UNIVERSITY OF TRENTO

DEPARTMENT OF INFORMATION ENGINEERING AND COMPUTER SCIENCE
DEPARTMENT OF INDUSTRIAL ENGINEERING
FONDAZIONE BRUNO KESSLER

Doctorate Program in Industrial Innovation

Design of Robots for Unstructured Environments

A Customisable Agile Quadruped, a Sensorised High-Force Gripper, and an Intelligent Drilling End-Effector

Edoardo Del Bianco

Advisor
Prof. Marco Roveri
Università di Trento

Co-Advisor
Dr. Nikolaos Tsagarakis
Istituto Italiano di Tecnologia

June 2026

Disclaimer

I, Edoardo Del Bianco (“the Author”), wrote this doctoral thesis in my personal capacity while employed at Leonardo S.p.A. (“the Company”), where I hold the position of Research Fellow within the Robotics Laboratory of the Innovation Hub & Intellectual Property organisational unit.

The views and opinions expressed in this thesis are solely those of the Author and do not necessarily reflect the official policies or positions of the Company.

This thesis has been prepared exclusively using open information sources, namely public-domain information obtained from unclassified sources, the majority of which are publicly available on the internet and not subject to any disclosure restrictions.

The thesis includes some results of research activities carried out at Leonardo S.p.A., to which the Author contributed or which were conducted under his supervision.

All cited sources (including texts, patents, data, and images) have been duly referenced where possible and where required. All cited trademarks and patents are acknowledged as the property of their respective owners, where applicable.

Nothing in this thesis shall be construed as granting, by implication or otherwise, any license or right to use any intellectual property owned by the Company or by third parties.

Any examples presented in this thesis are intended solely as the Author’s assumptions and do not reflect the position of the Company or of any third party. References to specific products, technologies, or organisations do not constitute endorsement or recommendation.

This thesis is provided for academic and research purposes only and shall not be relied upon for professional, commercial, or operational use.

The Author declares that this work does not intentionally disclose information subject to export control regulations, classified restrictions, or other regulatory limitations.

The Author has made reasonable efforts to ensure that all information and materials included in this thesis were accurate at the time of writing; however, no guarantee of accuracy can be provided.

The Author has not received any remuneration, consideration, or benefit for mentioning, reporting on, including, or commenting on any paper, program, product, policy, law, theory, hypothesis, or intellectual property.

Any remaining errors or inadequacies in this work are the sole responsibility of the Author.

Abstract

Robots for unstructured environments explore and physically interact in variable, uncertain, and unpredictable settings, as the contexts in which they are deployed are not adapted to facilitate their operation. Their technology is not yet mature for industrial use, but interest is rising for simple industrial inspection tasks.

The work presented in this thesis aims to facilitate the industrial deployment of robots for unstructured environments by providing robotic design case studies. Three novel devices are introduced, with the purpose of advancing agile quadrupedal locomotion, high-force grasping, and robotic power drilling. The first device is *Leon*, an agile quadruped designed from commercial actuators, eliminating the need for actuator development while retaining full access to the platform's hardware and software. Leon demonstrates a simple yet effective design approach, which simplifies agile robot design by using COTS components. The second device is *DAGANA*, a robust, modular, high-force-capable 1-DoF gripper that enables high-payload operations with everyday objects in unstructured contexts. DAGANA features a multimodal sensing system that mitigates sensor occlusion during grasping, and its modular design allows extension of its dexterity and sensing capabilities. The last device is *Smart Drill*, a sensorised robotic power-drilling end-effector that enables low-payload robotic arms to perform drilling operations. Smart Drill integrates intelligence into its design, allowing the end-effector to directly control the task execution in a robotic-platform-agnostic manner, facilitating seamless installation across different robotic arms.

While Leon's first prototype is still to be manufactured, its design is evaluated and validated through simulations and experiments on its actuator. Conversely, physical prototypes of DAGANA and Smart Drill have been fabricated and used in extensive laboratory experiments. The experiments not only assess the design's effectiveness but also showcase the applications of software pipelines appropriately designed to execute tasks relevant to real-world applications.

Keywords

Robotics for unstructured environments, Agile quadrupedal robot, High-force gripper, Power-drilling end-effector, Robotic industrial inspection

Acknowledgments

The work presented in this thesis was supported by the company Leonardo S.p.A. under the grant LDO/CTI/P/0020481/23 with the Università di Trento.

I express my gratitude to **Leonardo S.p.A.** for funding this research.

Looking back at these years of doctoral studies, the first person who comes to mind is my friend **Alessandro Garibbo**. I would like to thank him: without his effort and trust, this path would not have been possible.

I am also extremely grateful to **Navvab Kashiri** for sharing his deep mechatronic knowledge during the design of Leon.

I owe special thanks to **Pierpaolo Gambini**, **Alessandro Massa**, and **Rino Scervo** of Leonardo S.p.A. for encouraging my efforts and creating an inspiring research environment within the company.

The inspiration for my work comes from **Nikolaos Tsagarakis**, my supervisor and mentor, whom I sincerely thank. Nikos has always given me invaluable advice, and he is also, in my view, the best example of what a robotics scientist can be.

My gratitude also goes to my academic supervisor, Prof. **Marco Roveri**, for his constant support throughout these years.

I thank Prof. **Giovanni Berselli** and Prof. **Wesley Roozing** for their effort in reviewing this thesis; their feedback significantly improved the quality of the work.

I would also like to acknowledge my colleagues: **Giuseppe Alfonso** and **Marco Puliti** for their quick, reliable, and expert help with the experiments on Leon; **Davide Torielli** for his tireless experimental work on DAGANA; **Enrico Mingo Hoffman** for his guidance, particularly in the development of Smart Drill; **Andrea Zunino** for his encouragement and support; **Fabio Amadio**, **Gennaro Raiola**, **Andrea Testa**, **Luigi Raiano**, **Marco Laghi**, **Valentina Pericu**, **Simone Giampà**, **Andrea Monguzzi**, **Diego Vedelago**, **Arturo Laurenzi**, **Lorenzo Baccelliere**, **Luca Muratore**, and **Eamon Barrett**, not only for their valuable advice as skilled roboticists, but also for making the working days more enjoyable.

Special thanks go to **Federico Rollo**, an immensely competent engineer whom I am honoured to count among my closest friends. Federico contributed significantly to the work on DAGANA and Smart Drill.

Finally, I thank my family: my wife **Josien**, who patiently listens to all my ideas and helps me bring order to the chaos in my mind; my little daughters **Elizabeth** and **Isabel**, who put that order back into chaos; and my parents **Laura** and **Ernesto**, who lovingly support me and help me make the best decisions.

Contents

List of Tables

List of Figures

List of Acronyms

2D two-dimensional. 78, 108

3D three-dimensional. 16, 64, 73, 75, 78, 79

ABS Acrylonitrile Butadiene Styrene. 40, 42, 73

AGV Automated Guided Vehicle. 1

AI Artificial Intelligence. 42

AMR Autonomous Mobile Robot. 2

BMS Battery Management System. 61, 68, 70

CAD Computer-Aided Design. xiii, xiv, 12, 16, 44, 69, 70, 74, 75, 86, 96

CAE Computer Aided Engineering. 47, 81

CAN Controller Area Network. 34

CMOS Complementary Metal Oxide Semiconductor. 71

CNC Computer Numerical Control. 1, 22, 79

COTS Commercial Off-The-Shelf. xi, 3, 16, 17, 29, 30, 33–35, 42, 43, 87, 91, 93, 113

DC-to-DC Direct Current - to - Direct Current. xii, 54, 55, 61, 66, 69, 72, 73

DoF Degree of Freedom. 20, 48, 49, 114

FBW force-to-bodyweight. 29, 32, 83, 96, 111–113

FEM Finite Element Method. viii, xi, xiii, xiv, 36, 58, 59, 81, 83–86, 96

FFF Fused Filament Fabrication. xv, 38, 40, 42, 60, 73, 83, 86, 87, 90, 93

FoV Field of View. 42, 43, 60, 62, 63, 76, 109

FT Force - Torque. xv, 97, 98

GPIO General Purpose Input/Output. 70, 71, 77

GPS Global Positioning System. 17

HHCM Humanoids and Human Centered Mechatronics. 50

IIT Istituto Italiano di Tecnologia. xii, xv, xvi, 7, 15, 23, 48, 50, 51, 66, 97, 98, 101, 105

IMU Inertial Measurement Unit. xiii, 17, 40, 60, 61

IR Infra Red. 71

ISO International Standardization Organization. xiv, 75, 76

LIDAR Laser Imaging, Detection, and Ranging. 17, 24, 28, 42, 43, 113

MIT Massachusetts Institute of Technology. 8, 15, 16, 96, 113

MP Mega Pixel. 71

MPC Model Predictive Control. 86

NO Normally Open. 40

PA Polyamide. 38, 83

PC Personal Computer. 61, 62, 79

PCB Printed Circuit Board. 40, 70

PCM Protection Circuit Module. 68

PD Proportional - Derivative. 64

PnP Perspective-n-Point. 78

QDD Quasi-Direct Drive. xi, 7, 8, 16, 17, 29, 30, 32–34, 96, 113

RAM Random-Access Memory. 70

RANSAC RANdom SAmple Consensus. 78

RGB Red Green Blue. xiii, 50, 60, 61, 67, 101, 109

RGB-D Red Green Blue - Depth. 17, 19, 24, 28, 42, 113

ROS Robot Operating System. 61, 62, 67, 77, 79

RTC Real-Time Clock. 70

RViz ROS Visualization. xiv, 86, 87

SAR Search and Rescue. 6

SBC Single-Board Computer. xiii, 3, 28, 40, 42, 61, 62, 70–73, 76, 77, 79, 106, 107

SEA Series Elastic Actuator. xii, 7, 50–52, 114

TCP Tool Center Point. xvi, 102, 103

ToF Time-of-Flight. xiii, xvi, 60–62, 64, 67, 71, 77, 101–103

TPU Thermoplastic Polyurethane. 42, 60

TRL Technology Readiness Level. 2, 4

UDP User Datagram Protocol. 61

UGV Unmanned Ground Vehicle. 6, 111

UI User Interface. 78, 79

URDF Unified Robot Description Format. 32, 86

Chapter 1

Introduction

Industrial interest in the field of robotics, which arose in the 1960s after the introduction of the first Unimate industrial robot in a General Motors factory [1], has for a long time been limited to structured working conditions. Here, the robot is separated from the human operator and can perform predetermined tasks proficiently in controlled environments. Examples range from manufacturing operations (unloading and loading of Computer Numerical Control (CNC) machines, large-tolerance machining, welding, painting and surface finishing, pick-and-place tasks, and precision assembly) to quality checking and materials handling (palletising, automated packaging).

In the late nineties, Colgate and Peshkin introduced the idea of robotic arms collaborating closely with humans [2], giving birth to collaborative robotics. In collaborative robotics scenarios, the environment in which the robot operates is less structured and predictable than the closely controlled automation environment, and this is due to humans' unpredictable behaviours to which cobots must adapt. Technology was not mature, and it wasn't until the end of 2008, when Universal Robots sold its first UR5, that cobots became an industrial reality [135]. Today, collaborative robotics is one of the most relevant aspects of Industry 4.0 [3], and cobot applications span through all industrial sectors.

The exploitation of mobile robotic platforms in industry for material handling followed a path similar to that of robotic arms, expanding their capabilities from strictly structured to increasingly less structured environments. The first Automated Guided Vehicle (AGV) was implemented by Barrett-Cravens in 1953, and the technology quickly spread thanks to the advantages it brought [4]. AGVs operate only in structured environments, requiring the installation of dedicated guiding infrastructure in the factory. Recent developments in perception-based localisation and navigation have enabled the technological readiness to deploy more advanced mobile robotic platforms, Autonomous Mobile Robots (AMRs), capable of operating without any infrastructure for guidance and safety in increasingly less structured conditions [5].

It can be observed that, as robotics technology advances towards robots capable of operation in unstructured environments, industry leverages the technological readiness and expands robotic applications accordingly.

Robotics for unstructured environments, strictly speaking, refers to those systems designed to operate in variable, uncertain, and unknown settings that have not been modified or constrained to aid the robot's task execution. It is best expressed by mobile robots capable of exploring and manipulating the environment and performing partially defined tasks while coping with outdoor scenarios, unpredictable terrain, and obstacles. These robots, whether wheeled, tracked, or legged, are resilient to these challenging conditions. Their manipulators or limbs are developed for unpredictable contacts, and their structures are capable of withstanding the elements and resisting impacts.

The development of these platforms is much more complex than that of the robots currently adopted by industry. This is due mainly to the approach of industrial robotics: a robot is built to solve a specific problem by executing a set of tasks. In unstructured environments, the approach is the opposite: robots are built with the constraint of operating in the real world, and executing as many tasks as possible, with the general objective of mimicking human capacities to explore and physically interact with the world around them. In recent years, interest in these robots has seen a rise, encouraged also by the DARPA Robotics and Subterranean Challenges [6, 7]. Robots for unstructured environments are starting to demonstrate capacities that could enable them to replace humans in dangerous and challenging missions [8].

In general, for these types of robots, Technology Readiness Level (TRL) remains low, and industrial applications are still largely experimental. Yet, in recent years, quadrupedal robotic platforms are reaching a level of maturity that makes them relevant for limited industrial applications, and companies like the American Boston Dynamics, the Swiss ANYbotics, or the Chinese Unitree have started businesses in the sector. The prominent application proposed is industrial inspection, with limited yet effective manipulation capabilities. Here, the manufacturers of these robots propose architectures that are capable of autonomously tending to the safety of an industrial plant, opening doors, operating valves and switches [136, 137, 138].

Robots for unstructured environments are literally taking their first steps into the industrial world. The work presented in this thesis fits into this context, aiming to inspire further industrial expansion of this field of robotics by providing details on how these robots are designed and developed. Three robotic devices are developed: a quadruped, a gripper, and a power-drilling end-effector. The design process is reported, and the devices are tested and critically reviewed.

While quadrupeds and grippers of the type developed are already being used in the industrial-inspection examples provided before, power-drilling end-effectors are mostly confined to industrial production.

The quadruped, *Leon*, responds to the need for a research and product development platform that its users can customise in all its hardware and software layers. This is a critical capability that empowers researchers to explore new solutions, but it is restricted in commercially available robots. Developing a mid-sized agile quadrupedal platform generally requires years of research into actuator technology to realise appropriate leg actuators. This work demonstrates that it is possible to design an agile quadruped using mostly Commercial Off-The-Shelf (COTS) components and simple mechanical parts.

The gripper, *DAGANA*, enables robotic platforms to grasp and manipulate high payloads in unstructured conditions, and it shows how multimodal sensing can aid in the grasping operation, overcoming the problem of sensor occlusion that is typical of the final phases of grasping. Finally, the proposed approach demonstrates how modularity, at a hardware level, can expand the applications in unstructured environments: after a physical reconfiguration, the gripper can be applied to tasks previously impossible due to low dexterity.

The power-drilling end-effector, *Smart Drill*, demonstrates how a robotic drilling operation can benefit from a purpose-built, sensorised end-effector, and how drilling can also be performed by low-payload robotic arms. This is relevant not only to the fields of manufacturing (e.g., collaborative drilling of holes) and construction (e.g., collaborative installation of electrical systems on a wall), but also to the fields of inspection and exploration (e.g., drilling a hole on a panel to insert a probe). Yet, the main contribution of the proposed design is the definition of a new approach to end-effector management: thanks to an embedded Single-Board Computer (SBC), the whole operation (drilling, in this case, but the concept can be extended to other applications) is run inside the end-effector itself, on-edge, making not only the end-effector but also its related task robot-agnostic. With Smart Drill, a simple mechanical reconfiguration and the setup of a software interface are sufficient to replicate the operation on another robot.

The overall aim of the work, as stated, is to inspire further development of robotics for unstructured environments in industry. The hope is that, by presenting these simple yet effective designs, research and development groups around the world are stimulated to find new applications for these robots, increasing the TRL of these devices towards their large-scale diffusion in the industrial world.

The thesis is organised as follows: Chapter 2 analyses the relevant state of the art in the fields of unstructured environments, agile locomotion platforms, and grasping and power-drilling end-effectors. Chapter 3 presents the problems addressed by the proposed devices, while Chapter 4 describes the approach to solving these problems by detailing each device's mechatronic design. Chapter 5 reports the experimental testing and validation of the introduced devices, and Chapter 6 compares them with the relevant literature.

Chapter 2

State of the Art

2.1 Robotics for unstructured environments

In recent years, robotics for unstructured environments has become increasingly relevant, both in research and in product development [8, 9, 10, 11, 12].

The term "unstructured environments" identifies those working conditions that have not been modified to simplify the execution of a task by a robot [13]. Examples of these settings include an outdoor field, an underground cave [14], or the area around an industrial complex, but can be extended to extreme environments such as the deep sea [15], or space [16].

Mobile robots for unstructured environments need to execute exploration and physical interaction tasks in a priori unknown settings. They are currently of interest for their promising performance as substitutes for human operators tasked with performing dangerous and demanding tasks [6]. Examples of such activities include exploration of unknown environments [17], industrial inspection [18, 19], disaster and emergency response [20], civil security and public safety [21], heavy work and construction [22], and humanitarian demining [23]. Furthermore, robots for unstructured environments can perform tasks currently impossible for humans, such as nuclear waste decommissioning [24] or hazardous chemical processing [25].

The scope of these tasks is broad: some robots need to perform simple exploration in order to gather information from the field (such as scouting unknown or potentially dangerous areas while gathering information with their exteroceptive sensors). In contrast, others need to perform physical interaction with the elements in the field (such as manipulating objects in a disaster response scenario).

Therefore, robotic devices designed for operation in unstructured environments must meet design requirements that vary significantly depending on the task at hand. On the one hand, exploration tasks are constrained by the robot's capacity to locomote and navigate in harsh or uneven terrain, often under harsh environmental conditions, while maintaining agility and energy efficiency. On the other hand, interaction tasks require powerful mobile platforms equipped with high-payload robotic arms and robust end-effectors to exert high forces and perform power-tool operations in the environment.

The following sections analyse, from a robotic design point of view, robotic systems capable of operating in unstructured environments that enable:

- agile locomotion on uneven and unpredictable terrains
- powerful and perception capable grasping for high-payload operations
- robotic power drilling.

2.2 Agile locomotion

As technology advances, Unmanned Ground Vehicles (UGVs) are becoming increasingly relevant for complex field missions, such as inspection, exploration, and Search and Rescue (SAR), where a human operator's intervention would be undesirable. Conversely, terrain conditions in these unstructured scenarios are often rough and unpredictable, rendering wheeled or tracked UGVs ineffective or impractical. Here, legged robotic systems demonstrate a significant advantage: legged locomotion enables tackling uneven terrain, obstacles, confined spaces, or collapsed structures while maintaining stability and agility, as shown at the DARPA Subterranean Challenge [7].

Among legged robotic platforms, quadrupeds offer a compromise between simplicity, stability, and payload capacity, particularly when compared to bipeds, thanks to their large support polygon and simple balance control [26].

While legged mechanisms have been developed as early as the late 1800s [27], major developments in quadrupedal robotic systems began around the 1960s. Some milestone designs include the General Electric Walking Truck [28] and the KUMO and TITAN robots [29]. Much development followed [30], until in 2008, Mark Raibert and his team at Boston Dynamics introduced the quadrupedal platform BigDog [31], showing for the first time that a quadruped robot could achieve balance under significant external disturbances and traverse irregular outdoor environments, establishing the foundations of agile quadrupedal robotics. BigDog relied on an internal combustion engine to generate power and to hydraulically actuate its legs.

Hydraulic actuation was further developed and combined with electric actuation with the HyQ quadruped robot of Istituto Italiano di Tecnologia (IIT) [32], advancing actuator technology [33] and achieving notable later results (such as pulling a small passenger aircraft [34]).

Despite these advancements, the complexity, maintenance requirements, and efficiency limitations of hydraulically actuated systems proved detrimental to their large-scale development, especially when compared with the more recent electromagnetic actuators. Even the humanoid Atlas of Boston Dynamics, which adopted cutting-edge hydraulic actuation solutions, has been converted to fully electric actuation in its more recent versions [139].

While advanced, energy-efficient electromechanical actuation systems have been implemented in robotic legs [35, 36], the unpredictability of rough terrain necessitates the use of actuation methods with a simple and robust design that, thanks to some level of compliance, can withstand impacts and rugged use [37]. The most common actuation systems that offer these characteristics are the Series Elastic Actuator (SEA) [38] and the Quasi-Direct Drive (QDD) [39].

The SEA actuation paradigm couples an elastic element (typically a spring) between the actuator and its load. This approach makes the actuated joint impervious to disturbances and less prone to mechanical damage after an unforeseen impact, but the benefits come with trade-offs in control bandwidth, positional accuracy and stability. Despite these mechatronic design and control complexities, SEA actuators enable quadrupeds to use electric motors effectively in unstructured environments.

The StarlETH [40] and ANYmal of ETH Zurich [41, 42] are among the first examples of agile quadruped robots equipped with SEA actuators, configured for high speed and impact resilience. Together with its later commercial revisions, ANYmal [137] demonstrates agile behaviour in navigating unstructured environments, overcoming slopes, obstacles, and rough terrain.

SEAs also offer the possibility of obtaining stiffer interaction and a more human-like force range, as seen in the quadrupedal locomanipulation platform IIT CENTAURO, but the higher force capability comes at the cost of agility and ruggedness [43].

As an alternative to SEA-based solutions, QDD actuators compactly integrate a simple but torque-dense brushless motor and a low-gearing single-stage planetary gearbox [44]. Thanks to the low transmission ratios, the reflected inertia is minimised while maintaining sufficient torque output, allowing high backdrivability and simplified high-bandwidth torque control. This implementation produces simple, rugged actuators that are impervious to impacts and easy to control [45].

The most prominent examples of QDD-actuated robots are the Cheetah robots developed by the Massachusetts Institute of Technology (MIT), which show surprising agility, jumping, and manoeuvring capabilities and reduced cost of transport [46]. The initial developments at the MIT were centred on bioinspiration and energy efficiency [47]. Further developments enriched these concepts with economical manufacturing methods and simplified control strategies, producing Mini Cheetah, the first quadruped robot capable of performing a backflip [48]. These robots showed impressive running speed, ruggedness and resilience to disturbances previously unseen in electric quadrupedal platforms.

QDD actuators are also used in systems that explore alternative leg morphologies, such as SpaceBok [49], but, apart from these few examples, all agile robots feature simple leg architectures with hip-roll, hip-pitch, and knee-pitch joint configurations. Robots like ANYmal have their actuators mounted in-axis with the joint, increasing the upper leg's inertia. With QDD actuators, thanks to their intrinsic simplicity, it is possible to develop solutions that optimise the upper leg's inertia to achieve greater agility. Both the hip-pitch and knee-pitch actuators can be located at the top of the upper leg, closer to the quadruped's trunk. In this case, a transmission system actuates the lower leg. Multiple approaches are studied: the original MIT Cheetah uses a four-bar linkage [50], MIT Cheetah 3 uses a chain transmission, KAIST HOUND [51] uses a belt, and the high-payload quadruped Barry [52] uses ball-screw transmissions (also patented by Boston Dynamics [53]).

Other efforts in dynamic quadrupedal platform design have focused on designing research and development platforms with simplified mechanical architectures and open to high customisability. The Open Dynamic Robot Initiative [54] created the Solo12 quadruped [140], and another notable example is the small Stanford Doggo [55]. Other notable designs optimised for simple fabrication and open customisation have been developed at the Indian Institute of Science, both with small-sized quadrupeds [56] and larger chain-driven robots [57].

More recently, commercial exploitation of quadruped robots has begun. Leveraging the QDD concept, the company Unitree [141] commercialised AlienGO, Go1, and B1, and their successors, providing an effective solution for higher-level research and development in locomotion, navigation, and manipulation. The company DEEP Robotics soon followed Unitree with the X20 [142]. Nevertheless, these commercial products prevent users from developing their lower-level control and software architecture or upgrading their mechatronics design. This is primarily due to closed-source hardware and software and restricted commercial/legal practices. Still, it effectively limits the development of such commercial devices in a modular direction, making it extremely complex to interface with systems that expand their capabilities. The same limitation applies to other higher-end commercial quadrupeds (which offer purchasing opportunities to selected partners), such as Boston Dynamics Spot, Ghost Robotics Vision 60 [143], and others.

2.3 Grasping

As mobile manipulation platforms for unstructured environments advance and their technology enables higher manipulation payloads (as seen in humanoid robots [43, 58] or mobile platforms equipped with collaborative robotic arms [59]), gripping systems become critical enablers for developing high-force manipulation capabilities.

Gripping system designs can utilise various actuation paradigms, including electric, vacuum, pneumatic, and hydraulic actuators, each offering significant compliance levels for impact resilience and adaptability to specific tasks. To reduce overall dimensions and optimise inertia, the transmission of the grasping power is often performed using gears, cables, or linkages, allowing the actuator to be displaced from the grasping end-effector [60]. Furthermore, the grasping bodies can be developed with very different shapes (such as claws, fingers, or simple pads) and materials, often resorting to deformable elements or underactuated joints to add some level of compliance with the shape of the target object [61]. Innovative approaches, such as the jamming of granular material [62], show promising results and a different view on the basic principles that enable the gripping operation.

Robots in unstructured environments are tasked with interacting with everyday objects in a priori unknown settings. On the one hand, the target objects are often shaped considering the dexterity of the human hand, therefore requiring dexterous robotic end-effectors with fingered grasping mechanisms [63, 64]. Solutions range from grippers with few underactuated fingers [65, 66, 67, 68] to fully actuated anthropomorphic hands [69, 70, 71]. Nevertheless, high dexterity comes at the cost of added complexity, resulting in delicate mechanisms that are not appropriate for intensive use in unknown conditions. Furthermore, fully actuated solutions require complex actuation and transmission systems, which are difficult to maintain and increase weight and size. These factors limit the deployment of high-dexterity systems in real-world conditions.

On the other hand, tasks in unstructured environments can require high force, particularly when the robot is used to replace the human operator in dangerous and demanding conditions (as seen in Section 2.1). Wheeled quadruped robots have demonstrated their ability to perform interaction tasks (such as opening doors or carrying objects) through the use of strength and resilience to disturbances instead of dexterity [72]. Hand-type grippers are usually too complex and too weak for strong physical interactions, such as pushing objects and surfaces, because their fingers cannot exert high forces and their mechanisms can easily get damaged. Still, these high-force features can be embedded in simpler designs.

To address some limitations of traditional hand-type grippers, modularity in the finger-hand assembly is often employed. Rearranging the finger positions [67, 73] can enhance the capabilities of these grippers, enabling them to handle a broader range of tasks. Furthermore, modular designs are easier to fabricate and maintain due to the lower number of different components involved and the possibility of using preassembled subassemblies as spares [74].

Modularity benefits in particular two-finger grippers. In these simple designs, adjusting the position and shape of one of the gripping elements can further extend the dexterity, enabling these grippers to grasp a wide range of objects, as seen with the F1 Hand [75] and the M2 Gripper [76].

Furthermore, these simple two-finger designs, featuring only two gripping elements with just one being actuated, reduce complexity, lower the risk of failure, and increase overall robustness. They have the advantages of simplicity, cost-effectiveness, and good power-to-weight ratio, and for these reasons, they are widespread in all fields of robotics, with a high number of commercial solutions in the market ready to be used both in structured and unstructured environments [144, 145, 146].

Morphology, kinematics, and actuation methods of a robotic gripper are not the only active fields of research in grasping end-effector design. Gripper development also focuses on the integration of sensors in the gripper itself, aiming to add proprioceptive and exteroceptive sensing capabilities directly inside the end-effector.

On the one hand, proprioceptive sensors (like motor encoders and certain types of force/torque sensors) open remarkable possibilities to refine the actuation strategy in robotic grasping. On the other hand, exteroceptive sensors (like tactile sensors, distance sensors, accelerometers, and cameras) enable tasks that would otherwise be difficult or impossible. For example, tactile sensing [77] can be used to apply a specific grasping force [78, 79], or detect slipping [80]. Eye-in-hand vision systems can focus on the object while the arm and the target object are moving, demonstrating impressive use cases, like catching objects in flight [81, 82]. The advantages of vision sensors embedded in the gripper tool have been further elaborated in [79]. Embedded range sensors have shown their potential in enabling the accomplishment of otherwise impossible grasping tasks [83], and microphones can be used to fuse visual and audio data to improve the manipulation operation [84]. From a software point of view, integrating end-effector control and embedded perception capabilities enables easy and seamless task execution [85].

Robust grippers with a simplified structure and embedded perception are available commercially in the field of quadruped robots. One example is the end-effector mounted on the Boston Dynamics Spot quadruped robot [147]. While this end-effector is not extensively documented in the literature, its capabilities are showcased in [136]. Another example is the Unitree Z1 arm and its gripper mounted on the quadruped B1 for inspection tasks [138, 148].

Validation of grasping end-effectors to determine their capabilities is also a field of interest, as it is often difficult to relate the technical specifications of a gripper to its applicability in real-world tasks. Some studies introduce application-oriented benchmarks for evaluating the end-effector dexterity [86], or the capacity of manipulating everyday objects [87] and clothes [88]. Other works focus on intrinsic benchmarks, providing standards for measuring parameters such as forces applied by the fingers and grasping strength [89].

2.4 Power drilling

Drilling is a fundamental machining operation widely used in assembly, maintenance, repair, and construction. While it primarily enables the installation of mechanical fasteners, it has multiple other applications, such as inspection (probes can be inserted into drilled holes) and medical applications (e.g., orthopaedic surgery).

From a process engineering perspective, machine drilling is the most common material-removal machining operation. Its process parameters and execution are continually being developed and refined to achieve higher surface finish, reduce tool wear, and improve the accuracy and precision of the resulting hole [90].

Given its primary importance as a manufacturing operation, power drilling with robots has been investigated since industrial robots were first introduced into manufacturing contexts, as evidenced by the development of complex power-drilling end-effectors reported already in the 1980s [91, 92]. Power-drilling automation in robotic systems poses several challenges, including positioning accuracy, orientation control, force regulation, and interaction with heterogeneous materials [93].

In factories, which are a prime example of structured environments, robotic drilling is primarily used to increase throughput, repeatability, and quality in machining operations that require hole creation. Here, the workpiece, fixtures, and tools are known a priori, and industrial manipulators traditionally perform drilling using generic end-of-arm spindle tooling [94]. Research focuses on machining precision, improving positional accuracy of the drilled hole, its orientation relative to the surface normal, and the overall hole quality [95].

The aerospace industry is one of the earliest and most mature applications of robotic drilling in manufacturing. The assembly of an aircraft structure requires drilling and riveting millions of holes, posing challenges to machining repeatability and to work-related health issues for human operators. Since the early 2000s, task-specific end-effectors have been designed to refine a specific operation, such as aileron manufacturing [96]. Furthermore, end-effectors capable of combining drilling with support to secondary operations, such as countersinking, inspection, or fastening, have been developed [97, 98]. These devices are bulky and complex, but effective for predetermined tasks in industrial automation. Currently, well-known companies such as Electroimpact [149] provide mature combined solutions that enable the replacement of human operators in these contexts.

Industrial robotic drilling often encounters discrepancies between the Computer-Aided Design (CAD) model used for offline task programming and the dimensions of manufactured parts. Deviations are primarily due to manufacturing tolerances, part deformation, or fixturing, and result in holes drilled by the robotic system in positions outside of the maximum tolerance. This is true especially in the aerospace sector, where loosely toleranced sheet-metal panels are widely used. To address this challenge, vision-based measurement and correction strategies have been implemented [99], and the design of end-effectors has evolved accordingly, with the direct integration of cameras and related sensors [100] and the development of their calibration procedures [95]. In these cases, the correction of the drilling trajectory uses information directly provided by the end-effector rather than signals generated by an auxiliary external system.

The integration of sensors into end-effectors has proven beneficial for maintaining precision and accuracy with difficult-to-machine materials and challenging workpiece structures and fixtures. The integration of signals from multiple sensors (for example, by combining distance sensors and a camera [101]) has proven to be particularly beneficial for machining titanium structures.

Robotic power drilling is not only applied to the structured industrial automation environment. Indeed, the commercial availability of collaborative robotic arms has facilitated the expansion of robotic drilling to human-robot collaboration contexts. Still, the low payload and stiffness of cobots, as well as safety mechanisms that limit allowable forces and speeds, pose challenging control problems. Here, the robot can assist the drill operator, reducing the risk of fatigue and work-related health issues often associated with the awkward positions and repetitive motions required during drilling. Furthermore, studies show possible benefits by analysing how a collaborative robot can apply appropriate force profiles and support the operator to reduce positional errors and increase hole quality [102, 103]. Force control strategies have also been implemented using control methods derived from learning by demonstration [104].

In these works, drilling end-effectors have been developed to measure the operator's interactions, but no drilling end-effector has been specifically developed for the collaborative task. Indeed, the general approach is to clamp a small, commercial, battery-powered drill to the robot's end-effector flange and perform the drilling operation [85, 104], with little regard for the optimal orientation of the drilling axis relative to the robot's flange and no task-oriented optimisation of the end-effector's design or integration of sensing systems. Only for small-sized hole drilling, specific end-effectors are developed [105].

Even in the more unstructured scenario presented in [85], where the control of end-effectors for humanoids and lightweight robotic arms is investigated, drilling is treated only as a task to be performed by holding a commercial power tool in a humanoid hand, with no further strategy in end-effector development.

Unstructured environments open up new applications for drilling with small-sized robotic arms. Interest in drilling end-effectors for field tasks is emerging [106], and a notable example of power drilling in unstructured environments is presented in the context of autonomous pine-tree resin collection in forests [107]. Here, a functional, custom drilling end-effector is attached to an industrial manipulator mounted on a mobile base to drill irregular, biologically variable surfaces, often under low positional accuracy requirements. Since the task imposes no restrictions on payload or execution, the developed end-effector is a straightforward adaptation of the approach used in industrial contexts.

Another emerging, unstructured context for robotic power drilling is the use of mobile manipulators in construction. This field is particularly relevant for reducing work-related health issues [108], as drilling is a vibration-intensive task that requires impact-drilling strategies. The company Hilti is researching the automation of drilling operations in this scenario with its mobile manipulator Jaibot [150], and similar systems from the company nLink [151] are benchmarked against human operators in [109]. These integrated systems benefit from task-specific design and integration of end-effector, robotic arm, and mobile base with the specific aim of enabling drilling in construction. Yet, the end-effectors themselves do not seem to be directly applicable to other mobile manipulation platforms without major adaptations.

Similarly complicated end-effector designs are used in civil infrastructure maintenance research. Examples include those used in works on modelling and vibration reduction for bridge deck rehabilitation [110, 111], where a commercial power drill is modified and sensorised, and an additional actuated linear axis is included to control the feed motion of the drilling bit.

Task-optimised robotic drills also appear in space exploration to enable surface sampling. The Mars Science Laboratory Drill [112] is an example of such highly specialised drilling end-effectors.

Chapter 3

Problem addressed

The problem addressed by this work reflects the need to quickly and reliably deploy novel robotic systems that are ready for the challenging conditions of unstructured environments, simplifying research and development and enabling previously impossible tasks.

In particular, the work focuses on the mechanical design of robots and end-effectors, identifying and addressing limitations of current robotic systems in unstructured contexts for (i) agile locomotion, (ii) high-force grasping and (iii) power drilling.

3.1 Customisable agile quadrupeds

As seen in Section 2.2, agile quadrupedal robotic platforms are promising operators in complex missions of exploration, inspection, and physical interaction in unstructured environments. This is mostly due to their superior capability to overcome obstacles and uneven terrain, in which wheeled and tracked vehicles (or humanoids) have limitations. In recent years, research and product development groups have been prolific in the exploitation of quadrupedal robotic platforms, and their hardware has evolved accordingly.

3.1.1 Low-level access to hardware and software

Despite the relevance of quadrupedal design for research and development, few research groups or companies (e.g., Massachusetts Institute of Technology (MIT) [46], Istituto Italiano di Tecnologia (IIT) [32], ETH Zurich [41], Boston Dynamics [152], ANYbotics [137]) have developed their own agile quadrupeds in-house. These developments were made possible by each group's foundational experience in developing customised, next-generation actuators. The remaining hardware components of these platforms are custom mechanical structures or repurposed commercial devices, with varying levels of customisation. In fact, the literature shows that each group's publications on actuators precede the publications on their robots by some years [38, 113, 114, 115], while (from the hardware perspective) no other preliminary research enabling the development of the platforms is presented.

The introduction of the first quadruped (MIT Mini-Cheetah [48]) featuring a low-cost, low-gearing Quasi-Direct Drive (QDD) actuator by MIT marked the beginning of a new generation of agile quadrupeds. These proprioceptive actuators, thanks to their simplicity, robustness and ease of control, led to a new generation of research-oriented and commercial agile quadrupeds, thoroughly discussed in Section 2.2.

The low-cost commercial variants of this new generation of quadrupedal platforms (represented most prominently by the portfolio of Unitree [141]) allow research groups and companies to investigate quadrupedal locomotion and navigation problems without the need to develop their own quadruped robot. These devices are widespread, economical and easy to acquire. However, this accessibility comes at the cost of customisability.

Conversely, the manufacturers of these commercial platforms restrict access to low-level software in their products and do not disclose precise three-dimensional (3D) Computer-Aided Design (CAD) files of their designs. Hardware and software developments often require access to the low-level software and hardware of the robot, as this access permits customisation of system architecture and integration of custom-designed components, computing units and sensors. As a result, developers are forced to resort to reverse engineering and time-consuming workarounds to perform their research or product development. Furthermore, reported vulnerabilities in Unitree robots [153, 154] highlight the importance of having access to the low-level software, as that layer can hide potential cybersecurity risks.

The hype around QDD actuators has recently led to their commercialisation by companies (such as Cubemars [155] or, more recently, Unitree itself [141]). These simple QDD actuation units can now be purchased independently from the robots or devices for which they were developed.

To guarantee maximum compatibility in a wide range of applications, the firmware installed in the electronics of these Commercial Off-The-Shelf (COTS) actuators is generally accessible and configurable up to to the lowest level. Therefore, when these actuators are used in a custom robotic device, the user has complete control over the low-level software implemented in the robot, delivering an acceptable trade-off between customisability and the use of commercial solutions.

The complexity of the realisation of a fully customisable quadrupedal platform realisation could therefore be overcome by implementing a new approach to the development of their actuation systems, using commercially available actuators as a foundation.

3.1.2 Making an agile quadruped

This work aims to address the complexity of conducting low-level hardware and software research and product development in locomotion and navigation with commercial quadrupedal robots due to manufacturer restrictions. Given the possibility to independently purchase QDD actuators, it addresses the following question:

> *Is it possible to realise in-house an agile quadruped robot that can be fully customised at its lowest hardware and software level, without requiring the development of custom actuators from scratch?*

Such a platform would be developed using COTS components and avoiding custom actuator development by adapting existing components wherever possible. It would therefore be open to customisation from researchers and developers across all its software and hardware layers.

3.1.3 Commercial components and agility constraints

The realisation of a complete robotic platform requires the integration of several complex subsystems:

- **Actuation**: actuators and their proprioceptive sensing and low-level electronics
- **Sensing**: exteroceptive and proprioceptive sensors like Red Green Blue - Depth (RGB-D) cameras, Laser Imaging, Detection, and Ranging (LIDAR), Inertial Measurement Unit (IMU), Global Positioning System (GPS)
- **Computation**: computers dedicated to low-level communication with the actuators, middleware control and data processing from the sensors
- **Communication**: internal communication among computing units, actuators, and sensors, and external communication (wireless) to control the robot
- **Power**: battery, power management and safety

Sourcing the components that make up these subsystems from commercial catalogues presents various challenges.

On the one hand, these systems (when available commercially) are seldom provided in a state that can readily be integrated into a robot design, with problems spanning from bulky and heavy covers to power and communication interfaces. Their technical details and datasheets are sometimes not fully available, and some of their specifications have to be measured or inferred after procurement. On the other hand, commercial components are also prone to market-related issues: despite their presence in manufacturers' catalogues, they might be subject to minimum order quantities, regional availability, long production times and similar problems.

Furthermore, to have an agile quadruped, the mechanical design and integration of these components need to minimise and properly distribute the final inertia of the robot. Their supporting mechanical structures need to ensure protection and sufficient rigidity. Yet, they also need to be optimised for minimum weight, as the resulting quadruped must retain the agility properties that make quadrupeds effective in unstructured environments.

3.2 Grasping in unstructured environments

Grasping systems are critical for enabling the development of manipulation tasks in unstructured environments. As seen in Section 2.1, the robots for unstructured environments capable of manipulation are humanoids, mobile platforms, and quadrupeds equipped with one or more robotic arms. These platforms often feature robotic hands inspired by the human hand. Such systems have enabled dexterous robotic manipulation even in extreme environments such as the deep sea [116], effectively overcoming water pressure, temperature, and other environmental constraints.

3.2.1 Gripper payload, dexterity, versatility, and ruggedness

With the increase in payload capacity of small robotic arms and platforms for unstructured environments, it is critical that their grippers generate friction forces sufficient to pick up and manipulate heavier objects. Despite their dexterity, robotic hands apply low to moderate interaction forces, limiting the capability of the manipulation platform. Furthermore, they lack mechanical simplicity and ruggedness (key features for deployment in unstructured environments), as their fingers are mechanically delicate and are composed of many components and sensors.

The modular grippers analysed in Section 2.3, whether commercial or custom, provide simple two- or three-finger solutions featuring either angular or (more rarely) linear finger movement. Their grasping elements can be easily customised for the operation at hand, allowing designers to adapt the grasping jaws (or fingers) to a subset of tasks that the robotic platform is called to complete. This delivers a good compromise between simplicity and versatility, obtaining a reliable system that can be deployed for a variety of tasks. The implementation of custom fingers enables, at least for a limited subset of tasks and after a mechanical reconfiguration for the replacement of the jaws, the recovery of dexterity to a level closer to that of robotic hands. Nevertheless, these solutions also have relatively low gripping forces and (being designed for structured environments) have exposed mechanisms and ingress protection levels that are not appropriate for unstructured environments.

Drawing inspiration from nature, robotic grasping paradigms can be reimagined. Langowski et al. [117] observed the methods employed by animals to grasp objects around them, comparing their levels of power, dexterity and compliance. These observations can be extended to canines, which pick up objects with their mouths instead of their paws. Experience suggests that dogs securely grasp objects (e.g. a heavy toy, a rug, a rolled newspaper) and their cubs just with their bite, showing extreme versatility. They control their grasping force with their masticatory muscles, adjusting it according to the task at hand. A dog's mouth can be roughly modelled as a two-pad gripper with wide pads and one torque-controlled revolute joint that actuates only one of the two pads.

A similar approach is seen in the grippers of Boston Dynamics Spot [147] and Unitree B1 with the Z1 arm [148]. These large-size grippers are not available separately from their respective devices. They feature a single joint actuating one of two large grasping pads. Their declared grasping force exceeds that of commercial two-finger grippers, and their design follows paradigms of simplicity and sturdiness.

These grippers, while showcasing versatility and the capability to execute many tasks typical of unstructured environments (as seen in their respective presentation videos [136, 138]), cannot be repurposed for the task at hand without a significant redesign of their jaws, as they are integrated into the main body of the gripper.

3.2.2 Sensor occlusions in grasping

To drive the grasping, implementations with commercial grippers and robotic hands mostly make use of exteroceptive sensors (e.g. commercial Red Green Blue - Depth

(RGB-D) cameras) that are located on the robotic platform or on its arm (often with an additional flange [156]), leading to the possibility of occlusions of the sensors during the final approach phase of the grasping action. Few specifications are known about the Boston Dynamics Spot and Unitree B1 with the Z1 arm. Still, it is clear from observation and datasheets that these grippers include exteroceptive sensors in their large palms. Nevertheless, these sensors are deeply integrated in the gripper design and cannot be replaced or adapted to a new task without redesigning a significant part of the gripper.

3.2.3 Making a sensorised, rugged, and high-force gripper

This work aims to address the lack of a simple, robust and versatile gripper appropriate for exploiting the full payload of mobile manipulation platforms in unstructured environments and overcoming the problem of sensor occlusion in the grasping phase. It addresses the following question:

> *Is it possible to realise a gripper for unstructured environments unaffected by sensor occlusion and appropriate for high payload tasks, extending the sensing and manipulation capabilities of these robots to tasks currently carried out by human operators?*

Such a gripper would allow grasping and manipulation tasks in unstructured environments with heavy objects, extending the functionality of robots for unstructured environments further into the human-scale manipulation capabilities. Through mechanical reconfigurability, it would open the possibility to achieve, by developing custom jaws for a subset of tasks, higher dexterity than a generic equivalent. Its embedded exteroceptive sensors would overcome the problem of sensor occlusion that occurs during the final approach to an object to be grasped. Furthermore, with a physical reconfiguration of the sensing devices, it would be open to expanded sensing capabilities if a specific task requires it.

3.2.4 Actuation, mechanical design, embedded sensing

To realise this one Degree of Freedom (DoF) gripper, challenges regarding actuation, mechanical design, and sensor integration must be addressed.

Regarding the actuation system, it needs to be capable of both supplying high continuous torques and precisely sensing the delivered torque, even at low grasping forces. Furthermore, it must be able to withstand impacts during operation, and in terms of weight, it is crucial to have a high power-to-weight ratio.

From a mechanical design point of view, it is critical to minimise the mass of the structure, as for a given robotic arm payload, the actual payload that the robot can lift is diminished by the weight of the gripper. Furthermore, it is necessary to provide sufficient mechanical strength to withstand impacts, allow the robotic arm to use the gripper to push objects around (as seen in [136]), or even support the full weight of the robotic platform falling onto the gripper (as observed in [157]).

To ensure maximum compatibility of the gripper, it is necessary that the gripper can be mounted to the end-effector flange of the most widely used robotic arms for unstructured environments. Its electronics should likewise allow control using widespread protocols (such as EtherCAT [158]) that enable real-time control of the joint.

Modularity should also be addressed, allowing for a simple method of replacing the grasping pads and encouraging the development of customised grasping pads for various tasks. This enables the gripper to perform in applications that require more dexterity than what is possible with the standard grasping pads.

Finally, particular tasks may require specific exteroceptive sensors (for example, inspection tasks may necessitate the use of a thermal camera to assess the state of a hot component before touching it). In these cases, easy replacement of the exteroceptive sensors can be beneficial. Furthermore, the signals from these sensors need to be easily retrievable when the platform on which the gripper is mounted changes, ensuring maximum compatibility.

3.3 Power drilling in unstructured environments

Power drilling is one of the most ubiquitous machining operations, performed in both structured and unstructured environments by human operators and robots to produce holes in a wide range of materials. Its applications span from industry to construction, appearing in the manufacturing process of most human-made artefacts. Automation of the process is a traditional field of robot development in industrial shop-floor contexts, but it has recently gained relevance for human-robot collaboration in unstructured environments [150].

3.3.1 Drilling end-effectors and robots for unstructured environments

The examples analysed in Section 2.4 show that robotic drilling is easily achieved in structured environments, where geometries are predetermined, and machining conditions are predictable. Drilling end-effectors have adapted in this direction, evolving from end-of-arm spindle tooling derived from Computer Numerical Control (CNC) machines to solutions that aim to increase precision and combine multiple machining operations with a single end-effector.

Conversely, there are very few examples of robotic drilling in unstructured environments, where drilling operations are still mostly carried out manually by human operators.

Manual power drilling in unstructured environments is easy to deploy and highly versatile. The operator is equipped with a modern battery-powered drill and an appropriate set of drill bits. They arrive at the drilling site, manually measure and mark the drilling location, configure the power drill with the correct drill bit and speed setting and drill over the pre-marked spot up to the desired depth. They can then seamlessly reconfigure their equipment to drill other materials and in different locations. These operations are unmatched in terms of ease of deployment and versatility. The robotic drilling operation, by contrast, is more complicated to implement and less adaptable to varying circumstances.

The available robotic platforms for unstructured environments are either collaborative robotic arms or small robotic arms mounted on mobile bases (wheeled or quadrupedal [159, 118]). These robotic arms often have a limited payload [160], customised end-effector flanges and limited electrical power available at the end-effector [148]. Furthermore, the exteroceptive sensors of these platforms are limited, and their mounting positions (optimised for locomotion and obstacle avoidance) are not ideal for identifying drilling target points.

Adapting existing drilling end-effectors to these mobile platforms is either impossible or requires extensive reconfiguration of hardware and software.

These shortcomings can be addressed by redefining the concept of drilling end-effector for mobile platforms for unstructured environments.

3.3.2 Making a drilling end-effector

This work aims to address the absence of a robotic end-effector for drilling operations with the existing mobile platforms for unstructured environments, by addressing the following question:

> *Is it possible to design an end-effector that enables assisting or replacing the human operator in power-drilling operations in unstructured environments?*

The resulting system, deployed on existing mobile platforms for unstructured environments, needs to match human-operated power-drilling operations in terms of ease of deployment and versatility.

3.3.3 Limitations of robots for unstructured environments

To devise such an end-effector, it is necessary to analyse widespread mobile platforms for unstructured environments that are equipped with one or more robotic arms, assessing their compatibility issues with a power-drilling end-effector. These limitations are not specific to a single robot model, but recur across most mobile manipulation platforms designed for operation in unstructured environments.

1. Power limitation
2. Payload limitation
3. Transmission of axial drilling force
4. Variability of the mechanical coupling
5. Adequate exteroceptive sensing
6. Simplicity of low-level software integration
7. Simplicity of high-level software deployment

Power limitation

Small-sized robotic arms, such as cobots (e.g., Universal Robots UR5e [160] or Franka Research 3 [161], often embedded in mobile platforms, e.g. Robotnik Kairos [159]), or robotic arms integrated in robotic platforms like Unitree B1 with Z1 arm [148] or Istituto Italiano di Tecnologia (IIT) CENTAURO [43] provide the possibility to connect a device drawing a maximum of 50 W or no electrical connections at all. This obstacle must be overcome to integrate a power-hungry end-effector for drilling.

Payload limitation

Mobile platforms for unstructured environments, when equipped with a robotic arm, have a limited payload. This is even more critical in quadrupeds or humanoids, where the allowed payload varies with the position of the arm, as it affects the position of the projection of the centre of gravity on the support polygon. The advertised maximum payload is typically about 3 kg, but it varies significantly from device to device. A safe assumption is that an end-effector exceeding 2 kg can significantly reduce the available margin for force-controlled drilling. This limits the maximum permissible mass of the end-effector.

Transmission of axial drilling force

The literature discussion of Section 2.4 presents multiple instances of drilling end-effectors that have the axis of revolution of the drill bit out of alignment with respect to the wrist axis of the robotic arm (most often identified with the axis perpendicular to and concentric with the robot's flange). In these cases, when the drill bit applies an axial force to perform drilling, a torque is generated on the wrist, and the drill bit has the natural tendency to deviate from the desired drilling axis. The wrist actuators (which are normally the smallest actuators of a robotic arm) are therefore required to generate high torques to compensate for this misalignment, and their capacity can limit the maximum transmitted axial drilling force. Considering the size of the robotic arms mounted on mobile platforms, this misalignment can lead to required torques exceeding the capability of the arm, and thus should be minimised.

Variability of the mechanical coupling

The end-effector flanges vary among small-sized robotic arms. Some cobots comply with the ISO 9409 wrist-tool mechanical interface definition, although the dimensions vary as the size of the robot increases. Furthermore, customised platforms like the Unitree B1 present proprietary flanges. When connecting a new end-effector, it is often necessary to procure adapter flanges, slowing down the deployment process.

Adequate exteroceptive sensing

The exteroceptive sensors (i.e. Red Green Blue - Depth (RGB-D) cameras, Laser Imaging, Detection, and Ranging (LIDAR)) that aid in the localisation of the drilling target position are often positioned on the main body of the platform. Since a target drilling position is often on a benchtop or on a wall, the data derived from the exteroceptive sensors is incomplete or inaccurate, mostly due to occlusion of the sensors. This lack of information can substantially restrict the permissible operations, rendering the robotic drilling system less effective.

Simplicity of low-level software integration

Drilling end-effectors integrate a system for controlling their actuators and sensors through communication with their embedded electronics. This communication is not standardised and requires a considerable amount of development from the hardware and low-level software perspective. Furthermore, these developments are often non-portable to other robotic platforms, impacting the deployment time of the solution.

Simplicity of high-level software deployment

The high-level software necessary for the drilling operation ultimately allows the control of the robotic arm and the drilling end-effector to reach the target location, activate an appropriate control method and execute the drilling. To accomplish this mission, the software relies on the physical localisation and availability of the exteroceptive sensors, which are used to identify the target drilling location. The variations in sensor type and position from platform to platform can significantly influence the approach, slowing down the deployment of the high-level software associated with the end-effector.

Chapter 4

Proposed approach

The approach used to address the problems illustrated in Chapter 3 is based on the development of novel robotic devices for unstructured environments.

Following the listed problems, which concern (i) agile locomotion, (ii) powerful grasping, and (iii) power drilling, three novel robotic systems are introduced:

- the agile quadruped Leon (Section 4.1)
- the high-force, perception-enabled gripper DAGANA (Section 4.2)
- the intelligent power-drilling end-effector Smart Drill (Section 4.3).

While the mechanical design of Leon is complete and validated through assessments and simulations (Section 5.1), its first prototype has yet to be manufactured.

On the contrary, the prototypes of DAGANA and Smart Drill have been manufactured, and are validated through experiments in Sections 5.2 and 5.3.

4.1 The Leon quadrupedal robotic platform

This section describes the design of the quadrupedal robotic platform Leon, an agile robot open to customisation from researchers and developers. Its design addresses the problem presented in Section 2.2, which is useful to understand its objective and requirements.

4.1.1 Objective

Leon is an agile quadruped robot for unstructured environments that, unlike commercial devices, is fully accessible and customisable at its lowest levels of software and hardware.

Thus, research in locomotion, navigation or other fields is not restricted at the low level. It is realised without requiring custom actuator development.

4.1.2 Requirements

From the analysis of the problem and the technical challenges presented in Section 2.2, the design requirements can be determined. Leon satisfies the following:

1. Payload capacity appropriate for research in locomotion and navigation
2. Capability of performing agile motions
3. Unrestricted low-level software and hardware access
4. Simplicity and sturdiness
5. Custom actuators not required
6. Maximum use of commercially available components

Payload capacity appropriate for research in locomotion and navigation

The robot is capable of carrying a payload of at least 2.5 kg on its back, making it appropriate for research and product development in the fields of locomotion and navigation in unstructured environments.

Indeed, this research often requires equipping the quadruped with sensors and computational units to support specific activities, such as terrain exploration or industrial inspection. An example payload, used in navigation experiments [119], comprises a powerful Single-Board Computer (SBC), a Laser Imaging, Detection, and Ranging (LIDAR), and a Red Green Blue - Depth (RGB-D) camera. Its estimated mass, as detailed in Table 4.1, is less than 2.2 kg.

Table 4.1: Example exploration and inspection payload

Component	**Mass (g)**
SBC (Nvidia Jetson AGX Orin) [162]	870
LIDAR (Ouster OS0) [163]	522
RGB-D camera (RealSense D455) [164]	380
Support structure (estimate)	400
Total mass overall	2172

Capability of performing agile motions

The robot's inertial properties and actuators enable dynamic motions that can be considered agile. In order to estimate a robot's tendency to exhibit agile motion capability, the per-leg force-to-bodyweight (FBW) ratio [46] is used. It relates the maximum achievable purely vertical ground reaction force F_z of one single leg and relates it to the mass of the robot M_r.

$$\text{FBW} = \frac{F_z}{g\ M_r} \tag{4.1}$$

F_z is calculated, with the leg minimally extended, as:

$$F_z = \min_i \left(\frac{\tau_{\text{peak},i}}{l_{\text{link},i}} \right) \tag{4.2}$$

where i indexes the links of the leg, $\tau_{\text{peak},i}$ is the peak torque delivered by the actuator of link i, and $l_{\text{link},i}$ is the length of the leg's link i.

The robot ANYbotics ANYmal [41], which is considered an agile and is employed in use-cases similar to those of Leon, features a FBW ratio of 0.54 (as reported by Bledt et al. [46]). Leon is designed so that its calculated FBW ratio for Leon is higher than 0.55

Agility is also dependent on other factors, such as the actuator's technology and gear ratio. As seen in Section 2.2, Leon, with Quasi-Direct Drive (QDD) actuators and a satisfactory FBW, can be considered agile.

As a result of these agility properties, Leon is appropriate for locomotion on uneven and unpredictable terrains, commonly found in unstructured environments.

Maximum use of commercially available components

Leon uses commercial components wherever possible. When appropriate, the components are used as delivered, in a Commercial Off-The-Shelf (COTS) state. If necessary, they are minimally customised, e.g. to reduce the mass by removing a metal cover. This reduces manufacturing complexity and ensures maximum maintainability of each system.

Unrestricted low-level software and hardware access

As a consequence of creating a quadruped from minimally customised commercial components from scratch, each component's low-level software is accessible. Furthermore, the custom mechanical and electronics hardware necessary to integrate these components is in-house designed. Therefore, complete knowledge and access to these hardware components are guaranteed. This allows researchers and product developers full access to customise, fine-tune, and improve any of Leon's subsystems, acting independently and without restriction wherever needed.

Simplicity and sturdiness

Leon is developed for research and product development in the fields of locomotion and navigation in unstructured environments. For these reasons, its hardware is designed with simplicity and sturdiness as guiding principles. This allows easy maintenance and resistance to the possibly harsh conditions of unstructured environments. As a consequence, the three actuators of Leon's leg are identical in model and configuration, even if torque requirements may differ between joints, simplifying maintenance and tuning. Furthermore, the actuator's output bearings are overdimensioned to withstand high loads, including those from unpredictable impacts.

Custom actuators not required

Leon's actuation system is developed from COTS actuators. Modifications are made to its subsystems, but do not involve the electric motor or the gearbox. Therefore, it can be stated that Leon is a quadrupedal platform that uses commercial actuators, without requiring custom actuator development. This reduces manufacturing complexity and development time.

4.1.3 Conceptual design

Leon (see Figure 4.1) can be conceptualised as a mid-size agile quadrupedal robotic platform, developed by integrating minimally customised COTS components and using commercially available QDD actuators identical across all joints. Its legs are in a roll-pitch-pitch configuration, with fully symmetrical ranges of motion, with unlimited range at the knee-pitch joints. Its battery can be replaced for extended operation. In a closed position, the robot fits on the back of a human, as a backpack (see Figure 4.2). The total mass of the robot is 27 kg. Its estimated autonomy is 1.5 hours. It can carry a payload of 3 kg on its back without compromising its agility features. All its integrated systems are accessible at all levels, allowing users to customise and develop new solutions without restrictions.

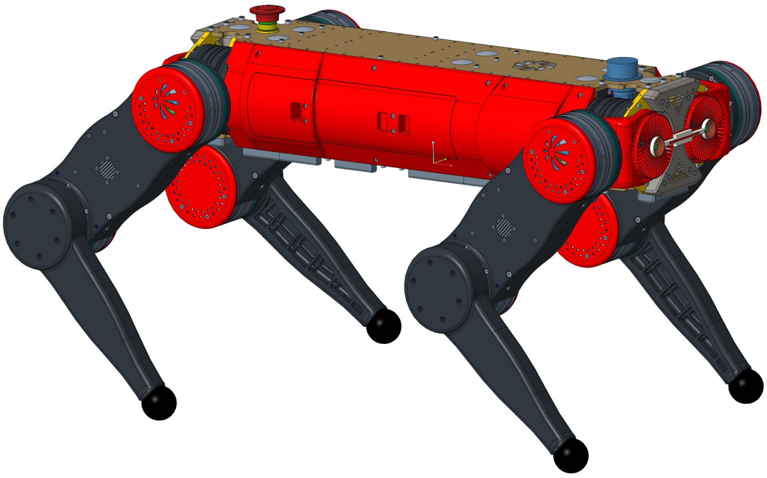

Figure 4.1: The quadrupedal robotic platform Leon.

Figure 4.2: Leon in folded position, close to the back of a mannequin carrying the robot as a backpack.

4.1.4 Customisation of a commercial actuator

The actuators of Leon are based on commercial QDD actuators with minimal customisation. This allows for rapid robot development without the need to invest time in developing a custom solution. The QDD technology, as shown in the literature (see Section 2.2), ensures agile robot performance when the actuator is correctly dimensioned.

Torque requirements

To determine torque requirements, a preliminary mass estimation of the robot is performed. Each subsystem's mass is estimated by summing up the known or estimated masses of its components and comparing the result to available data from other commercially available robots that use QDD actuators (such as the Unified Robot Description Format (URDF) of Unitree Robotics [165]). The result is a predicted total mass of up to 32 kg, as detailed in Table 4.2.

Table 4.2: Preliminary estimation of Leon's mass

Subsystem	**Mass (kg)**
Trunk	*10*
Computation units and other electronics	2
Battery	4
Frame and cover	4
Payload	*2.5*
(see Table 4.1)	
Legs	*20*
Actuators ($\sim$ 1 kg each)	12
Structural components($\sim$ 2 kg per leg)	8
Total mass overall	32.5

As seen in Section 4.1.2, given the torque capability, the FBW ratio can be used to ensure that the robot can perform with agility.

Using the Formulas 4.1 and 4.2:

$$\tau_{\text{peak},i} = \text{FBW}\ l_{\text{link},i}\ g\ M_r \tag{4.3}$$

where i indexes the links of the leg, $\tau_{\text{peak},i}$ is the peak torque delivered by the actuator of link i, and $l_{\text{link},i}$ is the length of the leg's link i, and M_r is the mass of the robot.

As indicated in Section 4.1.2, an actuation system can be considered satisfactory when it delivers a FBW of 0.55.

The length of the robot's links significantly impacts its performance. As stated in Section 4.1.3, Leon is a mid-size quadruped that can be carried on a human operator's back. This constrains its dimensions to a maximum length of 0.5 m to 0.6 m. Furthermore, the robot can be fully closed in a crouched position. This constrains the maximum length of the robot's lower leg link to ~ 0.25 m (considering the diameter of the actuator of ~ 0.1 m). To allow clearance between the upper legs' links, the upper legs' links are shorter than the lower legs' links. Therefore, considering the least favourable condition $l_{\text{link},i} = l_{\text{lower leg}} = 0.25$ m.

For simplicity in manufacturing and maintenance, considering that Leon is designed for research and product development, the same actuator is used in all joints. This simplifies $\tau_{\text{peak},i} = \tau_{\text{peak}}$.

Solving Equation 4.3 with FBW = 0.55, $M_r = 32.5$ kg, the minimum peak torque required from the actuators to ensure an agile behaviour is calculated as:

$$\tau_{\text{peak}} = \text{FBW}\ l_{\text{lower leg}}\ g\ M_r = 0.55 \times 0.25\ \text{m} \times 9.81\ \text{N kg}^{-1} \times 32.5\ \text{kg} = 43.8\ \text{Nm} \quad (4.4)$$

where $g = 9.81$ N kg^{-1} is the gravity of Earth.

Actuator selection and analysis

With the QDD market still undergoing significant expansion, at the moment of Leon's design, the only COTS actuator matching the torque requirements is the T-motor AK10-9/V2.0, later rebranded CubeMars AK10-9/V2.0 [155]. The actuator's specifications are: reduction ratio 9:1 with a planetary gearbox that ensures backdrivability, rated/peak torque 18/48 Nm, maximum speed 26 rad/s, rated/peak current 11.8/31.2 A and mass 0.960 kg. Its torque density, as advertised by the manufacturer, is approximately 50 Nm/kg. It is presented in Figure 4.3, on the left.

An analysis of the commercial actuator reveals three weak points.

1. **Bearing**
   The output crossed-roller bearing, which supports the link, is not properly clamped to the rotor and the stator as crossed-roller bearing manufacturers advise [166]. Its mounting consists of a simple press fit. Therefore, it is not protected from impacts, especially in the axial direction.

2. **Encoder**
   The integrated position sensor on the motor's side, an in-axis 15-bit magnetic

Figure 4.3: On the left, the COTS QDD actuator. On the right, the actuator modified for Leon. *Reproduced with permission from Springer Nature. First published in Springer Proceedings in Advanced Robotics, vol 32, pp 58–63, 2025 by Springer Nature* [120].

encoder which measures the position of the rotor before the gearbox, is not a multi-turn capable sensor. The simplicity of QDD actuators, together with their low gear ratio, allows them to be controlled with only one sensor on the motor side, before the gearbox. Nevertheless, to implement this strategy, a multi-turn encoder is needed. Furthermore, the encoder is not absolute. Therefore, it does not account for the robot's movements when the actuator is not powered, requiring a calibration procedure at each robot's startup.

3. **Electronics**
   The integrated drive electronics are fixed to the back of the actuator, increasing its overall axial dimensions. Since the motor's encoder is integrated in the electronics, they cannot be separated. This is particularly problematic for the upper leg, where the actuator's overall axial length determines the link's thickness. Furthermore, they provide only the Controller Area Network (CAN) bus communication protocol, whereas other alternatives may be more reliable and therefore preferred. For example, the use of the EtherCAT [158] protocol enables the implementation of modularity concepts that benefit research and product development environments [121].

To address these shortcomings, the following modifications and upgrades are performed. Figure 4.4 details the new components, while Figure 4.3 presents on the left the original actuator, and on the right its modified counterpart.

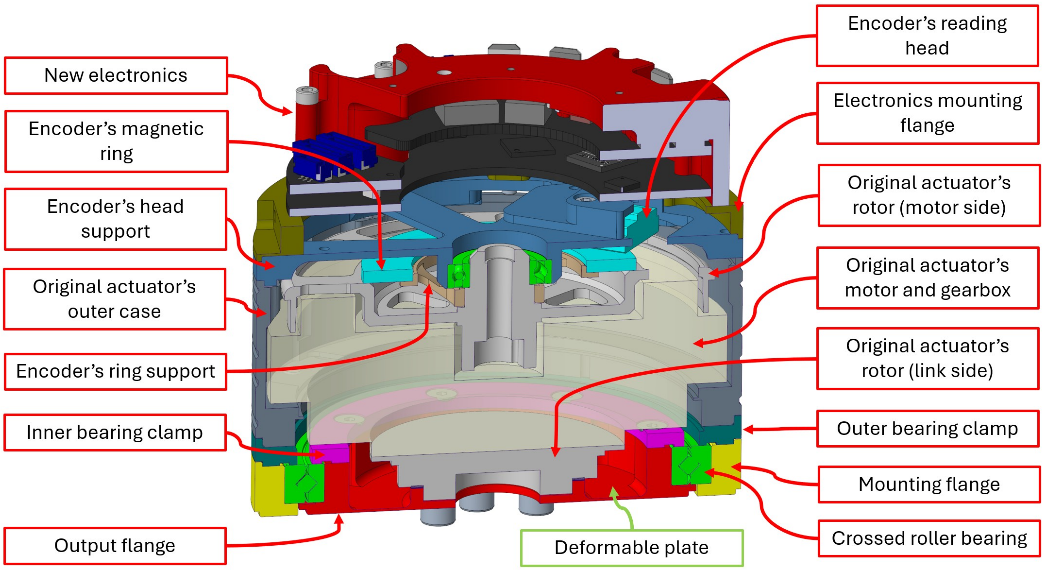

Figure 4.4: The internal parts of the upgraded actuator.

Bearing upgrade

The original bearing is replaced with a crossed-roller bearing of the maximum size that fits the cylindrical envelope of the actuator's main body, so that the final actuator diameter is not increased. The bearing used is the slim type, sealed IKO CRBS 708 V UU [166].

To verify its applicability, a maximum load equal to the load of the robot free-falling on one leg is considered in a quasi-static condition. Such an occurrence is unlikely unless the robot is dropped during transportation.

Following the procedure advised by the bearing's manufacturer to calculate the equivalent radial loads on the bearing [166], and using the preliminary estimations of the robot's mass ($M_r = 32.5$ kg) and of the least favourable link's length ($l_{\text{lower leg}} = 0.25$ m), the safety factors on the dynamic and the static loads are of 1.6 and 2.6 respectively.

Enhancing the functionalities of a COTS actuator poses the problem of having little or no information about the assembly tolerances of its internal components. This problem occurs during the design of the crossed-roller bearing's clamping flanges, shown in violet and dark green in Figure 4.4 (the bearing is shown in light green). In order to provide correct service, these bearings need to be clamped axially on both the inner and outer rings. Nevertheless, the tolerance on the axial position of the rotor is not known. Therefore, the inner ring of the bearing cannot be clamped without the risk of overconstraining the rotor. Among the actuators acquired, a 0.2 mm axial positional discrepancy of the rotor with respect to the stator was observed.

To solve this issue, the actuator's output flange (red in Figure 4.4) is designed as a deformable component which compensates for axial mismatch in the rotor's position. It is precisely positioned on the stator by clamping on the inner ring of the crossed-roller bearing, and it is then connected to the link's side of the rotor (of which the axial position is unknown) by means of a deformable thin plate. This deformable plate tolerates an axial deformation of up to 0.4 mm without breaking, permitting proper clamping of the actuator without overconstraining the system. The design of this flange is validated with a Finite Element Method (FEM) simulation, presented in Figure 4.5.

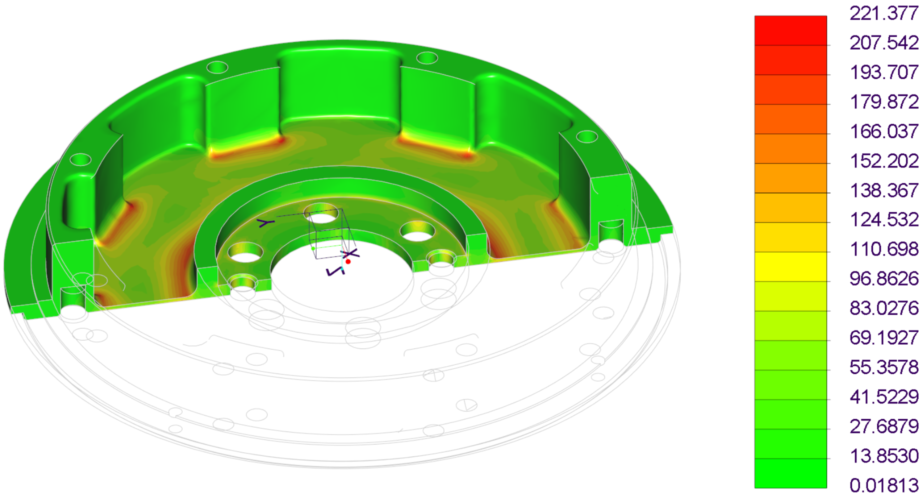

Figure 4.5: The FEM simulation validating the deformable output flange. A torque of 60 Nm (higher than the peak torque of 48 Nm) and a displacement of 0.4 mm are applied to the inner flange, while the bearing flange is fully constrained. The maximum Von Mises stress of 222 MPa is safely below the yield strength of the material used, Aluminium AL 7075-T6 [167], which is 503 MPa. *Reproduced with permission from Springer Nature. First published in Springer Proceedings in Advanced Robotics, vol 32, pp 58–63, 2025 by Springer Nature* [120].

Encoder upgrade

The original position sensor is replaced with the absolute magnetic encoder Bogen AKS 16, which provides 20-bit resolution and multi-turn counts. With a backup battery, it tracks the motion when the robot is off, during the replacement of the main battery, transportation or maintenance. Therefore, with this setup, a sensor on the output side (i.e. the link side) of the actuator is no longer needed.

To correctly assemble the sensor, the distance between the encoder's magnetic ring and the encoder's reading head must be kept within the manufacturer's tolerances. Nevertheless, the axial position of the rotor with respect to the stator is variable from actuator to actuator by 0.2 mm (similarly to what happens for bearing clamping). The encoder's head support is fastened on the original actuator's outer case (i.e. the stator (in dark blue in Figure 4.4), which defines its axial position. To compensate for variable rotor positions, the mounting element of the magnetic ring (in brown in Figure 4.4) can translate axially up to 5 mm during assembly. Once the correct distance from the reading head is determined, it is locked in position with set screws.

To protect the encoder's reading head from impacts, the encoder's head support features a cage in which the head is inserted (in dark blue in Figure 4.4, the sensor's reading head is in light blue together with the magnetic ring). Furthermore, this support flange allows the rotor to get proper ventilation while protecting the encoder head.

Electronics upgrade

The original electronics are replaced with an EtherCAT-enabled servo-drive, the Synapticon SOMANET Circulo 9 [168]. This integrated motor driver offers the option to interface with a separate position sensor via a wired connection, allowing it to be mounted separately in the robot's links (as shown in Figure 4.7). Nevertheless, thanks to its circular form factor, it can still be attached to the back of the actuator without increasing its overall diameter, as seen in Figure 4.4. This strategy is applied in the hip-roll joint. It features EtherCAT-enabled safety and communication.

4.1.5 Leg design

For simplicity and maintainability, all four of Leon's legs are identical, with no differences left to right or front to back. Likewise, all twelve actuators are identical.

The leg's joints, shown in Figure 4.6, are arranged in a roll-pitch-pitch configuration. The actuators are located in-axis with their respective joints, with the same approach featured by ANYbotics ANYmal [41]. This results in an extended workspace, as shown in Figure 4.14, at the cost of having less optimised upper leg inertia.

The hip-roll actuator is mounted on the trunk, and its electronics are attached to its back. The actuator's mounting flange, which houses the crossed-roller bearing, is fastened to a mounting plate that is solidly fixed on the trunk's frame.

The hip link, connecting the outputs of the hip-roll and hip-pitch actuators, is an L-shaped bracket manufactured with aluminium AL 7075-T6 and optimised for rigidity

Figure 4.6: Two views of Leon's leg.

and mass reduction.

The hip-pitch and knee-pitch actuators and their electronics are located on the upper-leg link. The upper leg, as shown in Figure 4.7, on the left, presents a symmetrical design. The two half-cell structures, each containing one actuator and its corresponding electronics, are identical and can be assembled and maintained separately. The half-cell bodies incorporate the actuator's mounting flange (in yellow in Figure 4.4), housing the crossed-roller bearings directly in their structures (see Figure 4.7, on the right). This approach avoids the need for a separate fastened connection between the actuator and the link, reducing overall thickness and maximising structural rigidity. The length between the hip-pitch and the knee-pitch joints is 215 mm.

The lower leg is connected to the output of the knee-pitch actuator. Its main body consists of a composite structure, fabricated with the Fused Filament Fabrication (FFF) method with carbon-fibre-reinforced Polyamide (PA) material. Its design features a stringer and frame ribbing, which optimises its mass without compromising structural rigidity. This ribbing is shown in the semi-transparent view of Figure 4.8. Since the lower leg is not sensorised, there is no wiring between the upper- and lower-leg links. Therefore, the range of motion of the lower leg is not limited.

A modified squash ball is used as a foot, similarly to Mini Cheetah [45]. The lower leg measures 244 mm between the knee-pitch joint and the centre of the foot.

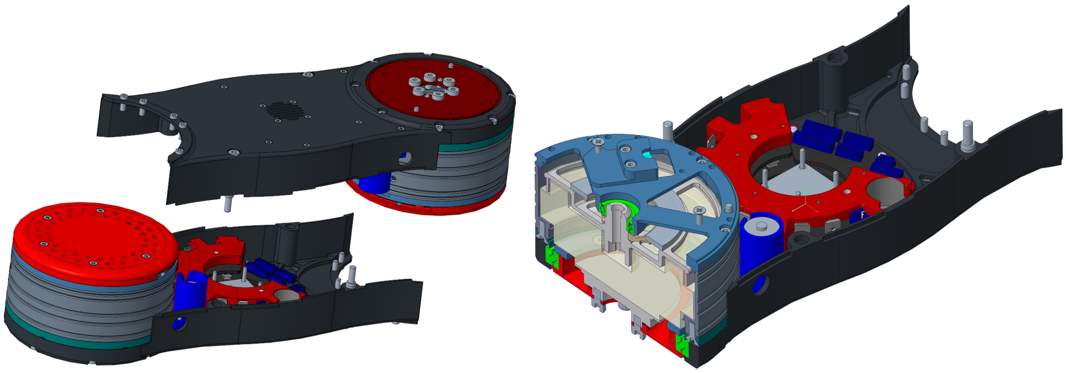

Figure 4.7: On the left, an exploded view of the upper leg link. The symmetrical design allows maintenance and replacement of either the knee-pitch or the hip-pitch joints with the same components. The motor's electronics are mounted off-axis to reduce the link's thickness. *Reproduced with permission from Springer Nature. First published in Springer Proceedings in Advanced Robotics, vol 32, pp 58–63, 2025 by Springer Nature* [120]. On the right, the actuator's sectional view shows the removal of the actuator's mounting flange, obtained by housing the crossed-roller bearing's outer ring directly in the link's structure.

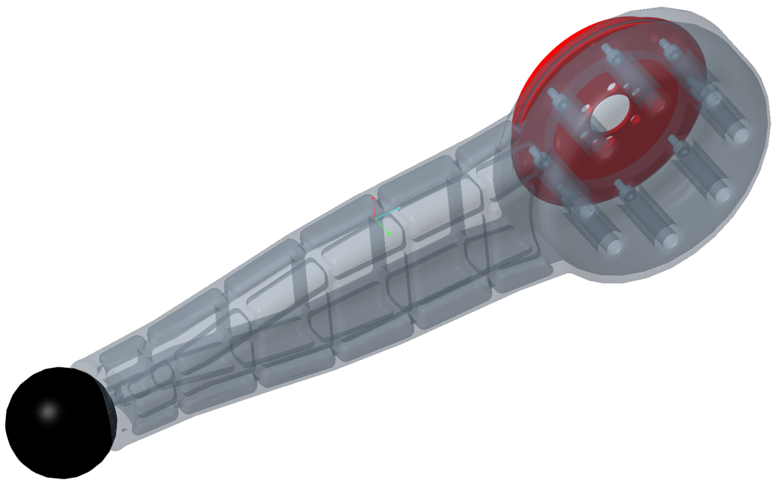

Figure 4.8: The lower leg of Leon, with its main body in a semi-transparent state to show the stringer-and-frame ribbing.

4.1.6 Trunk design

Leon's trunk houses all the components necessary for its communication and locomotion functionalities. These components are listed in Table 4.3. They include two computation units, one for low-level EtherCAT-enabled joint control and one for robot management and wireless communication, EtherCAT and Ethernet switches, an Inertial Measurement Unit (IMU), a battery and other power-related elements. The components needed for higher-level implementations, such as sensing and navigation, are instead located on Leon's payload and can be quickly modified for specific needs (see Section 4.1.7).

Table 4.3: Components in Leon's trunk, providing communication and locomotion functionalities to the robot

Function	**Component**
Control SBC	AAEON UP Xtreme i11 [169]
Manager SBC	Intel NUC 11 Pro [170]
EtherCAT switch	Omron GX-JC06 [171]
Ethernet switch	D-Link DGS-105 [172]
IMU & GPS	GABLE SE7-OEM-RA [173]
Lithium-ion battery	MAP BATTERIE IP48V15 [174]
Power gauge	Generic voltage meter (square hole 33 mm by 20.3 mm)
Power switch	Generic 50 A Battery switch (hole 22 mm)
Emergency switch	Generic mushroom-head switch (hole 16 mm)
Power up switch	GenericNormally Open (NO) switch (hole 22 mm)
Power board	Custom Printed Circuit Board (PCB)

Figure 4.9 shows the position of the internal components within the rigid frame structure, which connects the legs and fixes the payload.

The trunk's framing structure (shown in Figure 4.10) is designed with seven structural components. It consists of two identical bottom and top plates, connected by two identical internal frames and two identical front and back actuator supports. The internal frames, in conjunction with a sheet-metal box, form a confined battery bay that can be accessed from the right side of the robot, providing protection for the internal components from the battery and enabling fast replacement of the battery itself. Reusing the same elements twice (except for the sheet-metal box), totalling just four different parts, results in more economical manufacturing and simplified maintenance.

The covers are designed to provide maximum leg workspace while maximising the trunk's internal space and protecting the internal components. They consist of five Acrylonitrile Butadiene Styrene (ABS) structures fabricated with the FFF technology

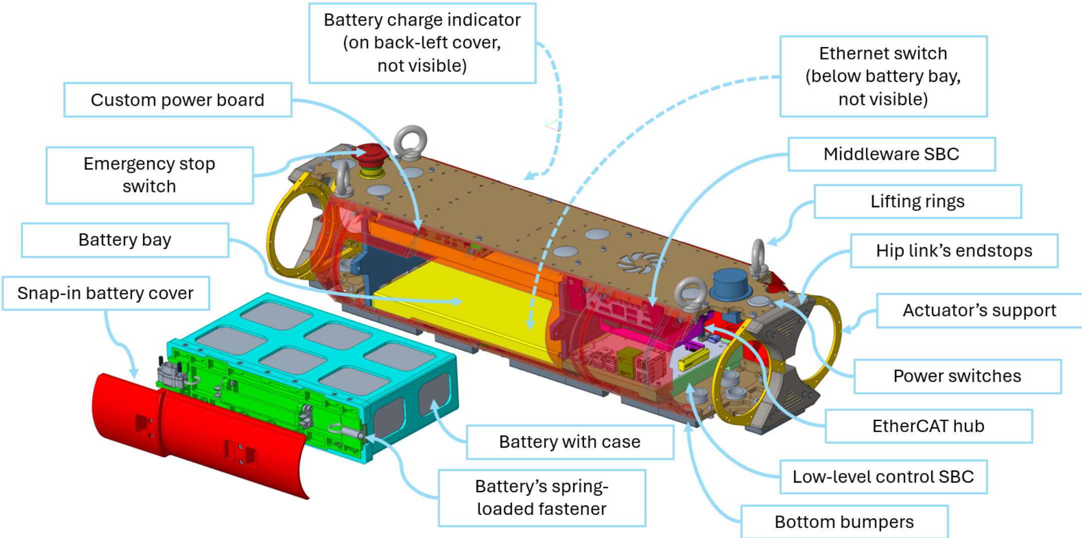

Figure 4.9: The components inside Leon's trunk

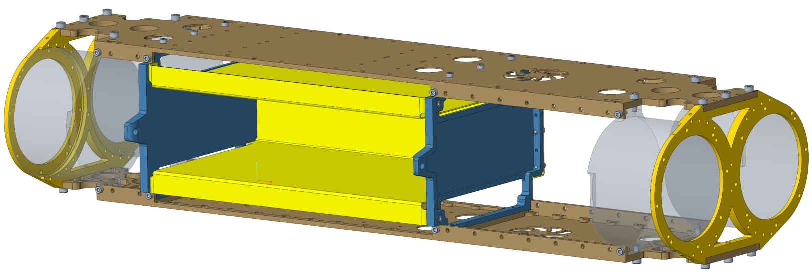

Figure 4.10: The structural components of Leon's trunk framing structure. The actuators are shown with semi-transparent placeholders.

and fastened with screws. They can be disassembled independently from the sides by undoing the fasteners, allowing easy access for internal cable routing and maintenance. On either side, there are two cover structures: a smaller one, in the front, provides access to the computation units and the EtherCAT switch. A larger one, in the back, covers the battery, power board, and Ethernet switch. The right-back cover protecting the battery on the side of the battery bay, as shown in Figure 4.9, is further split into two pieces. The internal piece, which snaps into place with COTS snap-in fasteners, allows easy battery removal. On the back-left cover, a voltmeter reads the battery's charge state.

The battery, as shown in Figure 4.9, features a FFF-fabricated ABS case which is secured on the framing structure with two spring-loaded pins. Considering similar systems [122] and the selected battery's capacity (720 Wh), the robot's autonomy is estimated to be 1 to 1.5 hours of normal operation.

On the front and back actuator's supports, Thermoplastic Polyurethane (TPU) rubber endstops fabricated with the FFF technology limit the workspace of the hip pitch links. If a particular payload requires further workspace restriction to prevent the legs from hitting its components, these rubber endstops can be quickly modified to meet the needs.

4.1.7 Payload

As seen in Section 4.1.6, the trunk of Leon includes all components that allow locomotion and communication. The components that enable exteroceptive sensing and additional computation capabilities are instead mounted on the top of the trunk, as a payload.

The standard payload of Leon consists of the following elements:

- an Artificial Intelligence (AI) capable SBC, the Nvidia Jetson AGX Orin [162]
- a forward-facing RGB-D camera for reliable depth sensing, the RealSense D455 [164]
- two side-facing stereo cameras for visual-inertial tracking, the Stereolabs Zed Mini [175]
- a LIDAR, the Ouster OS0 [163]

An aluminium AL 7075-T6 sheet-metal cage structure protects the sensors from impacts if the robot falls. Furthermore, it supports the sensors at a height that maximises their Field of View (FoV). Sheet metal is chosen for the LIDAR cage because it

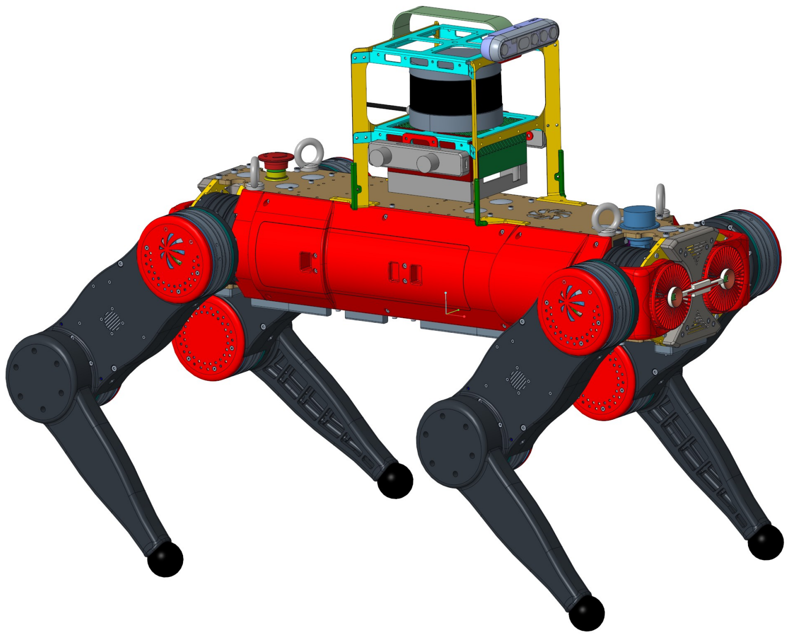

Figure 4.11: The Leon quadruped with its sensing and computation payload mounted on the trunk.

offers multiple advantages: (i) it is easy to manufacture, (ii) it provides rigidity, and (iii) it minimises the shadow created by the cage's vertical structures on the FoV of the LIDAR. The total weight of the cage structure is approximately 0.350 kg.

Additionally, a set of four lifting rings (visible in Figure 4.11) can be fastened on Leon's trunk. These rings, by allowing the robot to be lifted by a gantry crane that follows it, aid in the development of locomotion strategies, thereby preventing falls that can damage the robot's components.

4.1.8 Leg wiring

The COTS actuators used in Leon do not provide a through-hole design, which facilitates the wiring of robotic links. As a consequence, a wiring system is developed.

Since the hip-pitch and knee-pitch actuators and their electronics are located on the upper-leg link (as seen in Section 4.1.5), only one wiring harness is necessary for each leg, connecting the trunk to the upper leg. It features power cabling and EtherCAT cabling for the servo drives.

The cables, properly bundled together, exit the trunk close to the hip-roll actuators and enter the upper legs on their sides, close to the hip-pitch actuator. Four holes are present on the upper-leg body, so that the most convenient entry point can be selected.

To prevent failures, sufficient slack and chafe protection on the cables bundle and at the exit or entry points are to be employed during assembly. To preliminarily determine the appropriate cable length, a Computer-Aided Design (CAD) study involving extreme joint configurations is performed. It is presented in Figure 4.12.

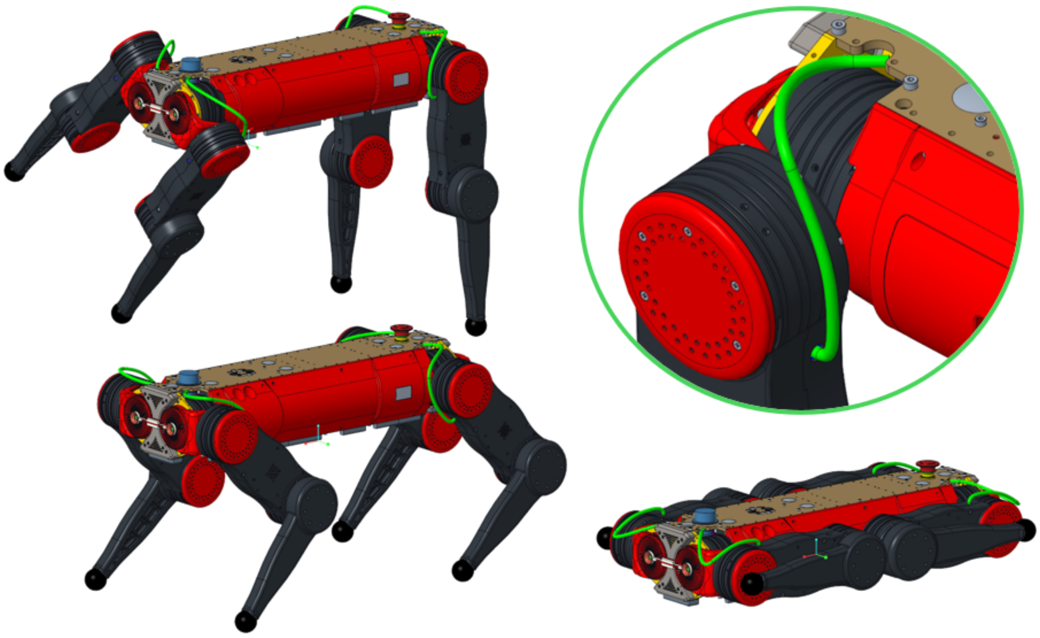

Figure 4.12: In light green, the wiring that connects the trunk to the legs of Leon, presented in operational and extreme workspace positions.

4.1.9 Technical specifications of Leon

The previous paragraphs have introduced Leon's components, describing its actuators in Section 4.1.4, its legs in Section 4.1.5 and its trunk in Section 4.1.6, while its standard payload is discussed in Section 4.1.7. The wiring of Leon's legs is described in Section 4.1.8.

The full assembly of Leon is shown in Figure 4.1.

This section reports the robot's final technical specifications, including its dimensions, mass and workspace.

Leon's actuators are capable of 18 Nm of continuous torque and 48 Nm of peak torque (as seen in Section 4.1.4).

The overall dimensions of Leon are visible in Figure 4.13. The most significant ones are reported in Table 4.4.

The workspace of each leg's joint is visible in Figure 4.14 and is reported in Table 4.5.

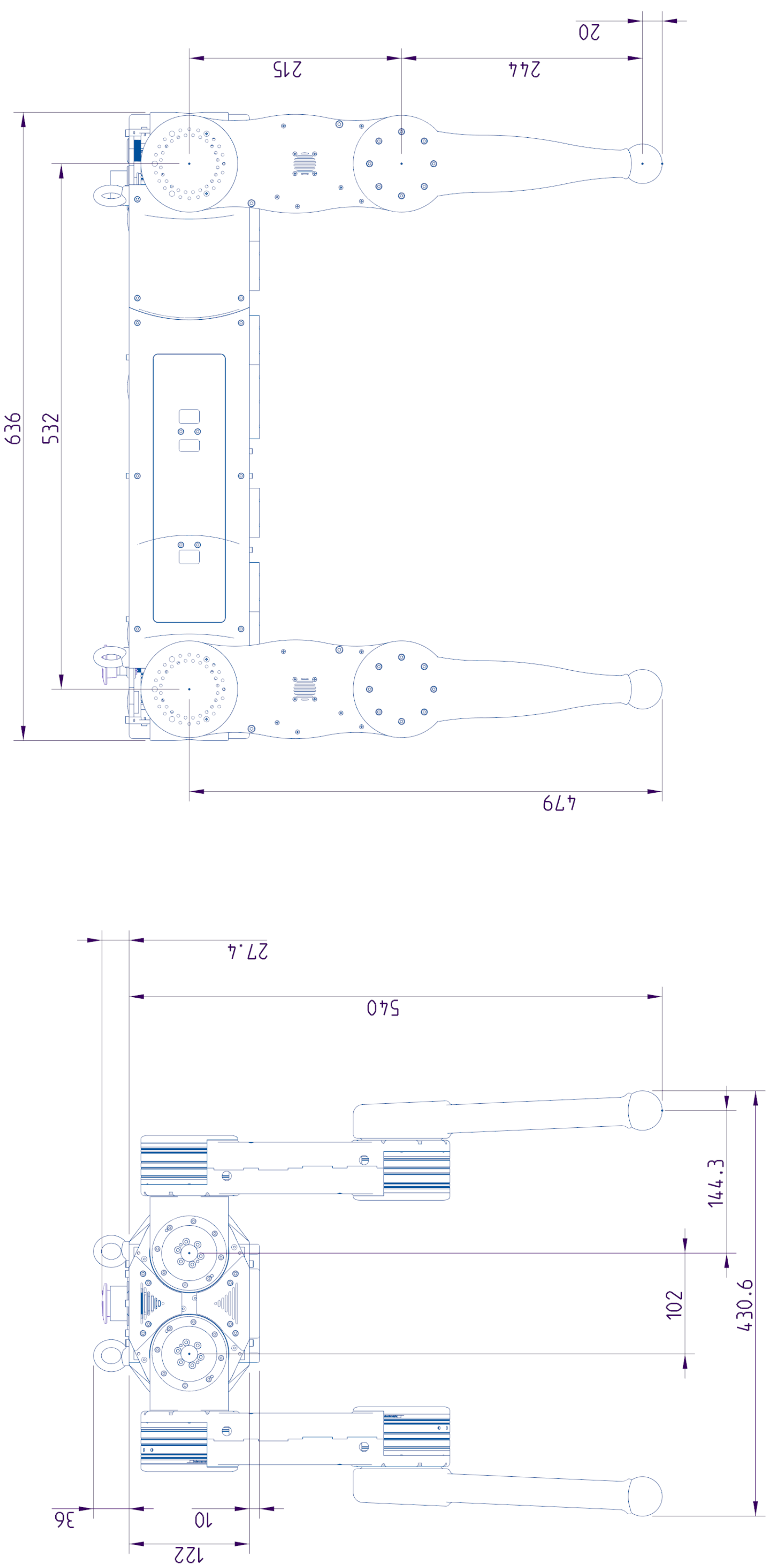

Figure 4.13: Technical drawing showing Leon's front and right views and presenting the robot's most significant dimensions.

The workspace of the hip-roll joint is 90° and completely symmetrical with respect to the vertical direction, while the workspace of the hip-pitch joint is 340° and is only limited by the presence of the electrical cables that go to the upper leg's link from the trunk, while the knee-pitch joint is unlimited.

The mass of Leon's subassemblies is reported in Table 4.6. The expected mass is 27 kg, while the platform is capable of carrying a payload of 3 kg.

Table 4.4: Significant dimensions of Leon, in mm.

Characteristic	**Dimension**
Length	636
Width	430.6
Trunk thickness (without ground bumpers and lifting rings)	122
Trunk thickness (with ground bumpers and lifting rings)	168
Upper-leg link's length	215
Lower-leg link's length (to the centre of the foot)	244
Lower-leg link's length (to the bottom of the foot)	264
Horizontal distance between hip-roll axis and foot	144.3
Payload mount plate height (legs fully extended)	540

Table 4.5: Leg's joints workspace. Angles in degrees referred to the pose of Figure 4.13.

Joint	**Angle MIN**	**Angle MAX**	**Range**
Hip Roll	-45	+45	90
Hip Pitch	-240	+100	340
Knee Pitch	–	–	unlimited

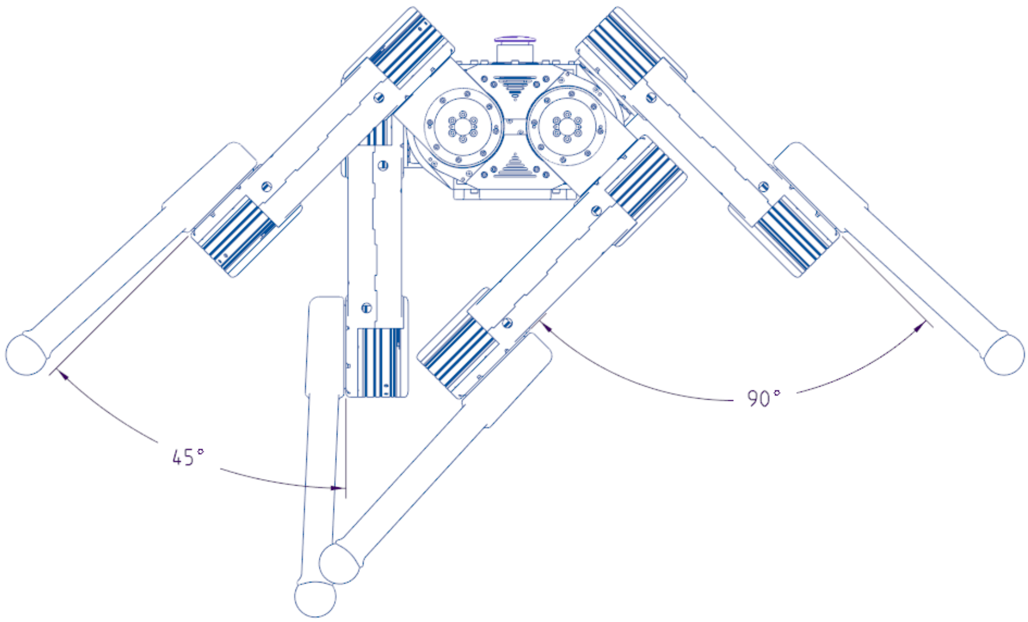

Figure 4.14: Technical drawing showing Leon's front view and presenting the workspace of the robot's hip-pitch joints.

Table 4.6: The mass of Leon and its subassemblies

Subassembly	**Mass (kg)**
Trunk[a]	9
Leg - Hip actuator[b]	0.9
Leg - Hip link[b]	0.9
Leg - Upper leg link[b]	2.2
Leg - Lower leg link	0.5
Payload[a]	2.7
Total mass without payload	**27**
Total mass with payload	**29.7**

Values rounded to the first decimal place.
[a] Considering a safety factor of 1.2 to account for cabling, connectors, and other elements that are not predictable with Computer Aided Engineering (CAE).
[b] Considering a safety factor of 1.02 to account for cabling and connectors.

4.2 The DAGANA gripper

This section describes the design of the high-force gripper DAGANA, a modular one Degree of Freedom (DoF) grasping end-effector equipped with multimodal exteroceptive sensing capabilities. Its design addresses the problem presented in Section 3.2, which clarifies its objective and technical requirements.

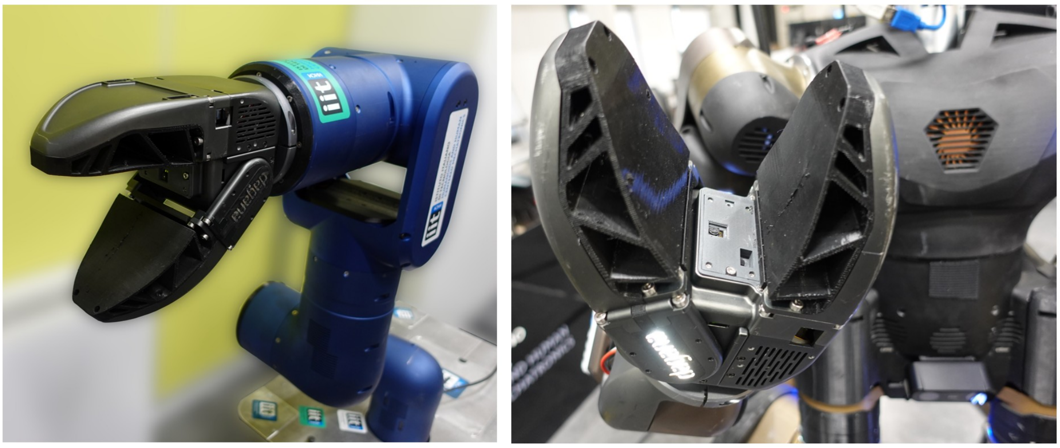

Figure 4.15: The high-force gripper DAGANA on the IIT RELAX [123] and IIT CENTAURO [43] robotic platforms.

4.2.1 Objective

DAGANA is a grasping end-effector for human-scale heavy-object manipulation with robotic platforms in unstructured environments. It overcomes occlusion of the robot's exteroceptive sensors during grasping and offers extended versatility through electromechanical reconfiguration.

4.2.2 Requirements

From the analysis in Section 3.2, which expands the problem and technical challenges addressed by this design, it is clear that DAGANA needs to satisfy the following technical requirements:

1. Simplicity and ruggedness
2. High-force capability
3. High force and impact resistance

4. Low overall mass
5. Embedded exteroceptive sensors
6. Reconfigurability of grasping elements and sensors

Simplicity and ruggedness

The gripper is a simple one DoF design, with large grasping elements (or jaws). It can operate in unpredictable environments without exposing its components to damage from impacts, dirt, or dust. These features make it optimal for working in unstructured environments, where the conditions are a priori unknown, and the task is not fully defined.

High-force capability

The gripper is capable of delivering a force higher than 100 N at its tip with a standard jaw configuration, thanks to a peak torque from the actuator higher than 15 Nm. This allows the gripper to exert high forces on the grasped objects, thereby producing friction forces between the target object and the gripper jaws high enough to support heavy objects.

High force and impact resistance

The actuator and the mechanical structure can withstand high loads and impacts not only related to its high-force operation, but also resulting from impacts and tasks in which the gripper is used to push objects and furniture (like doors).

Low overall mass

Any payload of the robotic arm used to support the weight of the end-effector reduces the free payload available for manipulation. As seen in Section 2.3, robots for unstructured environments and small collaborative robotic arms are moving towards higher payload capabilities, thus enabling high-payload manipulation. Nevertheless, it is important that this increase in payload is not absorbed by the mass of the gripper. Thanks to the optimisation of the mechanical structure and the high power-to-weight ratio of the actuator, the overall weight of DAGANA is below 2.5 kg.

Embedded exteroceptive sensors

The gripper includes exteroceptive sensors: a Red Green Blue (RGB) camera and a distance sensor, complemented by their data processing electronics. This allows the gripper to overcome the problem of sensor occlusion due to the end-effector obstructing the exteroceptive sensor of the robotic platform during the final phases of the approach.

Reconfigurability of grasping elements and sensors

A modular approach is used in the development of the gripper. In particular, its jaws are designed in a modular way, so that the gripper can be reconfigured with new mechanical components adapted for a particular task. This allows for the recovery of part of the dexterity lost with the choice of using a simple two-pad gripper with a revolute joint. Furthermore, its sensing system is modular, so that it can be replaced or upgraded with sensors more appropriate for a specific task.

4.2.3 Conceptual design

DAGANA is conceptualised as a high-force grasping end-effector of simple and rugged design, based on a single revolute joint. It features a high-power-to-weight actuator, and it is capable of withstanding impacts during operation. It is equipped with in-palm multimodal exteroceptive sensors. It is designed with a modular approach: its grasping module, normally equipped with two large grasping jaws, can be mechanically reconfigured to satisfy the requirements of a specific subset of tasks, while its sensing module can be expanded or replaced according to the needed sensing capabilities.

4.2.4 Actuator selection and customisation

While the gripper is designed to be adaptable to different robotic platforms, its initial design and operation are performed with the IIT CENTAURO [124] humanoid robotic platform.

The CENTAURO robotic platform includes 5 sizes of high-power-to-weight torque-controlled actuators with different harmonic gearing options. These high-performance actuators are developed by the IIT Humanoids and Human Centered Mechatronics (HHCM) research line as foundation technology and described in [43]. Thanks to their optimised Series Elastic Actuator (SEA) design, they are resilient to impacts, especially in their lower gearing configuration. They feature high-resolution (19-bit) position sensing on both the three-phase motor side and the output (or link) side.

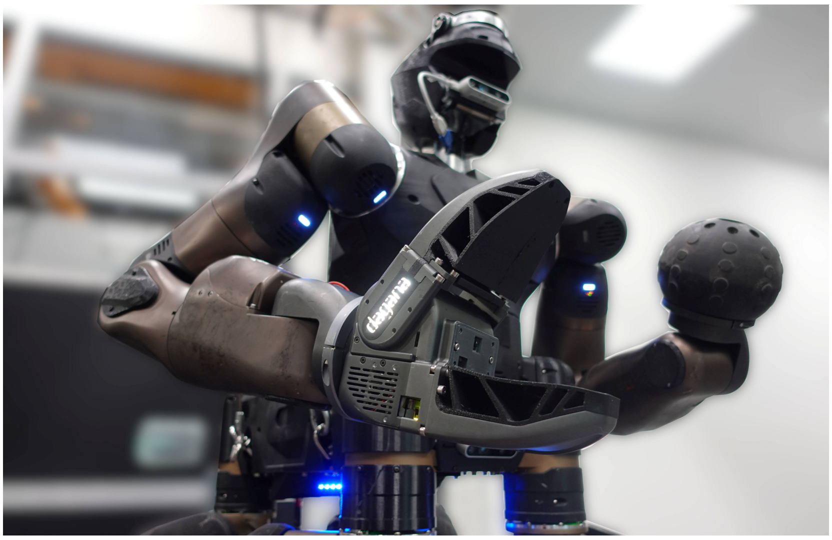

Figure 4.16: The DAGANA gripper on the IIT CENTAURO humanoid robot [43]. *Reproduced with permission from IEEE. First published in* [125]. © 2024 IEEE.

DAGANA uses one of these high-performance actuators, the Alberobotics Lime. As seen in the datasheet [176], this actuator has a mass of 0.87 kg, a length of 120 mm and a diameter of 82 mm. It features a continuous torque of approximately 10 Nm and a peak torque of 16.5 Nm. Considering a distance between the axis of the actuator and the tip of the grasping jaws of about 0.15 m, the peak pinching force at the tip (where the grasping force is lowest) is 110 N.

The torque-sensing capability enables precise force control during grasping, allowing regulation of impedance parameters (stiffness and damping), whereas the backdrivable low gearing (50 to 1), combined with the SEA approach, ensures a good impact resistance.

The actuator electronics used are custom and identical to those developed for CENTAURO, and are equipped with EtherCAT [158] communication. This enables seamless communication and control: DAGANA can be controlled as if it were just another of CENTAURO's joints.

The actuator output shaft is supported through an embedded crossed roller bearing.

Because the actuator's dimensions constrain the gripper's overall dimensions, the flange for mounting the actuator on the robot's structure was modified. The original flange (grey in Figure 4.17) is designed to provide a stable mounting through 6 screws and 2 pins assembled in the axial direction, requiring a higher actuator diameter to accommodate the mating surface. The new flange (red in Figure 4.17) is designed to provide tangential mounting, through 2 screws and 2 pins assembled in the tangential

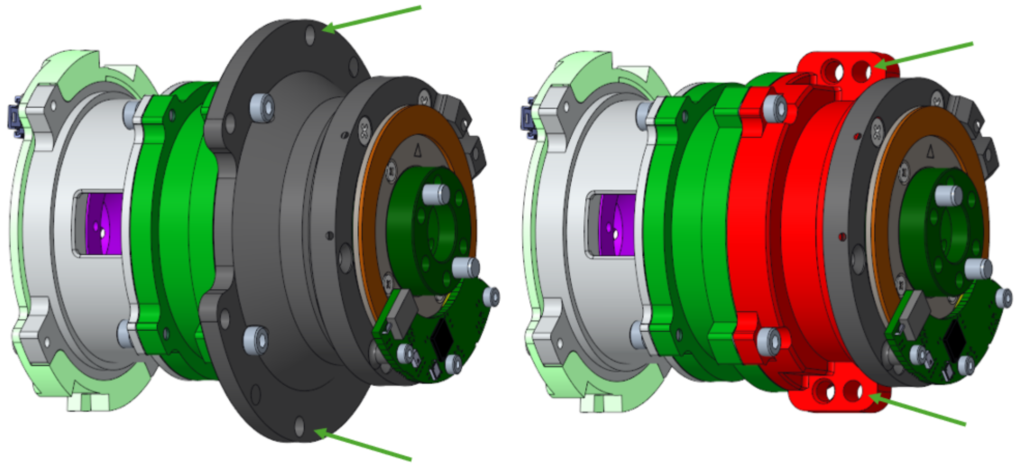

Figure 4.17: The Alberobotics Lime SEA. On the left, the original design with an overall diameter of 92 mm and axial fasteners, on the right, the customised design (new mounting flange in red) with an overall diameter of 70 mm and tangential fasteners. The green arrows indicate the holes for the fasteners.

direction. Furthermore, the lower-diameter cylindrical surface on the red flange and its axial steps have tight manufacturing tolerances. This allows creating a shape constraint wherever the two-screw mounting is deemed too weak for the specific application.

4.2.5 Modular mechatronic design

DAGANA is designed using a modular approach, which encourages the independent development of its elements and simplifies task-driven physical reconfiguration of its hardware. The 3 functional modules are connected with threaded fasteners and locating pins.

As shown in Figure 4.18, the following modules can be identified:

1. **Actuation module**
   Consisting of the main body of the gripper, it includes the actuator, its electronics and cooling system. It provides physical protection to these components through a cell design.

2. **Grasping module**
   This module consists of the grasping pads or jaws. They are fixed on the actuation module's interfaces and can be replaced easily according to the task at hand.

3. **Sensing module**

The sensing module contains the exteroceptive sensors. It is housed inside the main module, and its sensors are exposed inside the palm of the grasping module.

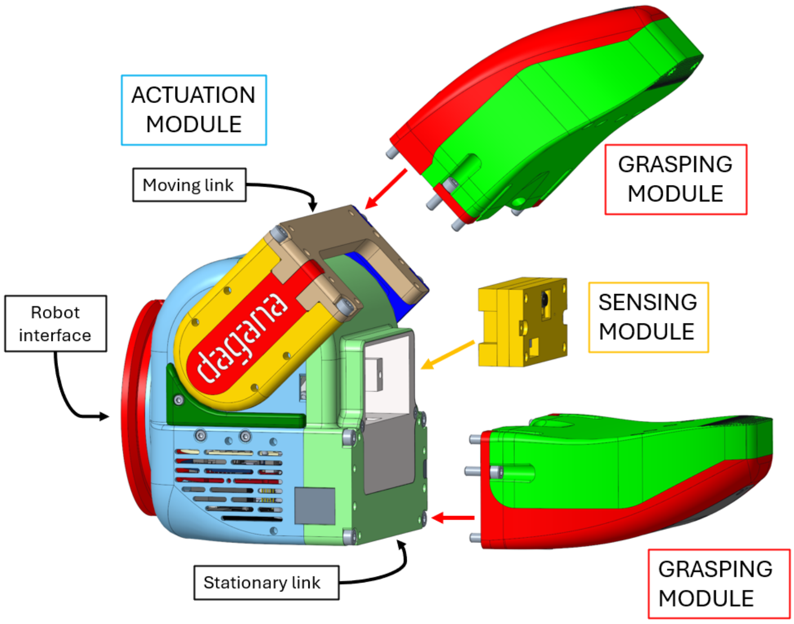

Figure 4.18: The modules of the DAGANA gripper.

The combined weight of the actuation and sensing modules is 1.5 kg, while the grasping jaws weigh 0.35 kg each, giving a total weight, in the standard configuration represented in Figure 4.18, of 2.2 kg.

Actuation module

The design of the main body of the DAGANA gripper follows the cell approach, with the actuator suspended inside a lightweight aluminium AL 7075-T6 cell structure identified in Figure 4.18 as the stationary link. The structure also creates a protective box for the actuator's power and communication electronics. Furthermore, it houses the sensing module, exposing its sensors to the palm of the gripper. This approach provides mechanical and ingress protection to the delicate actuation and sensing components.

A fan-forced airflow from the sides of the cell delivers cooling air through the actuator body and its electronics (see Figure 4.19). Thanks to the possibility of adding dust filters on the generously dimensioned air gratings on the sides of the cell, the cooling system can be made dust-proof.

The actuator is controlled through its custom-developed electronics. Nevertheless, to add flexibility to the design, an integration with commercial electronics is considered.

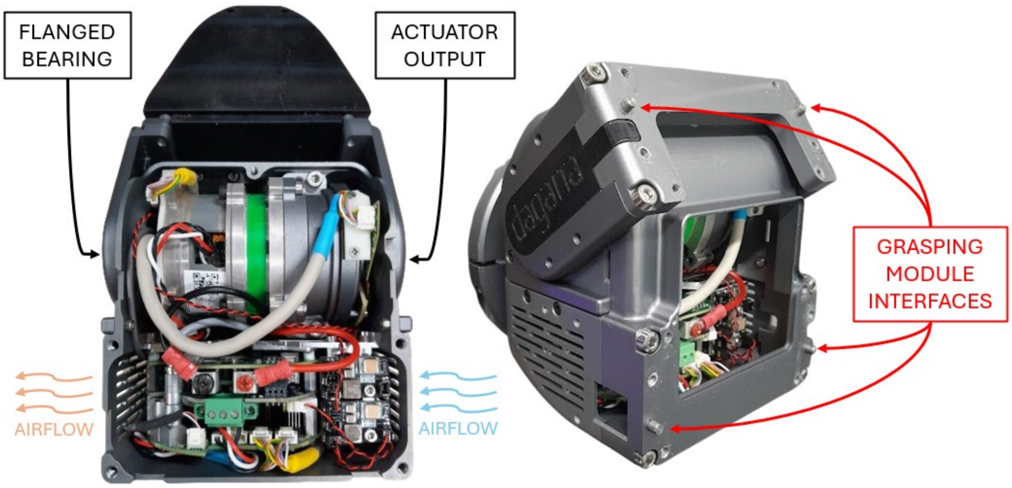

Figure 4.19: Left: a view inside the DAGANA's actuation module. A generous airflow, provided by a fan (not visible in the picture), cools the compactly assembled custom electronics. Right: the interfaces of the actuation module (pins and threaded holes), used to assemble the grasping modules. The aperture on the palm identifies the space reserved for the sensing module. *Reproduced with permission from IEEE. First published in* [125]. © 2024 IEEE.

As visible in Figure 4.20, the commercial Synapticon SOMANET Circulo 9 [168] electronics, appropriate to replace the original system, fit in the cell, and their installation only requires the replacement of the electronics mounting plate (in fuchsia on the left and violet on the right of Figure 4.20). From Figure 4.20, the compact assembly of the fan and the Direct Current - to - Direct Current (DC-to-DC) converters dedicated to the power supply of the sensing module can be seen.

A conical clamp-based electromechanical interface (red, on the left in Figure 4.18, visible in Figure 4.21) enables fast mounting of the gripper to the robot's wrist. It can be replaced to adapt the gripper to another robot flange type without modifying the actuation module's main structure.

The actuator is mounted via the developed tangential mounting flange (shown in Figure 4.17). The assembled actuator is visible in Figure 4.19, and its output shaft is sealed with a radial shaft seal of nitrile rubber that sits on the cell's structure. It prevents dust and particles from entering the actuator output link's area, which houses the output encoder, and is highlighted in Figure 4.22.

On the actuator output shaft, one arm of the moving link (blue in Figure 4.18) is assembled. As seen in Figure 4.22, the actuator features a four-point contact ball bearing, the SKF Kaydon KAA15XL0 [177], which ensures resistance to moderate moment

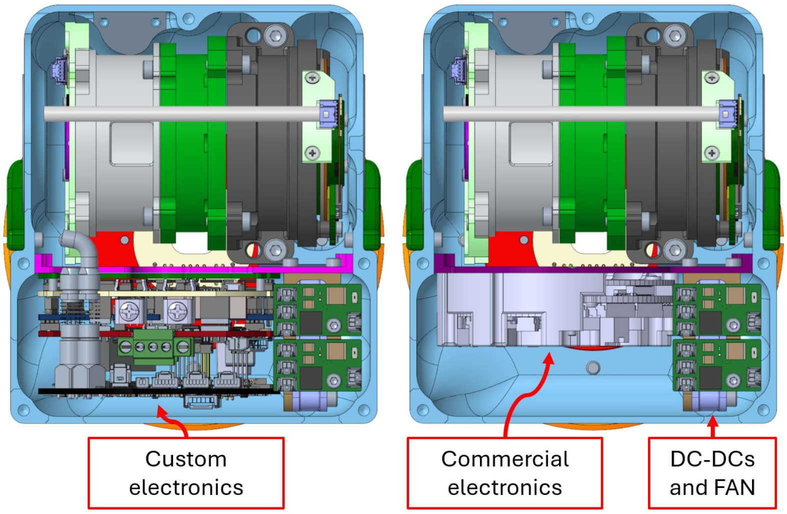

Figure 4.20: DAGANA's actuation module shown in two electronics configurations. On the left, the custom-developed boards. On the right, a commercial alternative, the Synapticon SOMANET Circulo 9 [168]. The DC-to-DC adapters and the fan remain unchanged in the two configurations.

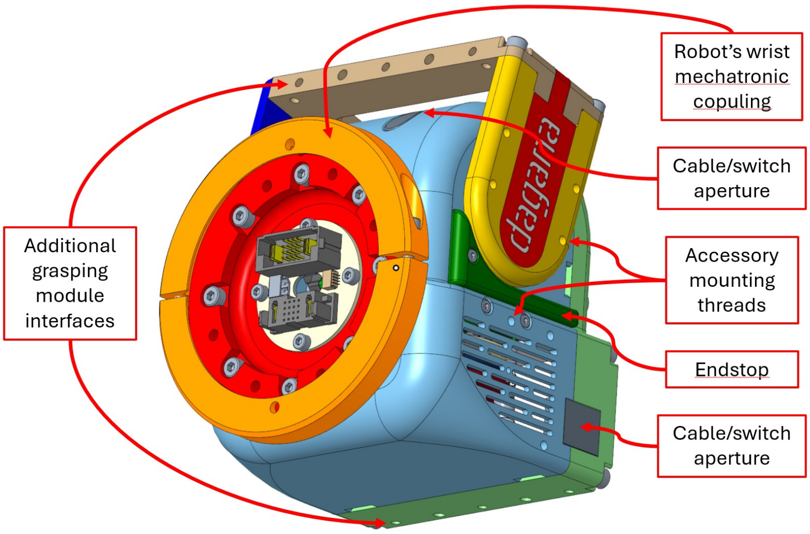

Figure 4.21: Details on the mechatronic coupling of DAGANA, the additional grasping module interfaces, and the features for mounting accessories and the easily replaceable endstop.

loads. The other arm of the moving link (yellow in Figure 4.18) is mounted on a flanged bearing, the MISUMI FL6805ZZ [178], assembled so that the distance between the two bearings' outer surfaces is 82.5 mm.

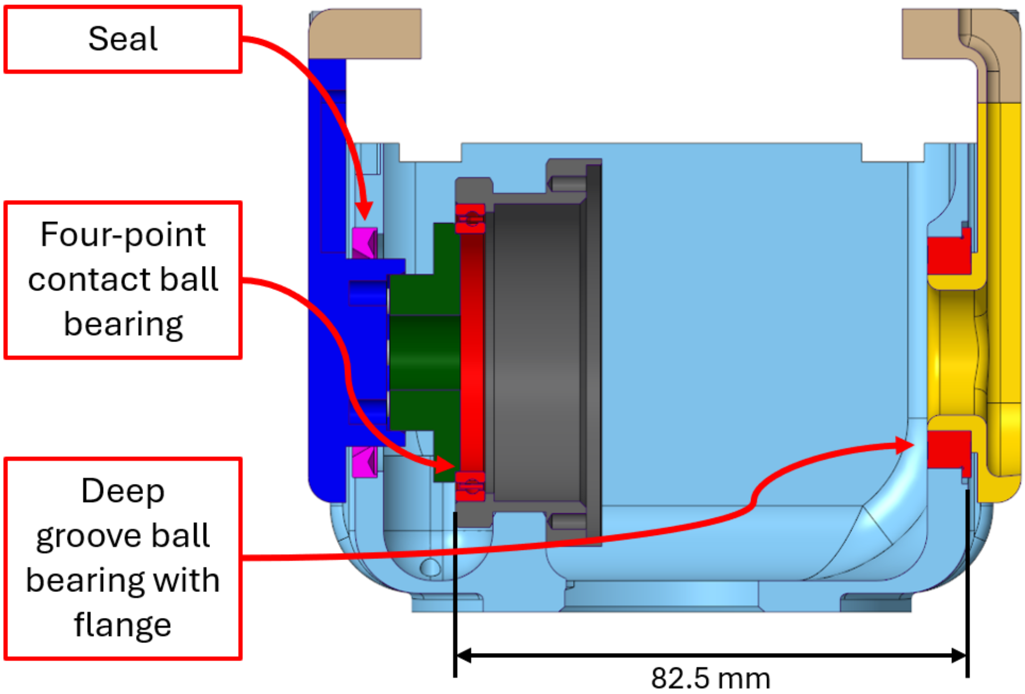

Figure 4.22: The bearing configuration of DAGANA. A four-point contact ball bearing is integrated into the actuator an additional deep groove ball bearing is fitted on the cell structure. A seal protects the output of the actuator, which houses the link encoder (not shown), from dust and unwanted particles. Note that, for visual simplicity, only a few of the actuator's components are shown.

This bearing arrangement allows higher protection from impacts and greater resistance to moment loads that what would be delivered by simply relying on the actuator's internal bearing, thereby satisfying the ruggedness requirement that makes the gripper effective for unstructured environments operation.

The basic static load rating of the actuator's four-point contact ball bearing is 2.71 kN. Considering the bearing's pitch diameter and a safety factor of 2, the maximum allowable moment on this bearing can be assumed to be approximately 30 Nm. By adding the flanged bearing, with a basic static load rating of 2.9 kN, the allowable maximum moment is determined by the admissible radial force on the bearings and their distance (which, considering the distance between the midplanes of the bearings, is approximately 76.5 mm). The maximum allowable radial force is constrained by the actuator's bearing (since its basic static load rating is lower than that of the flanged bearing). Using a safety factor of 2, the bearing configuration can be estimated to withstand moment loads up to approximately 100 Nm, which can be generated by a load of 667 N at the tip of the standard jaws used on DAGANA. Furthermore, the combination of the two bearings ensures that allowable radial loads are significantly increased. Thanks to the flange of the deep groove ball bearing, axial loads acting towards the opposite side of the actuator's output are supported by the flanged bearing, further protecting the actuator's bearing.

The integration of a second bearing on the DAGANA's moving link is performed though a specifically devised tolerancing and assembly strategy, with the aim of eliminating axial play between the moving link's arms and preventing overconstraining of the actuation system. Furthermore, this assembly strategy ensures that the actuator's bearing and the flanged bearing operate in tandem, delivering the desired impact protection and load capability. Figure 4.23 presents the assembly strategy. The actuator arm (blue) is locked on the actuator, and the bearing arm (yellow) is press-fitted inside the bearing previously installed on the cell structure. Then, the output faceplate is installed. Its alignment is ensured by the precisely machined slots and bosses, which allow small adjustments to compensate for inconsistencies in the axial runout of the flanged bearing and the actuator's output (motion shown on the left of Figure 4.23) and permit to minimise axial play between the arms (motion shown on the right of Figure 4.23). Oversized holes are used to lock with screws the output faceplate in the final position.

The moving link's range of motion is limited by two removable endstops (dark green in Figures 4.18 and 4.21), which can be customised to a lower angle of movement if a specific grasping module requires it.

The interface from the actuation module to the grasping module is visible in Figure 4.19. It consists of pins and threaded holes, and it is the same for the moving link and the stationary link. Additionally, on the bottom of the stationary link and on the top of the moving link, a set of threaded holes and pins is available for alternative mounting strategies of the grasping modules. These interfaces are visible in Figure 4.21, along with the threads and openings dedicated to mounting accessories, switches, or to be used as exits for wires.

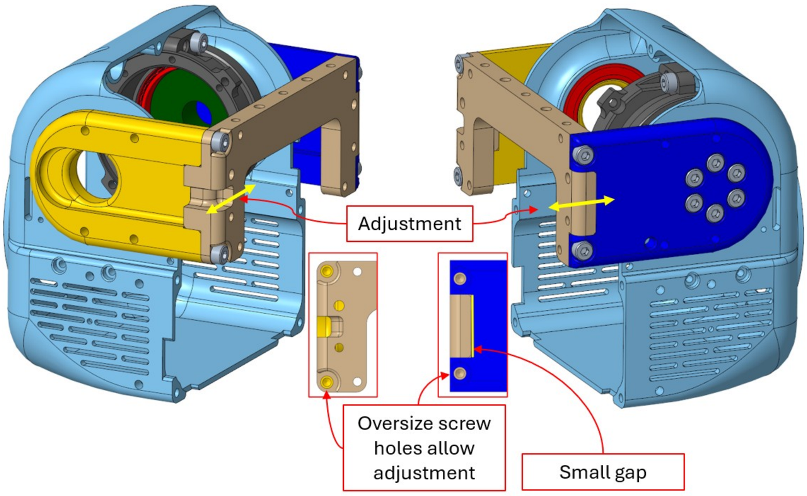

Figure 4.23: The moving link's assembly strategy, which aims to eliminate axial play between the link's arms and avoid overconstraining of the actuator's bearing. During assembly, the output faceplate of the moving link (in light brown) slides into the adjustment slots in the direction shown by the yellow arrows and is locked in position by tightening the screws that engage in the oversize holes. Note that, for visual simplicity, only a few of the actuator's components are shown.

Grasping modules

The grasping module enables DAGANA to perform the high-force gripping task. Two types of grasping modules are developed: (i) a generic set of grasping jaws, which can be satisfactory in most high-force applications, and (ii) task-specific grasping jaws, which increase the gripper's dexterity with objects of irregular shape (enabling enveloping or adapting to the grasped surface).

1. **Standard grasping jaws**

   The standard grasping module, developed as a set of generic grasping pads for the DAGANA gripper, consists of an aluminium AL 7075-T6 jaw structure complemented by rubber pads. The depth of the grasping pads is 110 mm, and the distance of the tip of the pad from the actuator's axis is approximately 0.15 m. Here, when the actuator is at peak torque of 16.5 Nm, DAGANA delivers a pinching force of 110 N.

   To ensure that this module can withstand not only the grasping forces, but also the loads related to impacts or derived from pushing objects around, a FEM validation is performed, as shown in Figure 4.24.

   Multiple rubber grasping pads are developed for these standard grasping jaws,

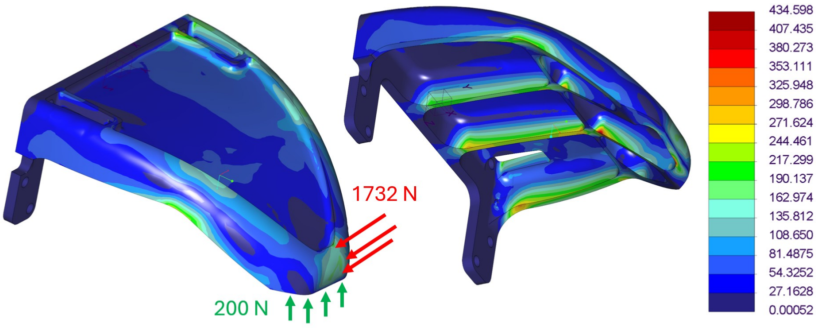

Figure 4.24: FEM validation of the standard grasping module's jaw structure. The loads considered are: a 200 N pinching force (equivalent to the maximum pinching force with a 1.8 safety factor) and a 1.7 kN pushing force (equivalent to the weight of the CENTAURO robot with a 1.8 safety factor).

Figure 4.25: Three different grasping modules developed for the DAGANA gripper. On the left, the standard jaws, in the centre, jaws for manipulating planar formwork, and on the right, jaws for grasping tubes. *Reproduced with permission from IEEE. First published in* [125].

adapting their rigidity and shape according to the desired task. Highly deformable pads are presented in Figures 4.15 and 4.16, while more stiff pads are used for the experiments presented in 5.2.2 and are visible in Figures 4.25 and 5.14. These pads are manufactured with Fused Filament Fabrication (FFF) of Thermoplastic Polyurethane (TPU) rubber, enabling rapid development of task-customised pads.

2. **Task-specific grasping jaws**
   As seen in Figure 4.25, additional grasping modules are designed. These modules enable DAGANA to grasp objects commonly found on construction sites, promoting the on-site deployment of the robotic platform. The first set of construction jaws (in the middle of the figure) is appropriate for grasping flat objects, such as planar concrete formwork. The second set (on the right of the figure) is appropriate for handling high-diameter pipes, such as large-diameter drainage pipes.

Sensing modules

Two different sensing modules are developed for the DAGANA gripper, both satisfying the requirements of being equipped with a RGB camera and a distance sensor. They are based on different processing units: (i) Arduino Nicla Vision [179] and (ii) Raspberry Pi Zero 2 W [180]. They both fit in the gripper's palm, and their sensor positions are optimised to exploit the maximum available Field of View (FoV).

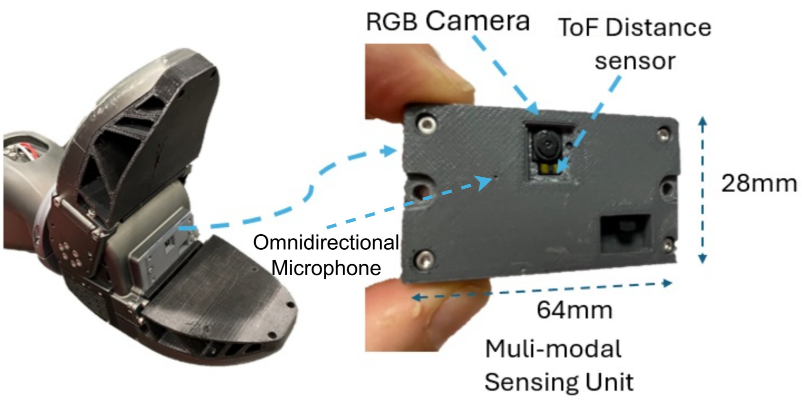

Figure 4.26: The battery-powered sensing module based on the Arduino Nicla Vision [179]. It includes a 6-axis IMU, a microphone, a 2 MP RGB camera, and a ToF distance sensor. The module, which can be easily removed from the palm for development, communicates via Wi-Fi and is independent from the robot's joint power supply. *Reproduced with permission from IEEE. First published in* [125]. © 2024 IEEE.

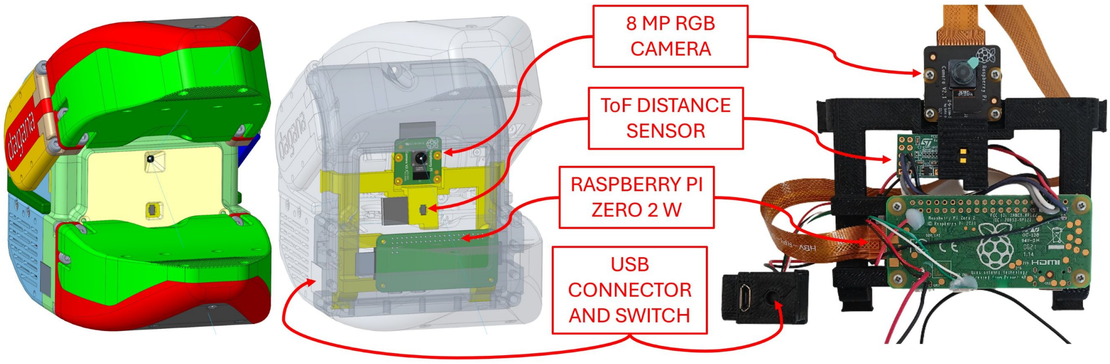

Figure 4.27: The sensing module based on the Raspberry Pi Zero 2 W [180]. It features the 8 MP RGB camera Raspberry Pi Camera V2.1 [181] and the ST Microelectronics VL53L1X-SATEL [182] ToF distance sensor. The micro-USB connector and the reset switch, connected to the SBC is assembled on the side of the stationary link.

1. **Module based on Arduino Nicla Vision**
   The module based on the Arduino Nicla Vision is a compact, self-powered sensing system. It is shown in Figure 4.26. Its customised box has been designed to include a high-capacity lithium battery, the Wi-Fi antenna and the sensor, with a switch to cut power when not needed. Its embedded camera's resolution is 2 MP, which is appropriate for high-speed image streaming, and its ToF distance sensor is accurate over a range of a few millimetres to 4 m. Additionally, it includes a 6-axis IMU sensor and a microphone.

   Thanks to an embedded Battery Management System (BMS), the battery can be recharged when the sensing unit is connected to the actuator's power supply (through the DC-to-DC converters seen in Figure 4.20). The fact that the sensor is battery-powered allows wireless communication to continue after the robot's joint is shut down, ensuring a more stable connection to the robot's network.

   The signals from the Arduino's sensors are streamed via User Datagram Protocol (UDP) to the robot's wireless network. They are then processed by a Personal Computer (PC) running the Robot Operating System (ROS) middleware [126], and the sensor information is made available as ROS topics dedicated to each sensor.

2. **Module based on Raspberry Pi Zero 2 W**
   The module based on the Raspberry Pi Zero 2 W is a powerful, intelligent sensing system. It is shown in Figure 4.27. Its design relies on the integration of commercial sensors: the 8 MP RGB camera, the Raspberry Pi Camera V2.1 [181], and

the ST Microelectronics VL53L1X-SATEL [182] ToF distance sensor.

The Raspberry Pi SBC directly processes the data stream from these sensors. It runs Ubuntu Linux [183] and ROS [126], directly streaming on the network the topics related to the sensor's data.

Since the module lacks a backup power source and relies on the robot's joint power supply, a reboot of the SBC is required whenever the joint is reset.

Compared to the module based on Arduino Nicla Vision, the module based on the Raspberry Pi provides higher-quality camera information and allows higher-level software implementations. This edge-computing approach, in which sensor data is processed directly on the end-effector, is further explored (with a more computationally powerful SBC) on the Smart Drill end-effector. The developments are described in Section 4.3.6.

4.2.6 Perception-driven grasping pipeline

To complement the mechatronic design of the DAGANA gripper, a software pipeline which makes full use of the gripper's perception capabilities is developed. It allows the gripper to autonomously detect, reach, grasp, and hand over a target object to the user in response to a user's voice command.

Since the pipeline uses vocal commands, it is compatible only with the sensing module based on the Arduino Nicla Vision.

This perception-driven grasping pipeline, presented in Figure 4.28, consists of 6 steps.

1. **Pre-scan**

   The gripper is initialised in front of a table on which several target objects are placed. The microphone is active and detects vocal commands, which are processed by the offline speech recognition toolkit VOSK [184] on the PC of the robot.

2. **Scan**

   The gripper searches for the objects to grasp within its camera's FoV, while the robot moves the wrist to extend the camera's field of view to the whole table. When an object is detected, it is classified with a network based on YOLO [127].

   Meanwhile, the user gives a vocal command naming what object they want the robot to grasp. The vocal command is processed, and the search for the target

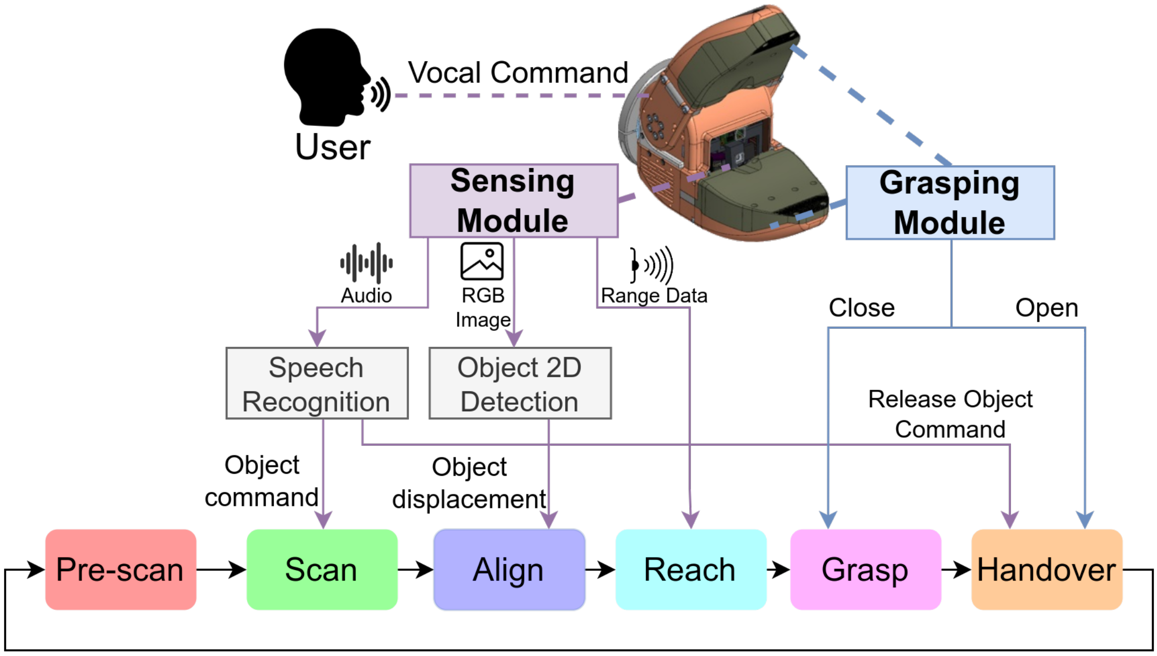

Figure 4.28: The perception-driven grasping pipeline which combines the gripper's sensing and actuation capabilities to reach, grasp and hand to the user a requested object. *Reproduced with permission from IEEE. First published in* [125]. © 2024 IEEE.

object begins. If one of the detected objects matches the user's request, the target is defined.

3. **Align**

   The centroid's horizontal and vertical coordinates, C_h and C_v, of the target object are obtained from the image by extracting the median point of the object's bounding box. Then, the horizontal and vertical angles (θ_h and θ_v) are computed with:

$$\theta_h = \frac{fov_h}{dim_h}(C_h - ref_h)$$
$$\theta_v = \frac{fov_v}{dim_v}(C_v - ref_v) \tag{4.5}$$

   where fov_h and fov_v are the FoVs of the camera, dim_h and dim_v are the dimensions of the image, ref_h and ref_v are the reference position that the object's centroid is desired to reach (as the camera is positioned in the centre of the palm of the gripper, $ref_h = \frac{dim_h}{2}$ and $ref_v = \frac{dim_v}{2}$).

The angles θ_h and θ_v are then used in a Cartesian Proportional - Derivative (PD) controller to align the gripper toward the target object. Considering that the x, y, and z reference axes follow the convention of x forward, y left, and z up and are centred on the robot's torso, and assuming that the gripper's approach is almost parallel to the x axis, the controller follows:

$$\begin{cases} x[i] = x[i-1] \\ y[i] = y[i-1] + K_p\theta_h[i] + K_d(\theta_h[i] - \theta_h[i-1]) \\ z[i] = z[i-1] + K_p\theta_v[i] + K_d(\theta_v[i] - \theta_v[i-1]) \end{cases} \tag{4.6}$$

4. **Reach**
   Once aligned, the ToF sensor data is used to produce a rough estimate of the object's three-dimensional (3D) position, and the gripper is moved towards the target.

5. **Grasp**
   When the target is in front of the gripper's palm, assuming that the orientation of the object is known or irrelevant for a successful grasping, the gripper is closed at a pre-set grasping torque, and the object is grasped.

6. **Handover**
   Then, the object is lifted from the table. When the user is ready to grab the object from the robot's gripper, they send the vocal command, and the gripper opens. The robot then goes back to the pre-scan phase.

4.3 The Smart Drill power-drilling end-effector

This section describes the design of Smart Drill, an intelligent power-drilling end-effector. Its conceptual design is inspired by the problem described in Section 3.3, which helps to understand its objective and technical requirements.

Figure 4.29: The Smart Drill end-effector.

4.3.1 Objective

Smart Drill is a power-drilling end-effector for small robotic arms used in unstructured and collaborative environments to aid or replace human operators, while matching the versatility and ease of deployment of manual power drilling.

4.3.2 Requirements

From the analysis of the problem and the technical challenges presented in Section 3.3, and in particular in consideration of the technical challenges related to the integration on a low-payload robotic arm, Smart Drill satisfies the following technical requirements:

1. Power independence
2. Limited overall mass
3. Alignment of the drilling axis with the robotic wrist axis
4. Easily replaced mechanical coupling
5. Embedded sensing
6. Embedded computation unit
7. Drilling capability

Power independence

The end-effector is battery-powered (like a cordless power drill for human operators), so that no power connections need to be implemented between the robot and the end-effector. This simplifies the following aspects:

- Some robots (such as Istituto Italiano di Tecnologia (IIT) CENTAURO [43]) do not include a power line at the end-effector that is independent from the power line of the actuators of the arm. If the robot is set in safe mode (e.g. by pressing the emergency button) the power line is cut, resulting in a complete shutdown of the end-effector and its associated computation units
- the end-effector's installation of a robot does not require the matching of the voltage supply from that of the robotic arm to that of the end-effector itself, avoiding the installation of a dedicated Direct Current - to - Direct Current (DC-to-DC)
- the end-effector is decoupled from the robotic arm, so that no concern is to be given to any power limitation at the robotic arm's flange.

Limited overall mass

The total mass of the end-effector is kept below 2 kg, so that Smart Drill is also compatible with the smallest commercial robotic arms for unstructured environments (like the Universal Robots UR3e [160]), and the free payload can be used to exert drilling force (e.g. in an overhead drilling application).

Alignment of the drilling axis with the robotic wrist axis

The axis of revolution of the drilling bit is aligned with the axis of the end-effector flange of the robot, so that the axial force required to perform the drilling operation does not generate moments on the wrist of the robot. This not only allows the drilling operation to be executed by smaller robotic arms (which generally have more limited torque capability on the wrist joints), but also ensures higher machining precision, as the natural tendency to rotate the wrist joints under the machining load is prevented by keeping the load direction aligned with the centre of the wrist.

Easily replaced mechanical coupling

The mechanical coupling between the end-effector and the flange of the robot can be replaced easily with one of different specifications, so that Smart Drill can be adapted to a new robotic arm in a short reconfiguration time.

Embedded sensing

To facilitate the execution of alignment and pointing tasks during drilling, the end-effector is equipped with an Red Green Blue (RGB) camera and a Time-of-Flight (ToF) distance sensor. These sensors open various possibilities to enhance the drilling operation. Firstly, they enable the development of robust drilling algorithms that are not dependent on the specific sensors provided by the robotic platforms and can therefore be fully portable to other robots for unstructured environments. Furthermore, they facilitate the exploration of sensor-fusion strategies like the one described in Section 4.3.6, which permits the use of these sensors to align the end-effector perpendicularly to the target surface and to locate the target drilling point.

Embedded computation unit

The end-effector features an embedded computer for edge-computing data processing and mechatronics control of the device. This allows for direct interface and control of the end-effector and of its sensors from a high-level software interface (like Robot Operating System (ROS) [126]), and to implement autonomous tasks as described in Section 4.3.6.

Drilling capability

The motor, gearbox, and chuck of a power drill are essential for identifying its capabilities in terms of the tasks it can perform. Smart Drill is required to execute the operations that a generic cordless power drill can, matching the processes performed by a human operator in industry, light-weight construction, or carpentry.

Considering the constraint of low weight, the system aims to match the capabilities of small 12 V cordless drills (like the Bosch Professional GSR 12V-15 cordless drill/-driver [185], the Milwaukee Tool M12 FUEL 1/2" Drill/Driver [186] or the DEWALT 12V XR Brushless Sub-Compact Drill Driver [187]), which are capable of holes in a wide variety of materials, can hold drilling bits up to 10 mm shank diameter and can be mechanically configured to limit the maximum delivered torque and to set the rotation speed of the chuck as high or low.

4.3.3 Conceptual design

Smart Drill is conceptualised as a lightweight drilling end-effector. Its chuck is mounted in-axis with the end-effector flange. It is equipped with a battery that powers not only its drilling motor, but also its embedded computation unit. It features a camera and a distance sensor. It is interfaced with the robotic system via an easy-to-replace mechanical coupling and high-level software running on the embedded computer.

4.3.4 Components selection

The design of Smart Drill primarily focuses on integrating commercial components in order to achieve a compact and lightweight end-effector. Instead of implementing a custom actuator and chuck for the drilling operation, the adopted solution is to repurpose the motor, gearbox, and chuck of a commercial power drill, reverse-engineering its internal components. To drive the motor, the internal electronics of the commercial power drill are retrofitted in order to be interfaced with the embedded computer.

A similar approach is dedicated to the battery. Power-tool batteries are widespread, easily recharged and reliable. Furthermore, they often incorporate a basic Battery Management System (BMS) or at least a Protection Circuit Module (PCM), which simplifies integration. Therefore, a solution utilising the battery from the power tool is adopted, following an approach similar to that presented by Katz for the first version of the Mini Cheetah quadruped [45].

This section presents the commercial components selected for integration into Smart Drill, which are:

1. Motor, gearbox and chuck
2. Battery
3. Motor controller
4. Embedded computer
5. Interface electronics
6. Camera
7. Distance sensor
8. DC-to-DC converter, power switch and fuse

Of each component, a Computer-Aided Design (CAD) representation is procured or, whenever not available, is realised in order to facilitate the mechatronic design.

Motor, gearbox, chuck

Among the small commercial drilling tools, models with a 12 V battery have the most promising capabilities in terms of low weight.

Of the models on the market, the Bosch Professional GSR 12V-15 cordless drill/-driver [185], the Milwaukee Tool M12 FUEL 1/2" Drill/Driver [186] and the DEWALT 12V XR Brushless Sub-Compact Drill Driver [187] are considered. Of these, DEWALT reports a weight of 0.87 kg for the bare tool, while Milwaukee Tools does not specify the weight. Bosch Professional reports a total weight of 0.98 kg, including a 2 Ah 12 V battery. Therefore, the Bosch Professional GSR 12V-15 is selected for its low total weight. Its maximum torque is 30 Nm, while its maximum speed is 400 RPM in the lower gear and 1300 RPM in the higher gear. It can accept drill bits with a diameter up to 10 mm.

Upon disassembly of the Bosch Professional power tool, the motor, gearbox, and chuck are removed for repurposing on Smart Drill.

The assembly of these components in the power tool is performed without the use of fasteners. In fact, the simple clamshell design of the power tool casing/cover integrates features to position and fix these components correctly.

The maximum output speed of the gearbox is selected by moving a lever on the body of the gearbox.

Battery

Regarding the battery, the one included with the Bosch Professional GSR 12V-15 is selected, as it is acceptable for running the SBC and the motor. It is the Bosch Professional GBA 12V 2.0Ah battery. A minimal BMS is integrated into its case, so the battery can be used directly to power components other than the motor controller (provided sufficient overcurrent protection is included). Its cover snaps inside shapes integrated into the pistol-grip housing, where a proprietary male connector is located.

Motor controller

The proprietary motor controller Printed Circuit Board (PCB) is necessary to drive the brushed DC motor properly. Replacing this component with a commercial alternative, while possible, would not provide an advantage in terms of capabilities for Smart Drill, as most robotic drilling operations in industry are performed at constant speed. Furthermore, it would be a major reverse-engineering exercise, as the specifications of the motor are completely unknown. Additionally, the motor does not feature any speed sensor, and control through higher-end servo controller electronics (such as Synapticon SOMANET Circulo 9 [168]) would not be possible without the integration of other additional components. Therefore, the original motor controller is extracted to be reused on Smart Drill.

When a human operates the drill, electromechanical switches complement the motor controller to reverse the drilling direction, and a trigger (which actuates a potentiometer) modulates the drilling speed. As these features are not required at the moment, these components are not CAD modelled.

Embedded computer

The embedded computer is required to connect to the sensors, process their signals and interface with the motor control electronics. Furthermore, it requires communicating with the computer of the robotic platform on which the end-effector is installed. To accomplish this, a Single-Board Computer (SBC) module with General Purpose Input/Output (GPIO) connectors and a dedicated camera connector is ideal.

Among the commercial alternatives that satisfy these requirements, the Raspberry Pi 4 Model B [188] with 8 GB of Random-Access Memory (RAM) is selected for its wide availability, low energy consumption, and acceptable computational capacity.

Since the Raspberry Pi 4 Model B does not include a Real-Time Clock (RTC) module, an additional RTC module (the Adafruit PiRTC DS3231 [189]) is installed to ensure the synchronisation between the SBC and the other computer(s) of the complete robotic system.

Interface electronics

Drilling speed control is not seen as an essential requirement, as robotic drilling operations in industry are normally carried out at a constant drilling speed. Therefore, the electromechanical switches and the trigger that initiate and regulate the drilling operation in the Bosch power tool are replaced with a simple ON/OFF logic. The potentiometer on the drill trigger that regulates the drilling speed is therefore replaced with a simple relay board. The board is chosen to be compatible with 5 V signals from a generic GPIO interface. From the SUNFOUNDER catalogue, the model TS0010 HL25S is selected [190].

Camera

As illumination conditions in unstructured environments are unpredictable, among the natively supported camera modules for the Raspberry Pi, the Raspberry Pi Camera Module 2 NoIR [181] is chosen thanks to its extended capabilities in challenging lighting conditions.

In fact, the NoIR camera module offers all the benefits of the standard Raspberry Pi Camera Module 2, based on the Sony IMX219 8 Mega Pixel (MP) Complementary Metal Oxide Semiconductor (CMOS) sensor, but does not include an Infra Red (IR)-cut filter in the lenses. This allows the sensor to perform better in dim lighting conditions or when shiny materials are used, provided that the light source also emits near IR light (e.g. in case of natural sunlight). However, this limits the ability to correctly identify colours (useful in specific vision applications, such as colour-based segmentation). In these situations, the NoIR module can be easily replaced with the standard module, as their dimensions and software interfaces are identical.

Distance sensor

The distance sensor selected is the ST Microelectronics VL53L1X [191], a ToF sensor that is precise up to 4000 mm and, thanks to its implementation on the ST Microelectronics VL53L1X-SATEL [182] breakout board, can be interfaced directly with the SBC through the GPIO connector using the I^2C interface.

DC-to-DC converter, power switch and fuse

To power the SBC computer from the 12 V power source of the battery, a DC-to-DC converter capable of delivering up to 3 A at 5 V is required. The Traco Power TSR3-1250 [192] is selected for its compactness and for its ability to handle lower input voltages than the nominal 12 V, thereby compensating for battery discharge.

Since the original battery is used to power both the SBC and the original motor controller, a 30 A power switch (the APEM 631H/2TK [193]) is used to cut the battery power, together with a regular 30 A fuse protection on the motor controller line and a 5 A fuse for protection of the SBC power supply line (following the recommendations of the supplier of the power supply).

4.3.5 Mechanical integration

The mechanical integration of the components listed in Section 4.3.4 aims to rely on a simple, widely available manufacturing technology, to devise an easy assembly process, and to obtain a strong yet lightweight mechanical structure.

Figure 4.30: Smart Drill, partially disassembled. On the left, the two semi-shell structures of the frame. In the top-middle, the front cover. In the centre and bottom-middle, the couplings. On the right, the battery and its cover.

The selected manufacturing process is Fused Filament Fabrication (FFF) three-dimensional (3D) printing using the Acrylonitrile Butadiene Styrene (ABS) plastic. This process ensures low cost (for a small production batch) and fast manufacturing, so that the final design can be quickly fine-tuned and later modifications or customisations can be rapidly deployed.

The use of ABS plastic offers a compromise between low cost, strength, electrical insulation, and wide market availability.

A view of all the Smart Drill's components is presented in Figure 4.30.

Frame

The design is based on a double-clamshell framing structure, identified as the frame (shown in Figure 4.31). The two halves of the frame, once joined, lock in position the motor, the chuck, the gearbox, the distance sensor and the battery male connector. The motor, gearbox, chuck and the battery connector are shape-constrained by features specifically determined to match the original assembly process of the power tool, despite the different manufacturing technology (as the pistol-grip frame of the tool is injection-moulded, instead of FFF fabricated, some features cannot be exactly replicated). These three components also provide alignment for the two halves of the frame, which are then joined with M4 bolts. The gearbox is permanently set at the lower speed (400 RPM), as this drill bit speed generates lower cutting forces on the tool and is appropriate for most materials.

Furthermore, the frame includes shapes that allow installing and removing the battery from the back of the end-effector in the same way as it is originally done with the power tool, namely through snapping plastic handles.

The framing structure houses the motor controller, the camera, the interface electronics, the DC-to-DC converter, the SBC and the power switch. These components, identified in Figure 4.32, are mounted on the outer surface of the frame with self-threading screws for plastic. This arrangement simplifies the wiring of all the internal components, as the wires can be routed directly on the exterior of the framing.

Robot couplings

The frame of Smart Drill, on its back and behind the motor power connectors, presents a 60 mm diameter cylindrical flange. This flange is equipped with a generously sized keyway and four radial bolt holes, which encapsulate at their internal end four M4 nuts. The encapsulated nuts are preferred over brass inserts, which are more common

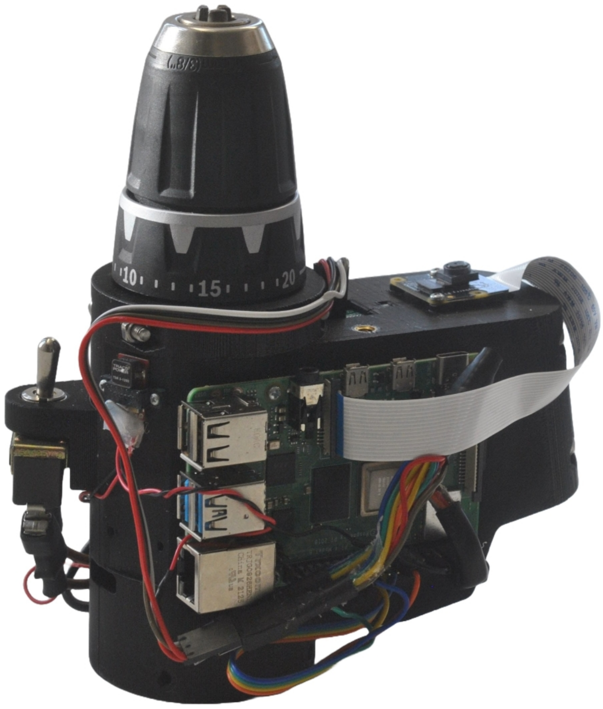

Figure 4.31: The frame of Smart Drill, housing all functional components.

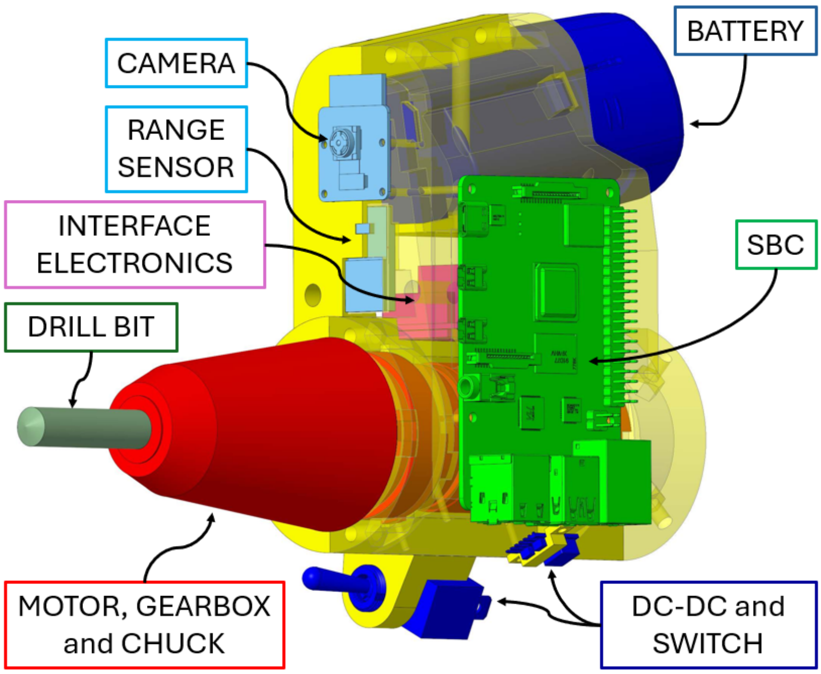

Figure 4.32: A CAD representation of the inside of Smart Drill, with its components labelled (the motor controller is not shown). *Reproduced with permission from IEEE. First published in* [128]. © 2024 IEEE.

on 3D-printed parts, for their shape-based retention and the strength of the material. Furthermore, this interface features a generously dimensioned keyway.

End-effector flanges of many of the widespread robots available on the market (e.g. Universal Robots [160] and Franka Robotics [161]) follow the method defined by the International Standardization Organization (ISO) standard 9409-1 [129], which requires screws to be fastened in the axial direction of the flange. As a consequence, end-effector mounting requires some sort of solution to access these axial screws during installation. The radial bolting method implemented with the flange of Smart Drill solves this problem. The mechanical coupling between Smart Drill and the robotic arm can, in fact, be installed on the robot in advance, inserting the axial screws if required. Then, Smart Drill is attached by using its flange and is secured with the radial bolts.

Furthermore, the use of radial bolts results in an axially compact fastening, thereby minimising the distance between the robot and the Smart Drill chuck. This lowers the overall end-effector inertia and keeps to the lowest possible the moments that can be generated by unexpected forces during operation.

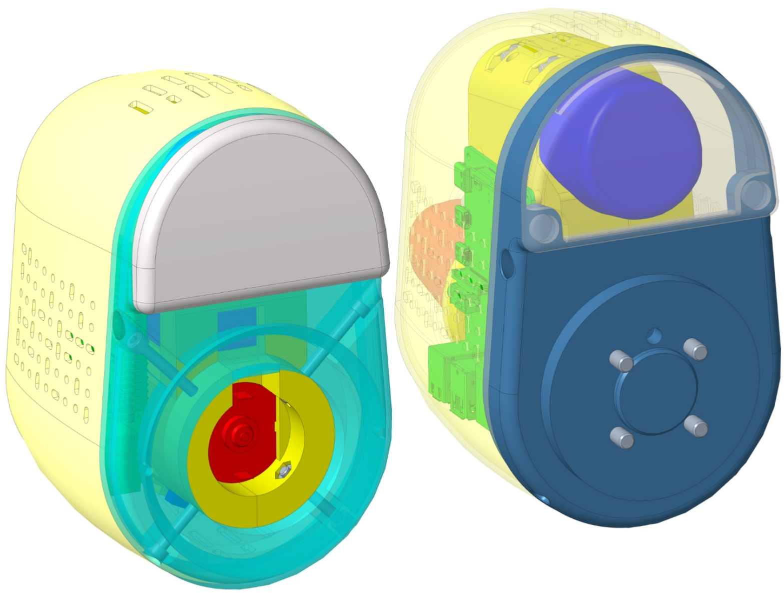

Figure 4.33: A CAD view of the Smart Drill's robot couplings. On the right, the coupling compliant with ISO standards. On the left, the coupling for the CENTAURO NEXUS humanoid, in a semi-transparent state to show the four radial bolts that connect the coupling to the frame.

In order to install Smart Drill on a different robotic arm, the only necessary step is to 3D print a new coupling, appropriate for the robot considered. As an example, two couplings were designed: one for the robot CENTAURO NEXUS [43], used to develop the experimental validation presented in Section 5.3, and one complying with the ISO standard used by the Universal Robots UR5 [160] and the Franka Research 3 [161]. The couplings are shown in Figure 4.33.

Cover

To protect the components and wiring installed on the outer surface of the frame and to offer a visually uniform shape for the finished end-effector, a three-piece cover is designed. Its middle part is integrated in the robot coupling, resulting in a compact use of space, as no axial length is wasted to fix the cover. From the front, an enveloping box is assembled on the middle part to provide protection to all external components. This box has ventilation apertures and shapes that guarantee no interference with the Field of View (FoV) of the sensors. On the back of the middle cover, above the end-effector coupling, a smaller cover is installed with magnetic locks. This small cover can easily be removed to access and replace the battery, which is slid into the frame from the back.

Total mass

The total mass of the design, in operating conditions (including a 10 mm drill bit mounted in the chuck), is 1.55 kg. This satisfies the requirements and allows Smart Drill to be used with small robotic arms of limited payload capability.

4.3.6 Software architecture

The software developed for Smart Drill can be differentiated into two levels: (i) the low-level software, dedicated to obtaining and abstracting sensor information and controlling the actuator, and (ii) the high-level software, which builds on the low-level software and the architecture of Smart Drill to implement a complete drilling task that is relevant for aiding or replacing the human operator while drilling in unstructured environments.

Low-level software

To address the tasks of sensor data processing and mechatronics control of Smart Drill, a set of software tools running on the embedded SBC is developed. The presence of the SBC enables wired and Wi-Fi network communication between the computers of the robotic system and Smart Drill, avoiding the need to develop and maintain lower-level interfaces.

These higher-level tools are developed using the Robot Operating System (ROS) middleware [126], running on the Ubuntu Linux [183] operating system installed on the SBC and on the other computers in the system.

The low-level ROS software development consists of three ROS nodes.

1. **Motor control node**
   To control the activation and deactivation of the motor, a dedicated ROS node is written. It initialises the GPIO pin of the SBC connected to the interface electronics and sets its status so that the motor is switched off. Then it creates a ROS service that, upon call, allows updating the status of the GPIO pin to activate the relay on the interface electronics and start the motor of Smart Drill. To include a level of operational safety, the service implements a safety watchdog that, every second, verifies that the ROS node which requested the activation of the motor of Smart Drill is still active. If the node is unresponsive, it resets the state of the GPIO pin, switching the motor off.

2. **Camera node**
   To stream the image of the camera sensor, a ROS node developed by the community (the `raspicam_node` [194]) is integrated in the project. It allows streaming the image of the camera on a dedicated ROS topic and exposes the camera parameters for seamless acquisition configuration.

3. **Distance sensor node**
   Likewise, a ROS node developed by the community (the `vl53l1x_ros` [195]) is also used to read the signal from the ToF distance sensor. It provides a fast sensor reading message on a dedicated ROS topic, and it exposes the configuration parameters to fine-tune the sensor settings.

Thanks to this low-level abstraction layer obtained with the ROS nodes, porting the Smart Drill to a different system is extremely easy (the only requirement being the presence of the ROS middleware). This simplicity of adaptation complements the simplicity with which Smart Drill can be reconfigured to work with robots having different end-effector flanges, seen in Section 4.3.5.

Semi-autonomous power-drilling pipeline

To complement the mechatronic design of Smart Drill, a software pipeline deployable in real-world power-drilling applications is developed. It allows a semi-autonomous drilling operation in an unstructured environment. Thanks to the availability of consistent sensor data even when the robotic platform changes (thanks to the embedded sensors), the full task execution is completely robot-agnostic.

Considering a configuration in which the robotic platform equipped with Smart Drill is brought in front of a surface on which a hole needs to be drilled over a pre-marked target point, this software enables Smart Drill to perform a semi-autonomous drilling operation that can be described as follows:

1. **Align the end-effector perpendicularly to the target surface**
   This task is executed by commanding the robot to perform with its end-effector a circular sweeping motion in front of the target surface while simultaneously acquiring the distances read by the distance sensor. The 3D points measured on the surface are registered in the reference system of the robot. Then, a plane (of general form equation $ax + by + cz + d = 0$) is fitted on these points by combining the standard Perspective-n-Point (PnP), the RANdom SAmple Consensus (RANSAC) algorithm, and determining the normal to the surface (identified by the normal vector components a, b, and c from the plane equation). Lastly, the end-effector of the robot is commanded to assume an orientation perpendicular to the surface.

2. **Acquire the target drilling point**
   Through a User Interface (UI) which displays the camera stream to the operator of the platform, the operator is required to select the desired drilling point on the image streamed by the camera. The two-dimensional (2D) image pixels $[u, v]^T$ are then converted into 3D points $[x, y, z]^T$ with the following formula:

$$\begin{bmatrix} x \\ y \\ z \end{bmatrix} = \begin{bmatrix} \frac{1}{f_x} & 0 & -\frac{p_x}{f_x} \\ 0 & \frac{1}{f_y} & -\frac{p_y}{f_y} \\ 0 & 0 & 1 \end{bmatrix} \begin{bmatrix} u \\ v \\ 1 \end{bmatrix} z \tag{4.7}$$

   where f_x, f_y, p_x and p_y are the camera intrinsic parameters (the focal lengths and principal points of the camera along x and y image axes), and the z coordinate of the 3D point represents the depth of the point with respect to the camera optical frame. It is estimated using the range sensor.

3. **Perform the drilling operation**
   This task is executed by commanding the robot to reach the target drilling point (keeping clear of the surface), start the motor, and perform a constant-velocity

trajectory to feed the drill bit into the surface, drilling up to the desired depth. The choice of a constant-velocity trajectory is justified by the fact that, in conventional and robotic Computer Numerical Control (CNC) machining operations, the feed speed is generally constant.

The code is based on ROS. Except for the UI interaction, which requires a Personal Computer (PC) with a screen and a mouse to be completed, the whole code runs on the SBC of Smart Drill.

Thanks to the combination of camera and distance sensor information, the system overcomes the limitations due to the monocular vision and the lack of a sensor that can provide direct 3D spatial information (such as a Red Green Blue - Depth (RGB-D) camera).

Chapter 5

Experimental results

This chapter presents the experiments performed with devices introduced in Chapter 4, validating the effectiveness of the designs with respect to the problems illustrated in Chapter 3.

The experiments regarding DAGANA (Section 5.2) and Smart Drill (Section 5.3) are conducted with physical prototypes built according to the design specifications. In contrast, Leon's physical prototype has not yet been manufactured. Only the physical prototype of one actuator has been obtained. Hence, Leon's validation (Section 5.1) relies on simulations and on bench-testing the actuator.

5.1 Validation of the design of the Leon quadruped

At the time of writing, the first prototype of Leon's customised actuator (see Section 4.1.4) has been obtained, assembled and tested. The detailed Computer Aided Engineering (CAE) design of the full robot has been completed to a manufacturing-ready level, as presented in Section 4.1. Yet the complete physical prototype of Leon is still to be manufactured.

Therefore, the design is validated by:

- assessing the robot's payload and agility performance according to the final design specifications

- confirming the structural soundness of the design through Finite Element Method (FEM) simulations of its most critical components, thereby ensuring that the final specifications of the robot (see Section 4.1.9) are realistic

- determining, through a dynamic simulation, the torques and speeds required from the actuators

- evaluating the actuator's performance on a test bench.

This validation was partially presented at the European Robotics Forum 2024 [120].

5.1.1 Payload capability

To assess the robot's capability to carry a payload indefinitely, the robot is presented in a moderately crouched stance with a clearance from the ground of 220 mm, as seen in Figure 5.1. In this condition, supposing an equal angle for the lower- and upper-legs links with respect to the horizontal of 36.2°, the joint in the least favourable position is the one actuating the lower leg.

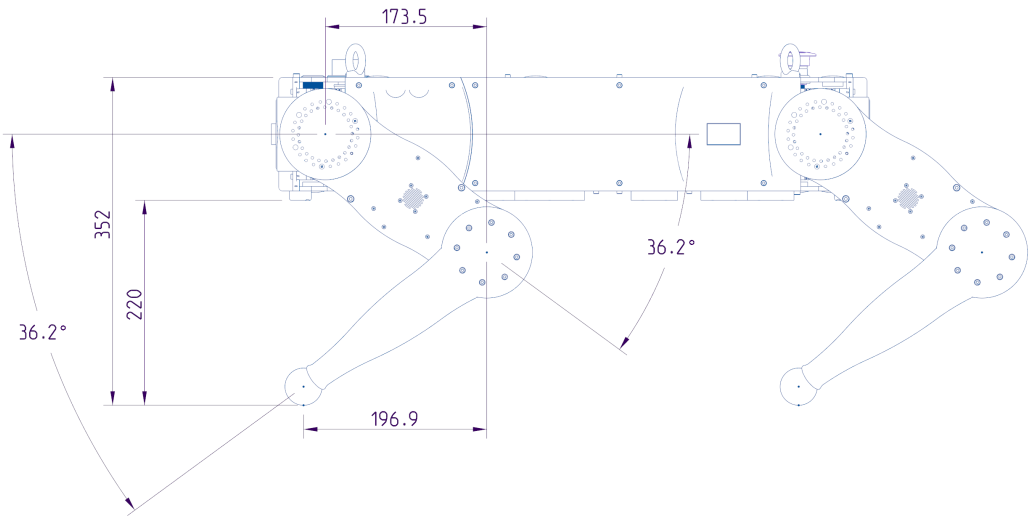

Figure 5.1: Technical drawing showing Leon in a crouched stance. The payload support is at 352 mm from the ground, while the clearance below the trunk is 220 mm.

The projected length of this link on the ground in these conditions is $l_{\text{lower leg, projected}} = 0.1969$ m, as reported in Figure 5.1. Since the payload is to be carried indefinitely, the continuous actuator torque of $\tau_{\text{continuous}} = 18$ Nm and the quadruped's mass without payload of $M_r = 27$ kg (from Table 4.6) are used to determine the payload carrying capacity with Equation 5.1.

$$
\begin{aligned}
M_{\text{payload,max}} &= \frac{N_{\text{legs}}\,\tau_{\text{continuous}}}{g\,l_{\text{lower leg, projected}}} - M_r \\
&= \frac{4 \times 18\ \text{Nm}}{9.81\ \text{N}\,\text{kg}^{-1} \times 0.1969\ \text{m}} - 27\ \text{kg} \\
&= 10.28\ \text{kg} \approx 10\ \text{kg}
\end{aligned} \tag{5.1}
$$

where $N_{\text{legs}} = 4$ is the number of legs that are supporting the payload continuously at the same time, $l_{\text{lower leg, projected}} = 0.1969$ m and $g = 9.81$ N kg^{-1} is the gravity of Earth.

Therefore, the maximum payload capacity of Leon in static conditions can be assumed to be about 10 kg.

5.1.2 Agility assessment

As seen in Section 4.1.2, the tendency of a robot to exhibit agile motion capability can be estimated with the force-to-bodyweight (FBW) ratio. Combining Equations 4.1 and 4.3, considering the lower leg link minimally extended (which is the least favourable condition, due to the link's length of $l_{\text{lower leg}} = 264$ mm), the fact that all the actuators are identical, the actuator's peak torque of $\tau_{\text{peak}} = 48$ Nm, and approximating the weight of the robot with the standard payload to $g\ M_r = 300$ N, the final FBW ratio of Leon is calculated in Equation 5.2.

$$
\text{FBW} = \frac{F_z}{g\ M_r} = \frac{\frac{\tau_{\text{peak}}}{l_{\text{lower leg}}}}{g\ M_r} = \frac{\frac{48\ \text{Nm}}{0.264\ \text{m}}}{300\ \text{N}} = 0.61 \tag{5.2}
$$

5.1.3 FEM simulations

The mechanical structures that compose the trunk and the legs of Leon are designed in order to minimise their weight and maximise their mechanical rigidity, while performing their specific function. To validate the design, FEM simulations are run, using the final design as input.

The materials used in the simulations are:

- Aluminium AL 7075-T6 [167], which features an ultimate tensile strength of 572 MPa, a yield strength of 503 MPa and a Young's modulus of 71.7 GPa
- Polyamide (PA) 12 or Nylon 12 thermoplastic filament reinforced with chopped carbon fibre, 35% by weight [196]. This material, due to the Fused Filament

> Fabrication (FFF) process, is anisotropic. In the flat direction (the direction in which a layer is printed), it features an ultimate tensile strength of 83.5 MPa and a Young's modulus of 9.46 GPa. In the upright direction (the direction in which printed layers are stacked together), it features an ultimate tensile strength of 32.7 MPa and a Young's modulus of 3 GPa.

The robot is subject to static and dynamic loads derived from locomotion, failures (e.g. the robot falling on the ground) and accidents during transportation. During the simulations, the mass of the robot is assumed to be 27 kg (see Section 4.1.9) plus a payload of 3 kg, for a total of 30 kg and a resulting weight approximated to 300 N.

The elements for which the design is more optimised for weight reduction are: (i) the framing structure of the trunk, (ii) the leg's hip link and (iii) the lower leg link. Conversely, the upper leg link (which is the only other structural element in the design) is less optimised for weight reduction. Its structure is of the cell type, and its thickness and load-bearing surfaces are more generously dimensioned to provide ingress and impact protection to the lower and upper leg's actuators. Therefore simulation is not required to validate its structural validity.

Trunk's frame

The trunk's structural rigidity is ensured by a frame structure, described in detail in Section 4.1.6. It consists of multiple components of Aluminium AL 7075-T6.

To validate the design under worst-case conditions, the weight of the robot (300 N, see above) is applied to one of the four hip-roll actuators (back-right), while the opposite hip-roll actuator (front-left) is fully constrained. The simulation is shown in Figure 5.2.

Leg's hip link

The hip link's design (presented in Section 4.1.5 and connecting the hip-roll and hip-pitch actuators) is FEM-validated, given its peculiar shape optimised for weight reduction. It consists of one component of Aluminium AL 7075-T6.

Considering a worst-case scenario, the robot's weight (300 N, see above) and the actuator's maximum torque (48 Nm) are applied to one of the link's flanges, while the other flange is fully constrained. The simulation is shown in Figure 5.3.

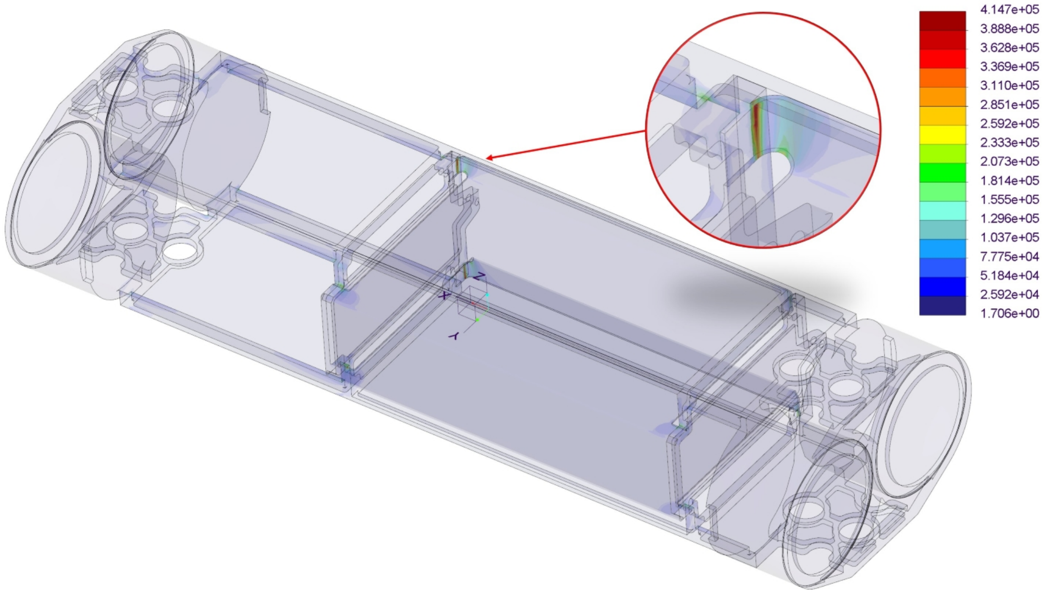

Figure 5.2: The FEM simulation on the trunk's frame. Von Mises stress in MPa. The frame structure is transparent, allowing visualisation of the maximum stress of 415 MPa, which is located in the battery box's sheet-metal structure.

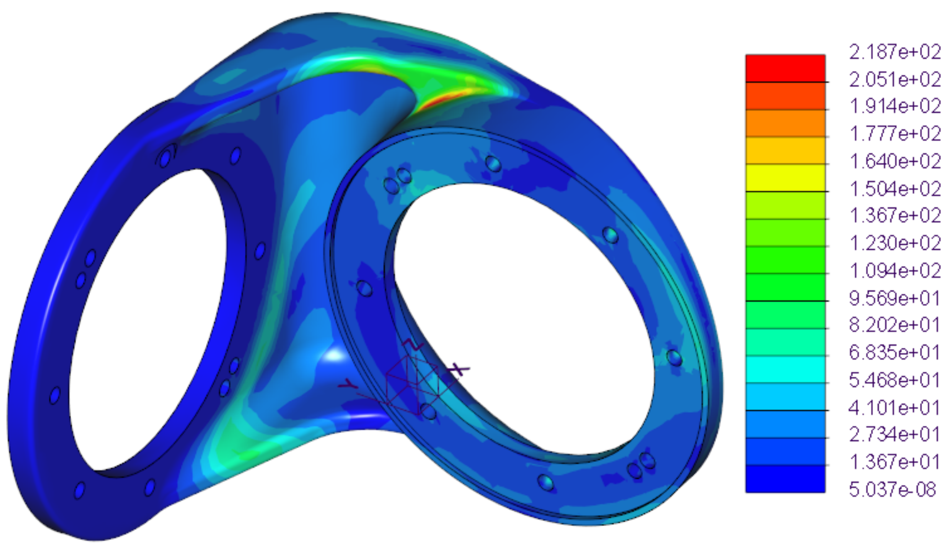

Figure 5.3: The FEM simulation on the hip link. Von Mises stress in MPa. The maximum stress is 219 MPa. *Reproduced with permission from Springer Nature. First published in Springer Proceedings in Advanced Robotics, vol 32, pp 58–63, 2025 by Springer Nature* [120].

Lower leg link

The lower leg link, presented in Section 4.1.5, is fabricated with FFF by stacking 3D-printed layers in the direction perpendicular to the actuator's flange.

To validate its structural properties, the scenario consists of the foot locked while the actuator is delivering the maximum torque (48 Nm). The simulation is shown in Figure 5.4.

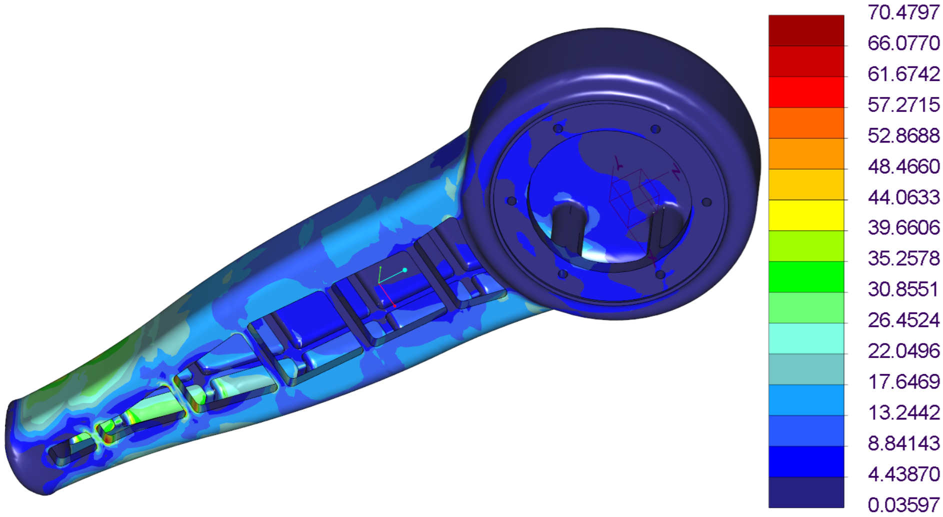

Figure 5.4: The FEM simulation on the lower leg link. Von Mises stress in MPa. The maximum stress is 70.5 MPa. *Reproduced with permission from Springer Nature. First published in Springer Proceedings in Advanced Robotics, vol 32, pp 58–63, 2025 by Springer Nature* [120].

5.1.4 Locomotion simulation

Using the information provided by the detailed design presented in Section 4.1.9 and by Leon's Computer-Aided Design (CAD) model, a Unified Robot Description Format (URDF) representation of the quadruped is developed. A dynamics simulation environment based on Gazebo [197] is used, implementing a Model Predictive Control (MPC) method to generate the control commands applied to the quadruped robot during locomotion simulations.

Figure 5.5 presents RViz views of the robot. Coloured curves are used to illustrate the time evolution of the foot and trunk trajectories in Cartesian space. The figure presents three simulated conditions: standing up from the ground, trotting in place (zero forward velocity), and trotting at a speed of 1 m/s. The joint positions, velocities, and torques recorded during these three simulations are presented in Figure 5.6 for the

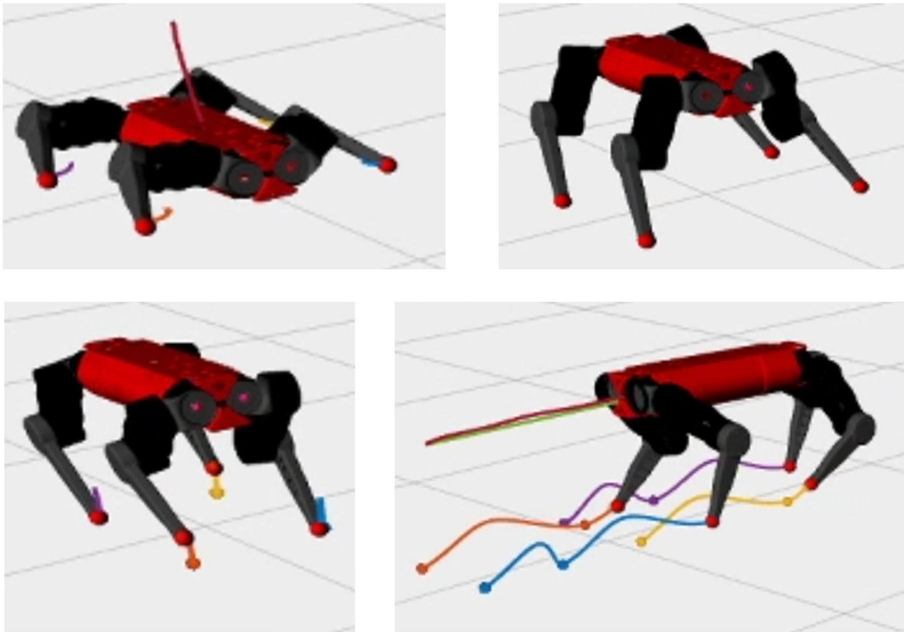

Figure 5.5: RViz views of Leon performing standing up from the ground (top), trotting in place (bottom left), and trotting with a forward speed of 1 m/s (bottom right). The coloured curves represent the Cartesian trajectories of the feet and trunk over time.

left-front leg and in Figure 5.7 for the left-hind leg. Given the symmetry of the gaits, only the left legs are presented.

The plots provide information on the required maximum torques and speeds to be reached by the customised actuator of Leon. A peak torque of 31.47 Nm is required to perform a trotting gait at a forward speed of 1 m/s, while the maximum speed reached is 7.26 rad/s.

5.1.5 Actuator characterisation

In order to determine the feasibility of the design, the actuator's rated data provided by the manufacturer the manufacturer [155] is used. Given the customisations and modifications required for the Commercial Off-The-Shelf (COTS) actuator to be integrated into Leon, one custom actuator was assembled and a dedicated test bench was developed.

The test bench relied on plastic and aluminium components that allowed to clamp the actuator to a sturdy bench (see Figure 5.8), as well as on a custom output link consisting of an aluminium profile rod mounted on a FFF-fabricated flange. 8 kg of gym weights could be mounted on the aluminium profile at an adjustable distance from

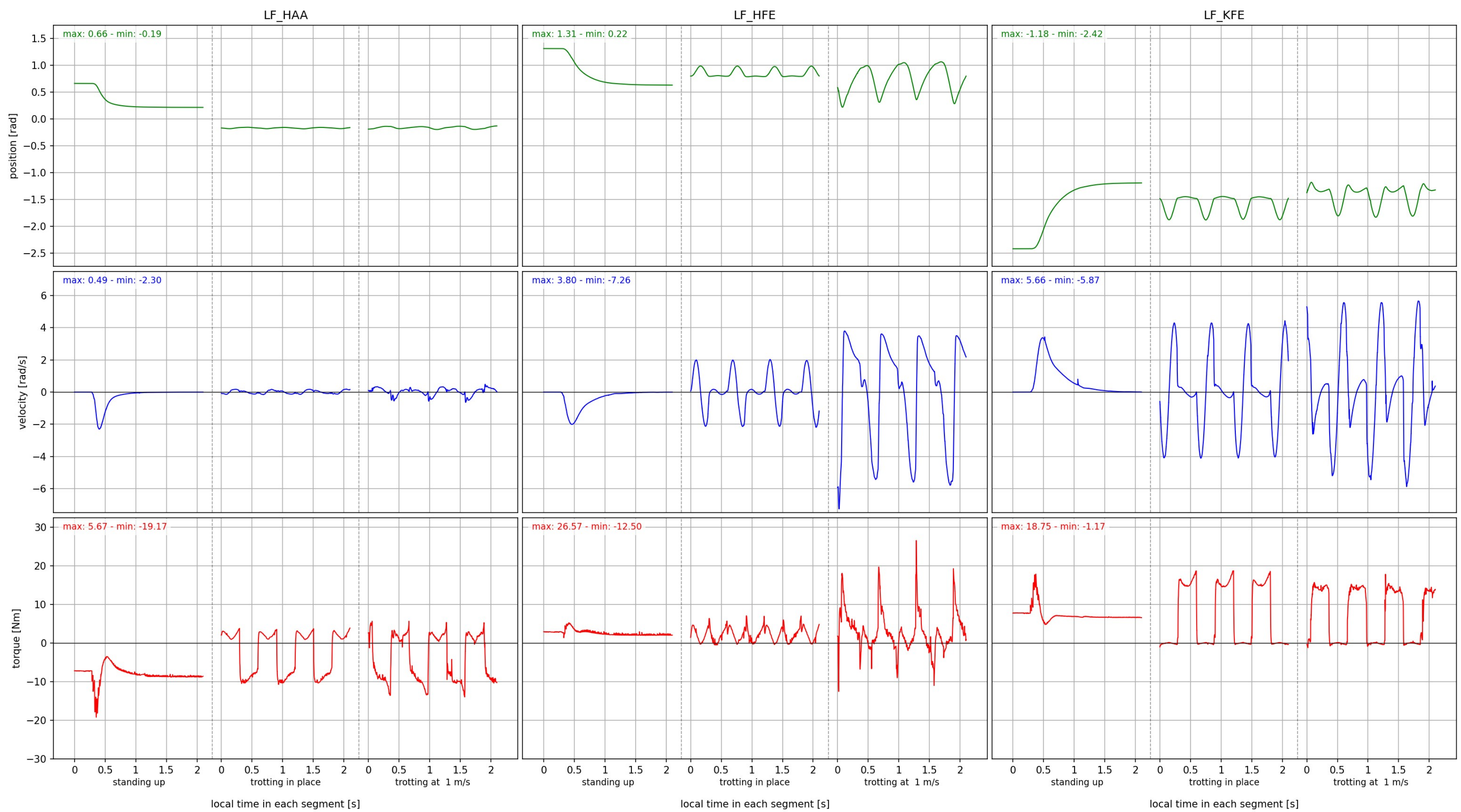

Figure 5.6: The left-front leg joint position, velocity, and torque computed in the locomotion simulation during standing up (left segment of each plot), trotting in place with zero forward velocity (centre segment), and trotting at 1 m/s (right segment). The three plots in the left column show the hip-roll actuator, the three plots in the centre column show the hip-pitch actuator, and the three plots in the right column show the knee-pitch actuator. The absolute maximum velocity and torque reached during the simulations are 7.26 rad/s and 26.57 Nm, respectively.

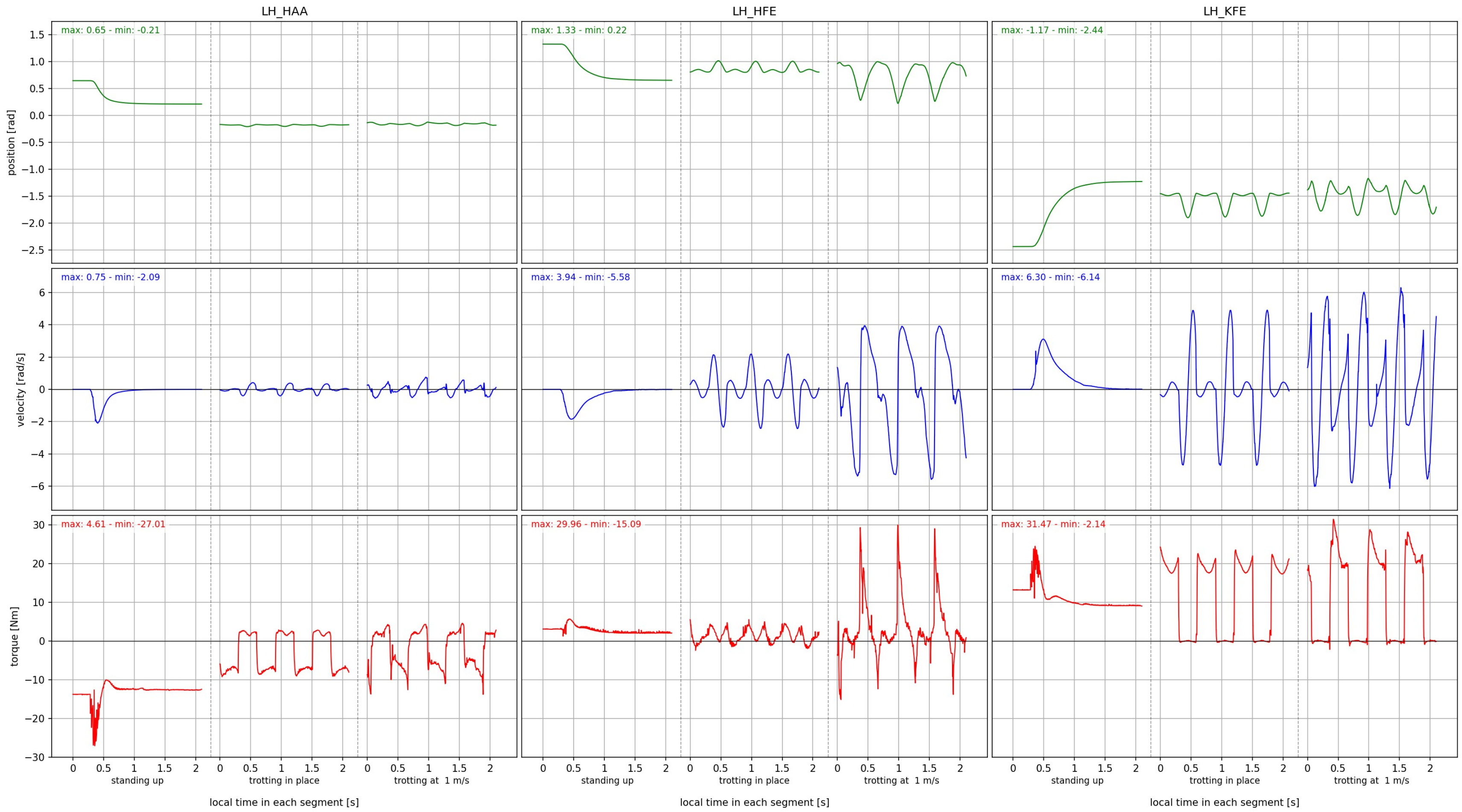

Figure 5.7: The left-hind leg joint position, velocity, and torque computed in the locomotion simulation during standing up (left segment of each plot), trotting in place with zero forward velocity (centre segment), and trotting at 1 m/s (right segment). The three plots in the left column show the hip-roll actuator, the three plots in the centre column show the hip-pitch actuator, and the three plots in the right column show the knee-pitch actuator. The absolute maximum velocity and torque reached during the simulations are 6.14 rad/s and 31.47 Nm, respectively.

Figure 5.8: Leon's customised actuator on the test bench. The actuator is configured as a hip-roll joint, i.e. with the electronics positioned on its back. It is mounted through FFF-fabricated components on an aluminium profile extrusion, which is clamped on the desk. Another aluminium extrusion, mounted through a FFF-fabricated output flange, acts as link, and gym weights (up to 8 kg) can be positioned at any distance from the rotation axis (up to 0.5 m).

the actuator axis.

The actuator was controlled through the software interface of the newly installed electronics (see Section 4.1.4). After a preliminary setup phase, the software allows speed and torque references (among other control modalities) to be sent to the actuator while recording motor current, estimated torque, temperature, and speed.

Three tests were executed, in order to assess the actuator's capability to reach (i) the rated torque, (ii) the peak torque required by the locomotion simulation (presented in Section 5.1.4), and (iii) the maximum speed.

Nominal torque validation

The nominal torque of the COTS actuator, according to the datasheet, is 18 Nm. To generate an approximately equal load torque, 4 kg of weight were installed on the output link. Considering the link's length of 0.5 m, the torque generated by the weight, when the link in horizontal position, is equal to 19.62 Nm.

The actuator was commanded increasingly higher target torques until the horizontal position of the link was reached. The load torque was calculated accordingly, using the position data from the actuator's encoder. Then, then position was held for approximately 20 seconds.

Figure 5.9 reports the recorded data of link position, torque (commanded and actual, as well as load torque calculated from the position), and motor coils temperature.

The increase in motor's temperature during the experiment was less than 4 °C.

Peak torque validation

The peak torque required according to the locomotion simulation (presented in Section 5.1.4) is 31.47 Nm, which corresponds to 66% of the rated peak torque of the actuator. Using a safety factor of approximately 1.2, the actuator was tested for a peak torque of 39.2 Nm. This load torque was generated by a weight of 8 kg at 0.5 m distance from the actuator axis, which corresponds to double the weight used in the nominal torque validation experiment.

The stages of the experiment can be observed in Figure 5.10. Contrary to the nominal torque test, the peak torque was only held for an instant: when the link reached the horizontal position, the actuator was switched off.

Figure 5.11, following the same structure of the nominal torque test presented in Figure 5.9, presents the position, torques and motor temperature recorded.

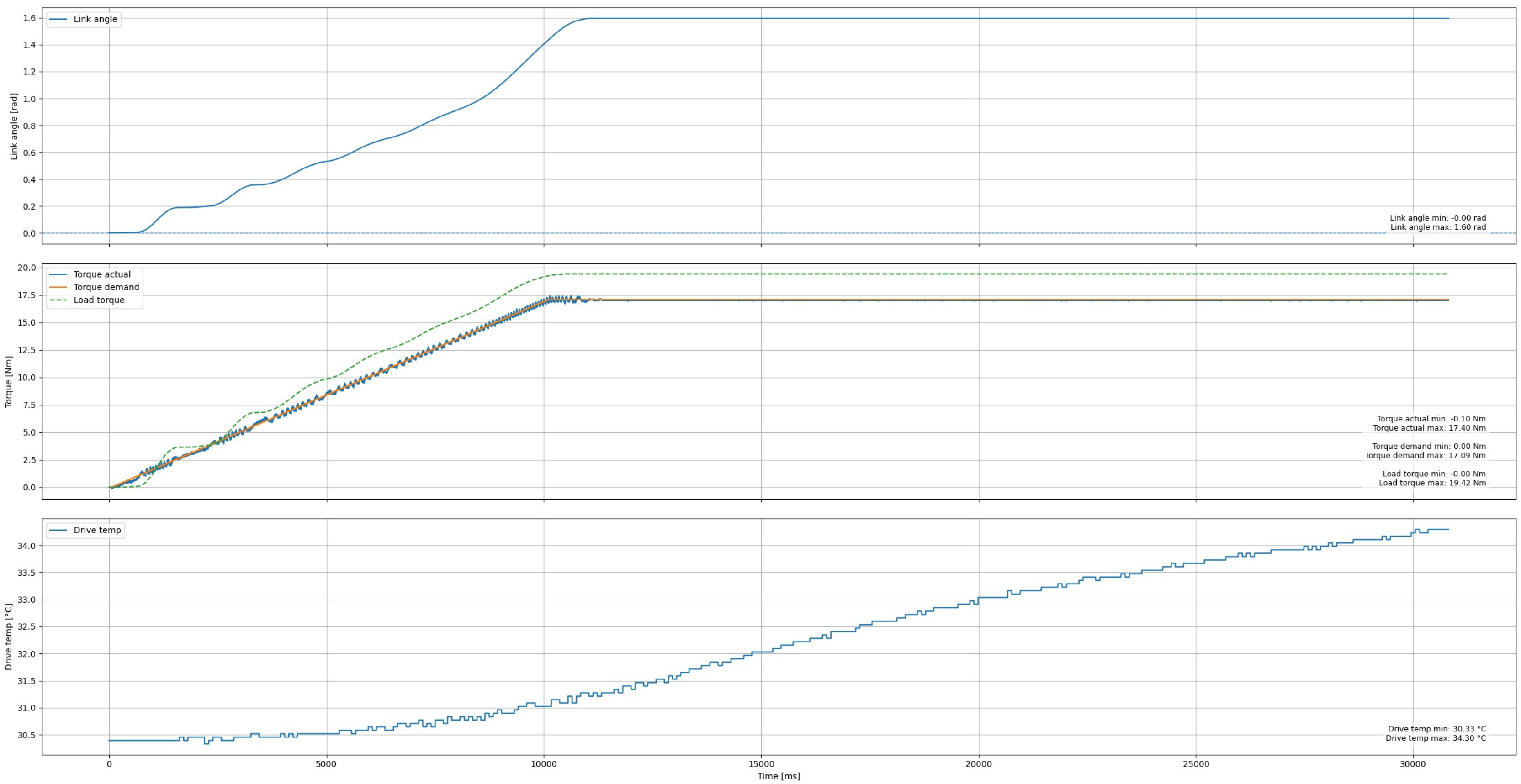

Figure 5.9: The results of the nominal torque test. The top plot reports the link's position, from which the load torque (green dashed line in the middle plot) e is determined. The middle plot reports the commanded (orange) and actual (blue) torque. A torque of 19 Nm is reached in approximately 10 s and held for 20 s. The bottom plot reports the evolution of the motor's temperature, which only increases by 4 °C in 30 s.

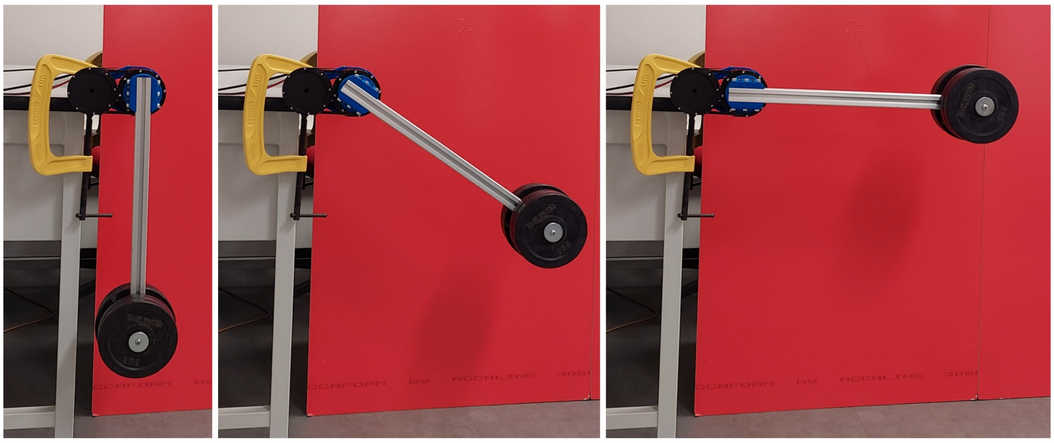

Figure 5.10: Leon's customised actuator on the test bench, during the peak torque test. The actuator lifted a load of 8 kg, composed by 4 disks of 2 kg each mounted at the end of a 0.5 m long link.

During the peak torque test, the increase in motor's temperature during the experiment was 2.5 °C.

Speed step response

The maximum speed of the COTS actuator, according to the datasheet, is 26 rad/s. To avoid overstressing the hardware, the test is performed by commanding a speed step to the actuator of 23 rad/s, equal to 88% of the rated maximum speed. As the maximum speed required according to the locomotion simulation (presented in Section 5.1.4) is 7.26 rad/s, the actuator in the test reaches a speed well above the requirements.

Figure 5.12 shows the actuator during a speed step response test. The only load on the actuator was the FFF-fabricated low-inertia link adapter visible in the figure in blue.

The data collected during the test is shown in Figure 5.13. The target speed is crossed after approximately 8 ms since the step command is applied, and the speed overshoots at 27.12 rad/s. To reach the target speed, a torque of 44.9 Nm is required by the controller, and the actual torque overshoots at 49.87 Nm.

5.1.6 Discussion

The evaluation of Leon is conducted on multiple levels. Firstly, using the final physical characteristics of Leon's design (presented in Section 4.1.9), simple assessments regarding Leon's payload capability and agility are elaborated.

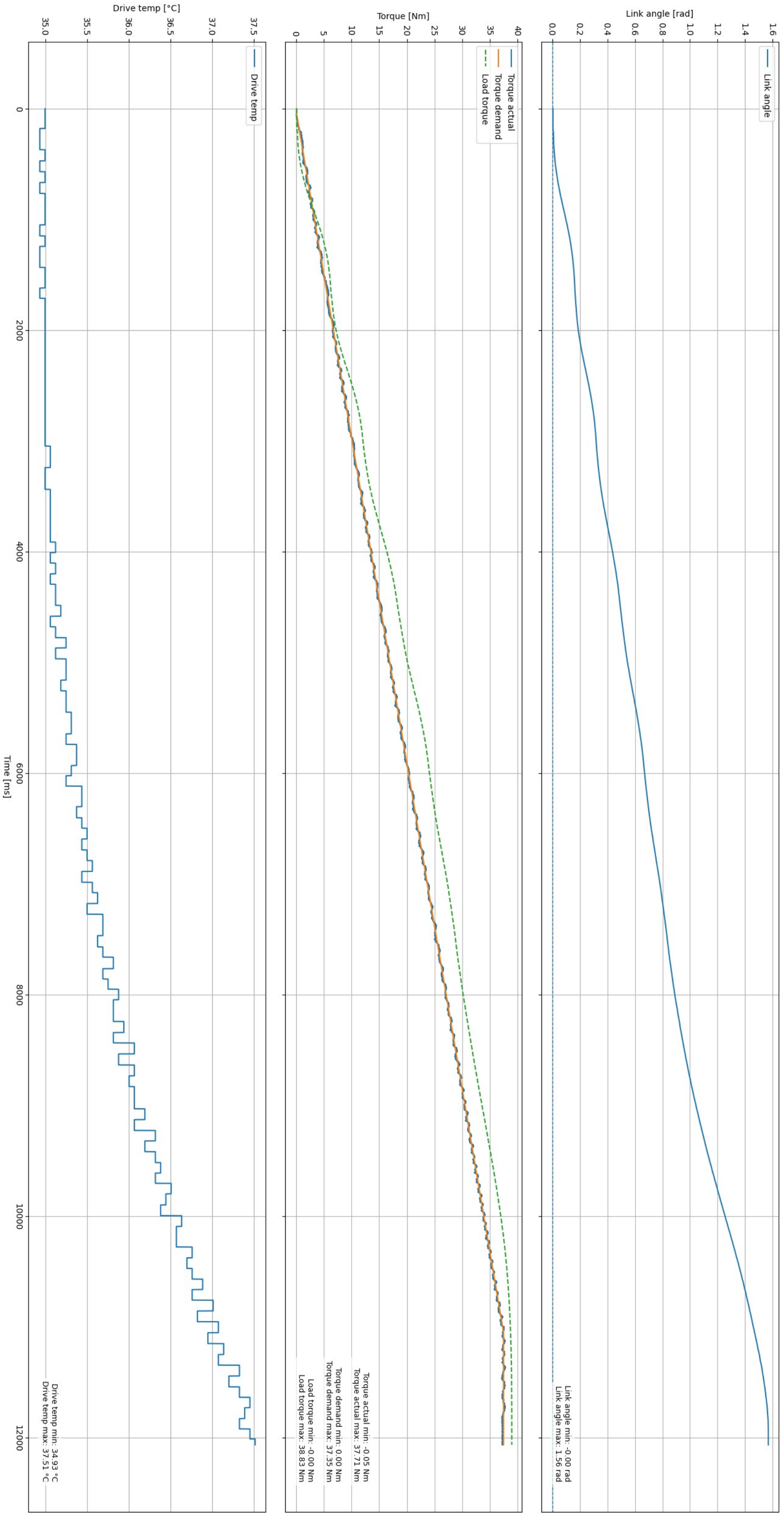

Figure 5.11: The results of the peak torque test. The top plot reports the link's position, from which the load torque (green dashed line in the middle plot) e is determined. The middle plot reports the commanded (orange) and actual (blue) torque. A torque of 38 Nm is reached and held for a few instants. The bottom plot reports the evolution of the motor's temperature, which only increases by 2.5 °C in the experiment.

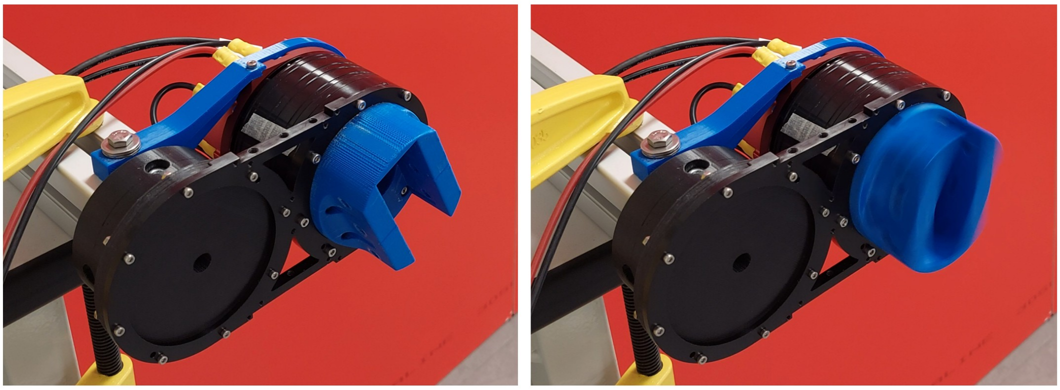

Figure 5.12: Leon's customised actuator on the test bench during a speed step response test. A low-inertia link adapter is mounted on the output flange. The actuator was driven with a step velocity command to reach its peak speed.

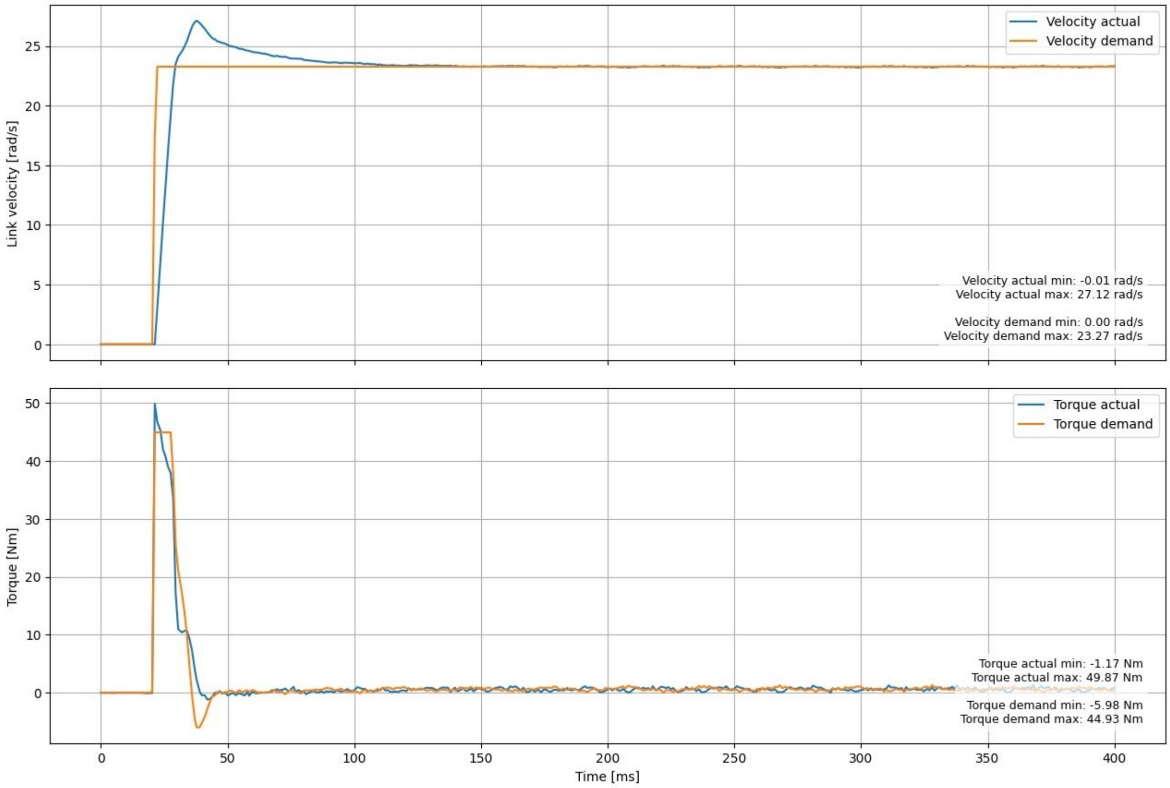

Figure 5.13: The results of the speed step response test. The top plot shows the commanded and actual speeds, while the bottom plot reports the commanded and actual torques.

Section 5.1.1 demonstrates that payloads up to 10 kg can be carried in moderately crouched positions. Section 5.1.2 uses the final design characteristics to estimate the FBW of the robot. The calculated value is 0.61, considering the standard 3 kg payload. As a reference, ANYbotics ANYmal [41] (which is moderately agile) features a FBW ratio of 0.54 [46], while Massachusetts Institute of Technology (MIT) Cheetah 3 (which is highly agile) features a FBW ratio of 1.6. This value, in conjunction with the Quasi-Direct Drive (QDD) actuation paradigm and the actuators' low gear ratio (9:1), suggests that the platform's behaviour is dynamic and agile.

These evaluations rely on the device's specifications, which are determined through the CAD model and reported in Section 4.1.9. To ensure that these quantities (particularly the masses) are realistic and reliable for the design assessment, the quadruped's structural elements are analysed. These components are designed to minimise weight, as the quadruped's agility depends directly on their low inertial properties. At the same time, they are subjected to high operational loads, making their structural integrity essential to the feasibility of the design. The performance of these components is therefore validated through FEM simulations, presented in Section 5.1.3, which demonstrate that Leon's structural elements can withstand the predicted operational loads.

To further validate the design, a dynamic locomotion simulation is performed and reported in Section 5.1.4. Its results confirms that the robot is able to perform agile trotting gaits. The data gathered during the simulation give estimations on the actual torque and speed requirements for the actuators, and show that even the the most challenging motions (standing up and trotting at 1 m/s forward speed) require torques and speeds that are below the actuator's rated capabilities.

The whole design relies on the customised actuator's capacity to deliver its rated torque and speed. This is confirmed in Section 5.1.5, which describes the tests that were performed with the actuator's physical prototype on a test bench. The actuator's performance confirms the predictions, demonstrating that the nominal torque can be held without significant temperature rises, that the peak torque is achievable and that the actuator can reach the rated speed.

Overall, the simulations and experiments confirm the validity of the design. Its characteristics position the device among mid-size agile quadrupedal robotic platforms, satisfying the design requirements. In conjunction with other factors deriving from the design choices (such as low-level software and hardware accessibility), Leon can be proposed as a completely customisable, easy-to-maintain, agile quadruped that does not require custom actuator development for fabrication.

5.2 Validation of the DAGANA gripper

The design of the DAGANA gripper was validated through several experiments. The first set of experiments aimed to demonstrate that the gripper is capable of delivering a high grasping force and therefore enables carrying a heavy payload, while the second set aimed to validate the perception-driven grasping pipeline.

Figure 5.14: The DAGANA gripper pinching a FT sensor on a lightweight robotic manipulator developed by IIT [130]. *Reproduced with permission from IEEE. First published in* [125]. © 2024 IEEE.

The experiments presented in this section were carried out in the context of the work presented at the 2024 IEEE-RAS 23rd International Conference on Humanoid Robots (Humanoids) [125].

5.2.1 Payload capability

As seen in Section 2.3, most grasping end-effectors' performances are presented as peak and continuous grasping force or payload. To validate the DAGANA gripper's payload capabilities, a more comprehensive set of tests was developed. These tests also take into account the thermal dissipation limits of the actuator at higher torques and the dynamic effects of robot motion in determining the maximum payload. This allows for a complete assessment of the gripper's capabilities in high-force grasping conditions.

Grasping force evaluation

This experiment measured the grasping force at different torques delivered by its actuation system. In order to have a direct measurement of the force (instead of a measurement of the applied torque and of the distance at which the resulting force is delivered), an external FT sensor [198] was used, using the setup presented in Figure 5.14. The sensor was at a distance of 0.15 m from the actuator's axis.

Figure 5.15 presents the increments in the commanded torque (up to the actuator's peak torque of 16.5 Nm) and the corresponding force, up to the maximum of 110 N.

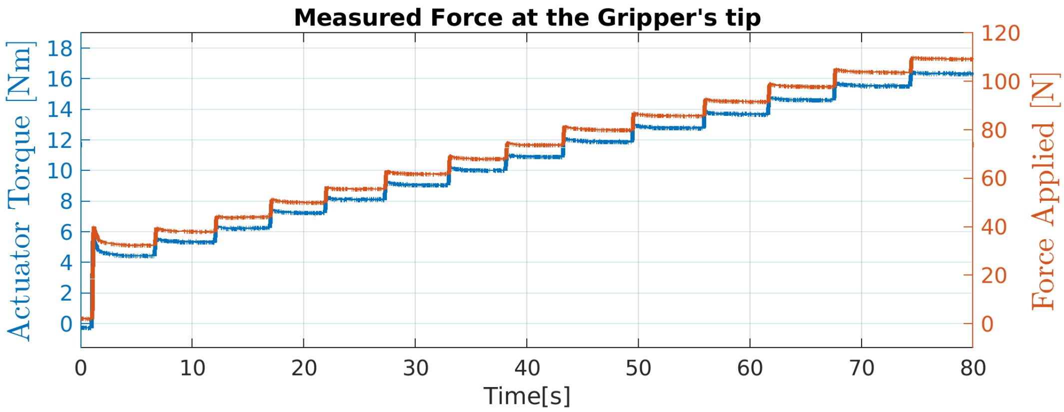

Figure 5.15: The torques commanded to the DAGANA gripper's actuator and the corresponding forces measured by the external FT sensor. *Reproduced with permission from IEEE.* ©2024 IEEE, *first published in* [125].

Thermal limit evaluation

This experiment measured the temperature rise over time for 10 different commanded torques. The measurement was performed using the actuator winding's temperature sensor, and torque was cut when the temperature exceeded 85 °C to avoid damage to the actuator (the actuator's datasheet reports a maximum limit of 130 °C). The results are shown in Figure 5.16. The peak torque 16.5 Nm (at which the gripper generates 110 N of pinching force) could be safely maintained for almost 80 seconds, while the continuous torque of about 10 Nm could be kept for more than 15 minutes.

Static payload evaluation

This experiment aimed to evaluate the capability of the DAGANA gripper, mounted on the IIT CENTAURO robot [43], to hold a given weight in static conditions. The

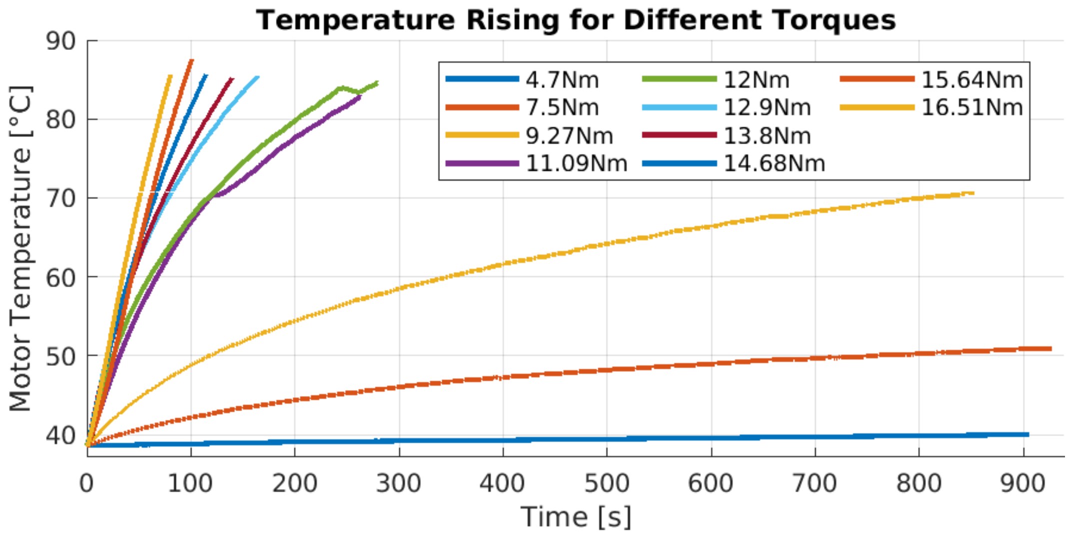

Figure 5.16: The actuator's temperature profiles over time, measured for several commanded torques. *Reproduced with permission from IEEE. First published in* [125].

payload consisted of a set of weights with a small wooden panel used as a handle, while the DAGANA gripper was equipped with high-density rubber pads mounted in the standard jaws (see Figure 5.17). Given a statically held payload and a gripping torque sufficient to support it, the torque was lowered until the payload slipped.

The results were reported in the plot of Figure 5.18: for the given materials in contact (rubber pads and wooden panel), the robotic system can hold a payload of 8 kg for an indefinite amount of time, while to hold a 10 kg payload, a torque of 12.5 Nm must be delivered. As seen from the plot of Figure 5.16, this torque can be held for a maximum of 3 minutes before risking overheating the actuator.

Dynamic payload evaluation

This experiment was an expansion of the static payload evaluation and aimed to assess the gripper's capability to hold a given weight in dynamic conditions, i.e. by accelerating the gripper in the vertical direction.

DAGANA was equipped with the standard jaws and high-density rubber pads, while the payload consisted of a set of metal weights. The applied torque was 10.6 Nm, which (as seen in the plot of Figure 5.16) is the maximum torque that can be held indefinitely. During the experiment, the robot was commanded to move along the direction of gravity with increasing speed, as seen in Figure 5.19. The peak Cartesian acceleration along the z axis, which occurred at the highest and lowest points of the linear trajectory, was

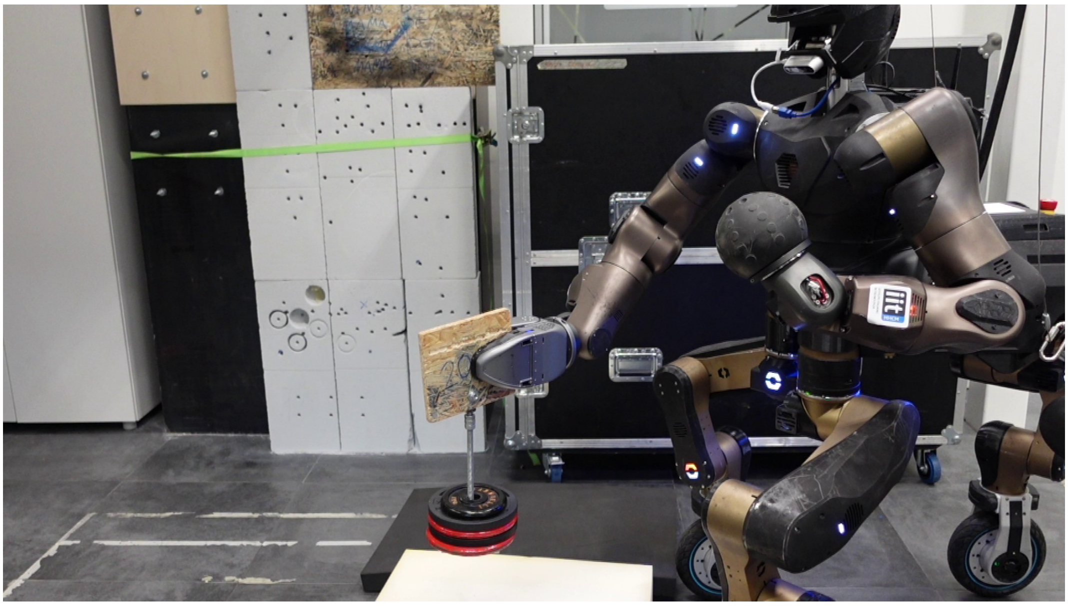

Figure 5.17: The DAGANA gripper on the CENTAURO humanoid, holding a 9.4 kg weight statically. *Reproduced with permission from IEEE. First published in* [125]. © 2024 IEEE.

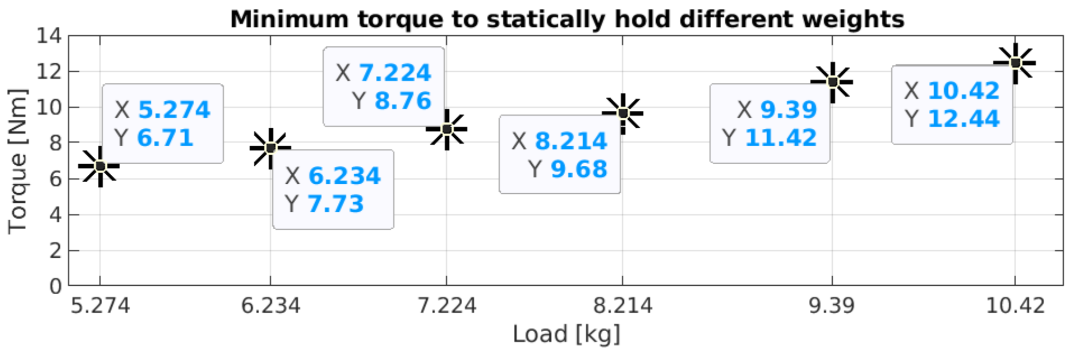

Figure 5.18: The minimum torque required to hold a set of payloads with the DAGANA gripper in static conditions. *Reproduced with permission from IEEE. First published in* [125]. © 2024 IEEE.

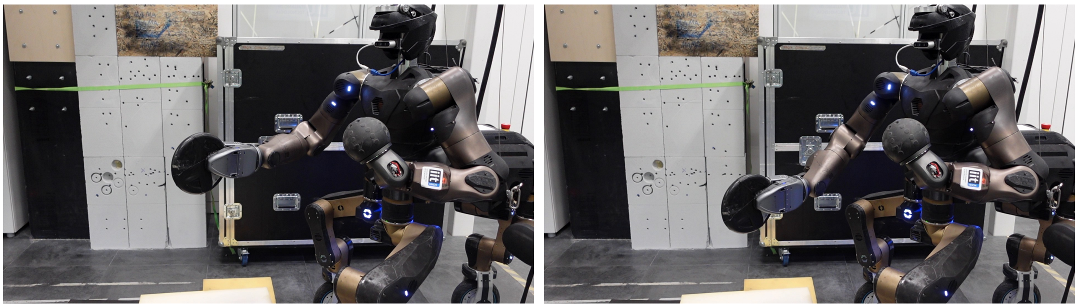

Figure 5.19: The DAGANA gripper on the CENTAURO humanoid, holding a 5.9 kg weight while moving its arm up and down. *Reproduced with permission from IEEE. First published in* [125]. © 2024 IEEE.

recorded.

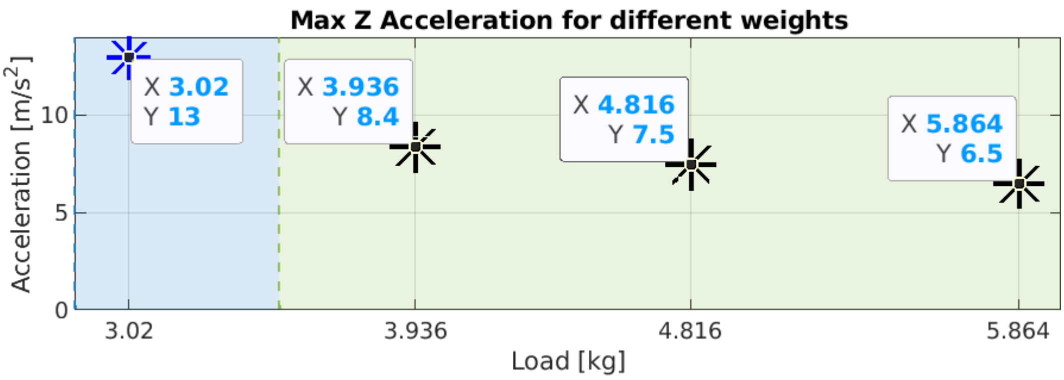

Figure 5.20: The maximum acceleration at which a set of payloads slipped. The blue area indicates conditions in which the experiment failed, not because the payload slipped, but because the robot's joints reached the maximum allowed acceleration. *Reproduced with permission from IEEE. First published in* [125]. © 2024 IEEE.

The plot presented in Figure 5.20 reports, for each payload, the maximum vertical acceleration measured before slipping occurred.

5.2.2 Perception-driven grasping experiment

This experiment employed the perception-driven grasping pipeline presented in Section 4.2.6 and made full use of the sensors developed with the integration of the Arduino Nicla Vision as a sensing module: the microphone, the Red Green Blue (RGB) camera and the Time-of-Flight (ToF) distance sensor.

The experimental setup consists of the IIT CENTAURO humanoid robot [43] with the DAGANA gripper on its right arm, positioned in front of a table on which a cup and a bottle are lying.

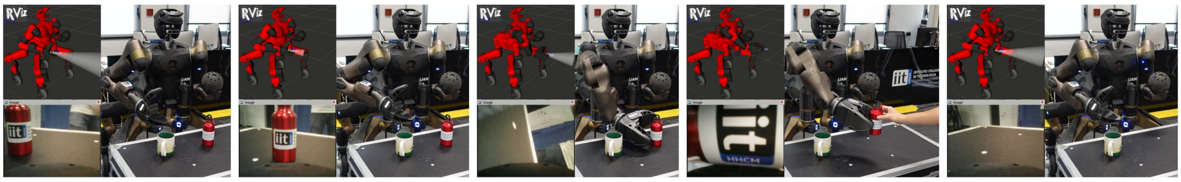

Figure 5.21: The perception-driven grasping experiment. (i) Pre-scan phase: the robot is scanning the table and awaits commands (ii) Scan and align phases: after the user commands “bottle”, the robot aligns (iii) Reach and grasp phases: after the bottle is reached, the gripper grasps it (iv) Handover phase: the robot, in the handover position, opens the gripper at the user’s “open” command (v) The pre-scan phase is activated again. *Reproduced with permission from IEEE. First published in* [125]. © 2024 IEEE.

Figure 5.21 shows the phases of the experiment. While the robot was scanning the table, the user requested an object (either pronouncing “cup” or “bottle”). The robot, using the gripper’s sensors, identified and grasped the object autonomously and presented it to the user. The gripper opened as the user was grasping the object from the robot and issued the command “open”.

The pipeline was run multiple times with success, positioning the objects in different locations and orientations. The recordings of the pose of the end-effector’s Tool Center Point (TCP), the angles calculated by the image processing software and used in the Cartesian controller of the arm to align to the target, and the readings from the ToF distance sensor throughout the multiple runs of the experiment are presented in Figure 5.22.

5.2.3 Discussion

The experiments fully demonstrated the capabilities of the DAGANA gripper.

On the one hand, the experiments presented in Section 5.2.1 evaluated the high-grasping-force performance of the gripper. The conditions imposed in the experiments are not different from those in industrial and construction tasks, where a robot may be required to move heavy wood panels or heavy metal objects. This fact reinforces the claim that the DAGANA gripper can be an essential tool in mobile manipulation in unstructured environments. Furthermore, the testing approach defined a new method for benchmarking a high-force-capable grasping end-effector that goes beyond the maximum force ratings of commercial grippers. Using information from the thermal evaluation and the static and dynamic payload capability tests, it is possible to define

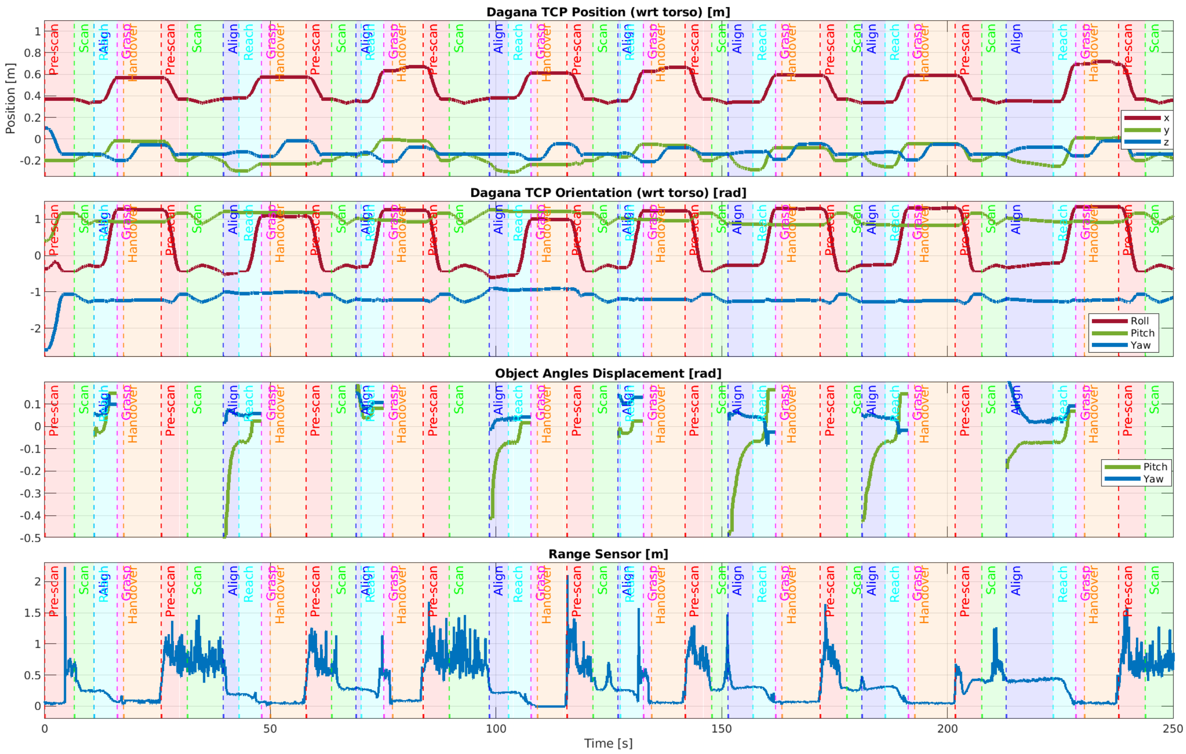

Figure 5.22: The data recorded in the perception-driven grasping experiment. Each phase is highlighted with colour. The first two rows show the end-effector's TCP pose. The third plots the object displacements computed from the RGB images. The fourth row presents the data recorded by the ToF distance sensor. *Reproduced with permission from IEEE. First published in* [125]. © 2024 IEEE.

a workspace of safe operational conditions (relevant to the industry or construction environment) in which the gripper is guaranteed to operate as claimed.

The experiments presented in Section 5.2.2 aimed, on the other hand, at showcasing the perception-enhanced features in a real-world application with everyday objects. Some simplifications with respect to a real-world setting were used: the assumption that the gripper's approach is almost parallel to the robot's x axis and the assumption that the orientation of the object is known (which is true for cylindrical objects positioned on a flat surface). Nevertheless, these simplifications (also presented in Section 4.2.6 for each relevant phase) do not diminish the qualitative result of the experiment: multimodal sensing at the end-effector can be beneficial for grasping applications, enabling otherwise impossible semi-autonomous manipulation with robots in unstructured environments.

5.3 Validation of the Smart Drill end-effector

The validity of the design of Smart Drill was assessed by performing two semi-autonomous drilling experiments with a robotic platform for unstructured environments. These experiments aimed to evaluate the end-effector's drilling capability and the precision of its sensing systems by running the semi-autonomous drilling pipeline presented in Section 4.3.6 in two different conditions.

The experiments presented in this section were carried out in the context of the work presented at the 2024 IEEE 20th International Conference on Automation Science and Engineering (CASE) [128].

5.3.1 Use case identification and experimental setup

The use case identified and replicated through the experiments is a construction or carpentry application, such as the application of plasterboard or the installation of electrical systems on a wall. The human operator marks on a wall target points that need to be drilled to perform the activity, and the robotic platform is brought in front of the surface to aid the operator in the drilling activity.

Figure 5.23: The IIT CENTAURO NEXUS [43] drilling a plywood panel with Smart Drill. *Reproduced with permission from IEEE. First published in* [128]. © 2024 IEEE.

This setting was replicated in the laboratory (see Figure 5.23) using the CENTAURO NEXUS [43] humanoid, developed by IIT and available at Leonardo S.p.A.

Robotics Laboratory. The robot was chosen for its ready availability and high-force capabilities, but any other robotic platform with sufficient payload capacity would produce analogous results, as the experiment did not use any platform-specific sensors and relied only on the equipment of Smart Drill. In fact, the robot was controlled in position control by sending to its controller the target positions of its end-effector directly from the Single-Board Computer (SBC) of Smart Drill. This simple approach focused on the assessment of the capabilities of Smart Drill rather than the determination of the most appropriate kinematics and control method to execute the drilling (which was outside of the scope of the experiment).

5.3.2 Drilling capability test

This test aimed to assess the robustness of the system by stressing its drilling capability and drilling a larger-than-usual hole. It was performed by commanding the system to drill a 10 mm hole on a 6.5 mm-thick plywood panel, thereby assessing the strength of the mechanical structure of Smart Drill. The 10 mm hole corresponds to the largest drill bit shank diameter of Smart Drill and is therefore regarded as appropriate to represent a large hole drilling example. The plywood material was selected as it represents a widely used material in construction. A red cross was marked on the target drilling point.

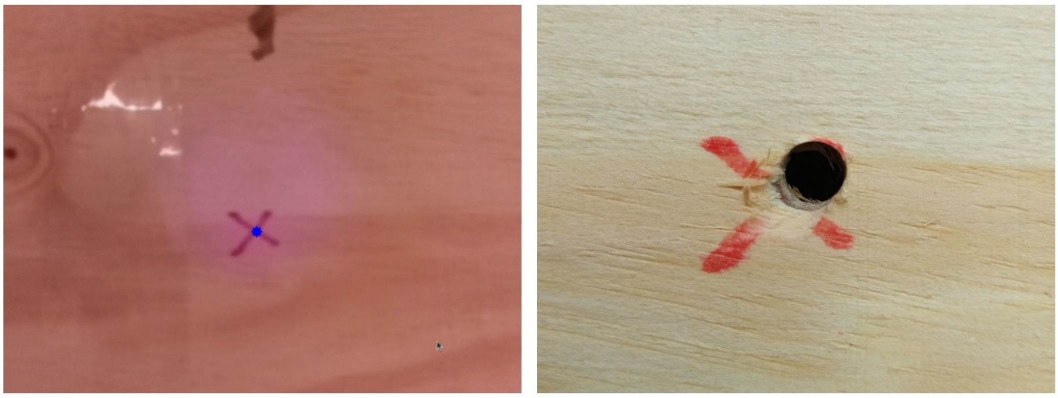

Figure 5.24: On the left, the view from the Smart Drill's camera stream. The operator selects the target point (dot on the red cross). On the right, the drilled hole. Slippage occurred: the drilling started in the correct position (the red cross is cancelled in the centre), but the final hole is 4 mm from the centre of the cross. *Reproduced with permission from IEEE. First published in* [128]. © 2024 IEEE.

The semi-autonomous pipeline was executed, and the robot drilled the wooden panel successfully. The experiment was repeated 3 times. Nevertheless, the drilling was not precise: by the visual analysis (see Figure 5.24) of the resulting hole, the drilling was initiated at the correct location, but the drill bit slipped on the wood while the robot was pushing on the surface, and the final hole was displaced approximately 4 mm from the target point. Close inspection indicated that the support structure of the plywood panel had slipped during the drilling operation.

5.3.3 Precision test

This test aimed to determine the effectiveness of the sensing system and its related data processing performed by the SBC using the previously described pipeline. It was performed by commanding the robot to drill 36 holes (using the same 9 points as a target for 4 times) on a soft substrate, so that any deviations related to the high-force interaction between the robotic system and the environment were eliminated. The drill bit installed was 5 mm in diameter, while the panel material was low-density polystyrene plastic. To provide a deterministic set of target points, a pre-marked A3 sheet of paper was attached to the plastic panel. This sheet presents a grid of 25 target points, equally spaced at 50 mm, and is visible in Figure 5.25.

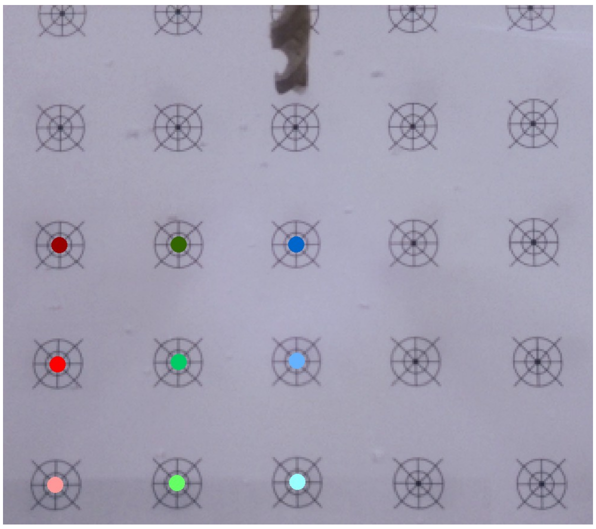

Figure 5.25: The Smart Drill's camera stream showing the target grid of 25 points, equally spaced at 50 mm. The points used in the experiments are identified by coloured dots in the bottom-left corner of the grid. *Reproduced with permission from IEEE. First published in* [128]. © 2024 IEEE.

The autonomous drilling operation was triggered (after the alignment of the end-effector with the drilling surface) over 9 of the 25 points, located in the bottom-left quadrant of the field of view of the camera. These points were chosen so that they did not require a reconfiguration of the arm of the robot to be reached. The operation was repeated 4 times; therefore, 4 paper sheets and supports were drilled, collected and a two-dimensional (2D)-scan of each was obtained.

The 36 drilled locations on the images were then reconstructed and measured using the software ImageJ [199], determining the distance and angle from each target point. The data are collected and presented in the polar plot of Figure 5.26, on which a black cross represents the mean distance from the target, and the grey area represents the standard deviation. In the plot, each drilled point is correlated with its pre-marked target location on the paper grid by using different colours; therefore, four points per colour (one for each paper sheet and support drilled).

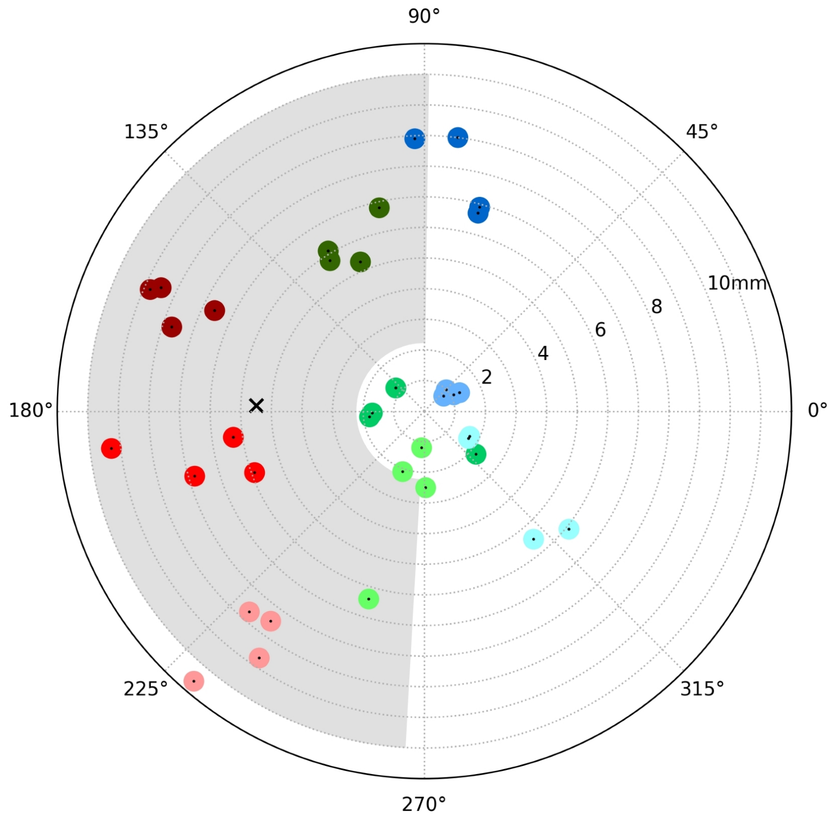

Figure 5.26: Polar plot of the drilling error from the precision test. The error is measured from the target point to the drilled hole, obtaining distance and angle. The drilling location is identified using the colours of Figure 5.25. *Reproduced with permission from IEEE. First published in* [128]. © 2024 IEEE.

The mean error (or distance from the target) is 5.5 mm (with a standard deviation of 3.3 mm), and the mean angle is 188° (with a standard deviation of 89°).

5.3.4 Discussion

The experiments demonstrate that Smart Drill is a functional drilling end-effector for low-payload robotic arms. Thanks to its embedded sensing and computation, along with its complementary software, it can effectively aid the human operator working in unstructured environments.

The first experiment demonstrated that the mechanical structure of the end-effector can support the loads characteristic of drilling a medium-hardness material, common in carpentry. The slippage that occurred during the operation can be attributed to the control strategy of the robot (which used a constant-velocity linear trajectory to feed the drill bit during cutting), specifically to an excessively high feed speed, which generated forces that the support structure of the plywood panel could not withstand. A further refinement of the control strategy, either by implementing force control to limit transmitted forces or by reducing the feed speed of the drill bit (through a reconfiguration of the constant-velocity trajectory), could improve the result.

The second experiment assessed the precision and accuracy of the sensing system and its associated software. From the results, presented in the polar plot, it is evident that the system is not accurate, as most of the holes were not drilled at the target point. Nevertheless, a colour-based clustering of the drilling points can be inferred from the plot. Points related to the same drilling location (identified by the same colour on the plot) are closest together. This indicates good repeatability of the system, which can therefore be considered sufficiently precise. Furthermore, correlating the position of the target within the Field of View (FoV) of the camera and the measured error, it can be inferred that the error is larger for the targets that are located farther to the left of the centre. To confirm, the standard deviation (grey area) is located to the left of the centre of the plot. These facts suggest that the error is likely due to camera distortion, which increases as the target is farthest from the centre of the FoV. A refinement in the calibration of the sensor, or the upgrade to a higher-quality Red Green Blue (RGB) camera, could improve the result.

Chapter 6

Related work

This chapter compares the robotic systems introduced and validated in the previous chapters with similar devices, highlighting their novelty and relevance to the current state of the art. Specifically, the following sections compare Leon, DAGANA, and Smart Drill, respectively, with similar quadrupedal robotic platforms (Section 6.1), high-force and perception-capable grippers (Section 6.2), and custom power-drilling end-effectors (Section 6.3).

6.1 Leon in the context

In this section, Leon is compared to the Unmanned Ground Vehicles (UGVs) for unstructured environments analysed in Section 2.2.

Table 6.1 reports Leon's and other agile quadrupeds' actuator type, leg size, mass and corresponding force-to-bodyweight (FBW) ratio (used in Section 4.1.2 and introduced in [46] to assess the capability of a quadruped to perform agile motions).

Despite Leon still being in the design phase, its expected characteristics make it a promising quadrupedal platform well aligned with the state of the art. Its predicted agility is comparable to that of the direct competitors in terms of size and mass, and its unique design approach, based on commercial components up to the actuators, makes it interesting for research and product development. To reinforce these claims, Leon is compared in terms of dimensions, agility, manufacturing process and customisability, equipment, and possible uses.

Table 6.1: Comparison of agile quadrupeds, ordered by year of introduction.

Name	**Year**	**Actuator type**	**Leg size[a] (m)**	**Mass (kg)**	**FBW ratio[b]**
BigDog [31]	2008	Hydraulic	1.00	109	–
HyQ [32]	2011	Hydraulic	0.70	91	0.66
StarlETH [40]	2012	SEA	0.40	23	0.66
MIT Mini Cheetah [48]	2013	QDD	0.39	9	1.7
HyQ2Max [33]	2015	Hydraulic	0.70	80[c]	0.84[c]
ETH Zurich ANYmal B [42]	2017	SEA	0.60	30	0.54
MIT Cheetah 3 [46]	2018	QDD	0.68	45	1.6
HyQReal [34]	2019	Hydraulic	0.74	130	0.49
Spot [152]	2019	Electric	0.75	32	–
ANYbotics ANYmal [137]	2021	SEA	0.66	50	–
Barry [52]	2022	QDD	0.80	48	0.74
Go2 [141]	2023	QDD	0.45	15	–
B2 [141]	2023	QDD	0.80	60	≈ 0.6
Keyper [200]	2023	Electric	0.75	43	–
A2 [141]	2025	QDD	0.8	42	≈ 1
PUDU D5 [201]	2025	Electric	0.7	61	–
Leon	–	**QDD**	**0.48**	**30**	**0.61**

[a] Leg size corresponds to the sum of the lengths of the upper and lower leg links. When not available in the respective reference, the value is reported from [52] or estimated.
[b] From [46] or estimated using data from the respective reference, whenever the peak torque with the leg minimally extended is provided for the actuator in the least favourable condition.
[c] Calculated with the power system offboard.

Dimensions

Firstly, Leon, with its characteristics and expected performance, can be classified as a small-to-medium-sized quadruped, larger than Mini Cheetah and StarlETH but smaller than ANYmal or Spot. Its dimensions are comparable to those of Unitree Go2, while its simplified arrangement of lower-leg actuators (in-axis with the knee-pitch joint) is the same as in ANYmal. Its mass of approximately 30 kg includes a standard inspection payload, making it a direct competitor of ANYmal in terms of functionalities. Lighter quadrupeds excel in agility, but their standard payload is less appropriate for locomotion and navigation research and development, while bigger quadrupeds are not as conveniently-sized for indoor exploration.

Agility

Compared to ANYmal, Leon shows a better FBW ratio, suggesting that Leon's agility is sufficient. Additional agility could have been obtained by optimising the internal components and the automation systems, reaching values similar to those of Unitree robots [141], Keybotic Keyper [200] of PUDU Robotics D5 [201], which feature similar actuators but a highly integrated trunk design and an optimised lower-leg inertia. This approach would nevertheless have been detrimental to Leon's simplified sourcing and manufacturing objective. Bigger quadrupeds, except those optimised for agility (Massachusetts Institute of Technology (MIT) Cheetah 3 and possibly Spot, although no definitive data is available to calculate the FBW ratio), show similar agility. Barry (optimised for high payload) shows superior agility while still using a Quasi-Direct Drive (QDD) actuation system. Still, its actuator design and leg kinematics are highly developed and not as easily sourced and manufactured as Leon's.

Manufacturing process and customisability

One of the main objectives of Leon's design is to prove that an agile quadruped can be manufactured from the integration of minimally customised commercial components and a few simple custom mechanical components. In this, Leon excels, as it is the only quadruped developed with Commercial Off-The-Shelf (COTS) actuators that does not require prior actuator development experience, cutting development time and making the system more attractive for research and development contexts without prior mechatronics experience. The extensive use of commercial components, integrated in a way that permits agile behaviour, is another point of interest of the design. Internal components can be readily accessed, replaced, or expanded. Hardware and software are open to the user at all levels, as no previously integrated commercial subassembly is included. This differentiates Leon from the widely used commercial robots like Spot or Go1, making it more suitable for research.

Equipment and possible uses

While Leon has been developed as a multi-purpose research and development platform for studies in quadrupedal locomotion and navigation, its equipment (Laser Imaging, Detection, and Ranging (LIDAR), Red Green Blue - Depth (RGB-D) cameras, powerful computation units) and its expandable payload (up to a total of 10 kg of sensing equipment) make it appropriate for the growing commercial task of industrial inspection, which is the current market target of ANYmal [137], Spot [136], and Unitree quadrupeds [138] and many other companies and startups.

6.2 DAGANA in the context

This section compares the DAGANA gripper with other grasping systems previously analysed in Section 2.3.

DAGANA is a rugged one Degree of Freedom (DoF) sensorised gripper specifically designed for operation in unstructured environments. Similar devices are the end-effector mounted on the Boston Dynamics Spot quadruped robot [147], and on the Unitree B1 quadruped with the Z1 arm and its gripper [148]. Nevertheless, few specifications of these grippers are known due to commercial interests. For what can also be inferred from videos showcasing these products [136, 138], these grippers show similar kinematics and functionalities to those of DAGANA.

In terms of grasping force, Boston Dynamics declares for Spot's gripper a maximum pinching force of 130 N at the tip of its 90 mm deep palm [147], while DAGANA showed a pinching force of 110 N at the tip of its standard 110 mm deep palm (see Section 5.2.1). If the gripper palm of DAGANA were the same size as that of Spot's gripper (90 mm instead of 110 mm), the pinching force (at DAGANA's actuator maximum torque of 16.5 Nm) would be 127 N. Therefore, DAGANA and Spot's gripper are comparable in size and capacity.

Nevertheless, DAGANA shows a higher level of reconfigurability than Spot's and Z1's grippers, both in the grasping pads and in its sensing systems. This feature is a result of DAGANA's modular design. It extends the gripper's applicability to more use cases: the jaw modules can be quickly replaced to address new use cases requiring different jaw shapes and materials optimised to accommodate grasping a particular tool or object. Modularity in the grasping pads, with specific pads installed to perform tasks otherwise impossible, has been shown to work in other one DoF grippers such as the F1 Hand [75] and the M2 Gripper [76]. DAGANA applies the concept to much higher force scales, allowing the manipulation of metal formwork and tubes (see Figure 4.25).

DAGANA's robustness and impact resilience are exceptional for grippers. They are favoured by the use of a Series Elastic Actuator (SEA) actuator. This actuation method is the favoured choice in collaborative robots. However, in robotic grippers, SEAs have been used only rarely, with low torque ratings [131]. DAGANA's SEA actuation system delivers high torque, derived directly from the actuation system used in high-torque-to-weight-ratio robotic arms and humanoids.

The sensing systems used in DAGANA also feature a tightly integrated yet modular design, allowing sensing capabilities to be extended when needed while protecting the sensors within the gripper's main body. This level of integration, obtained while maintaining full modularity, is a novelty with respect to other systems that use eye-in-hand vision, microphones or range sensors that are either external [79, 84] or tightly integrated [138, 83, 147]. Furthermore, the correlated sensing software is also developed in a modular way, aligning with the state of the art for easy, seamless exploitation of sensor information during task execution [85].

Another contribution of the work on the design and validation of DAGANA is the implementation of an extensive gripper-testing method, particularly regarding its payload capacity. This is uncommon for grippers. In fact, other works [65, 66, 67, 68, 69, 70, 71, 74, 75] and commercial products [144, 145, 146] seldom present such detailed evaluations, limiting the information to reporting maximum grasping force capabilities in papers or datasheets. The approach used for DAGANA (see Section 5.2.1) outputs information that enables the prediction of the gripper's behaviour in real-world tasks, extending the maximum grasping force evaluation to the real payload capability during manipulation and considering also the thermal limits of the actuator.

6.3 Smart Drill in the context

In this section, the Smart Drill power-drilling end-effector is compared with existing robotic drilling end-effectors analysed in Section 2.4.

Drilling end-effectors for small robotic arms, such as those used in collaborative contexts and in mobile platforms for unstructured environments, are most often implemented by clamping a commercial power drill to the end-effector flange, as seen in [85, 104], or by creating custom drilling end-effectors that are optimised for collaborative human handling [102, 103].

Smart Drill extends this approach by reconfiguring commercial drilling components into a robot-optimised end-effector. Its power-drilling components are still derived from a small commercial power tool. Nevertheless, these components are spatially arranged to optimise the transmission of drilling force to the robot. When drilling, Smart Drill does not generate moments at the robot's wrist joints, which are generally rated for lower torques. This reduces the robotic arm's drilling effort and enables drilling operations to be carried out with smaller robots.

The idea of creating a drilling end-effector from commercial power drills is also explored in research on power drilling in construction [110, 111]. Still, these end-effectors are mounted on large robotic arms that are less sensitive to the optimisation of the drill's orientation to reduce drilling effort. Nevertheless, the Smart Drill's approach could improve the operation's precision, as errors in the wrist joints in these configurations immediately cause the drill bit to deviate from its feed direction.

In the literature, sensorisation of drilling end-effectors is often applied, mostly with bulky designs optimised for high-payload industrial robotic arms [96, 97] to enhance the precision or capabilities of an industrial drilling operation. The Smart Drill's sensors are instead integrated in a way that minimally affects the end-effector's size and weight. They not only improve precision during a conventional drilling operation, but also enable drilling in positions where the robotic platform sensors would be ineffective due to occlusions. While Smart Drill still requires upgrading to reach, with its embedded sensing systems, precision, and capabilities comparable to those seen in industrial environments [95], it shows how the integration of sensors can be beneficial even in small-scale robotic applications, where sensors are already present in the mobile platform.

The conceptual design of Smart Drill combines a sensorised end-effector for enhanced performance, as seen in industry, with the reuse of commercial power drill components, as seen in construction and collaborative environments. This hardware combination approach is then completed with an embedded computation unit, which not only interfaces with the sensors but also controls the robot and the collaborative drilling experience, as seen in Section 5.3. This edge-computing approach, which translates the task definition and execution directly into the end-effector that enables the task, to the best of the author's knowledge, has not been reported in the literature and constitutes the novelty of the proposed design. With this approach, Smart Drill demonstrates a new method in which the end-effector takes control of the operation, and the same operation can therefore be translated to another robotic arm with minimal effort.

Chapter 7

Conclusions

This thesis concerns the design and validation of three robotic devices for unstructured environments: the agile quadruped Leon, the high-force gripper DAGANA, and the power-drilling end-effector Smart Drill.

The devices have been described in detail, and experimental results validated their effectiveness in relation to the problem their design aimed to solve. Still, much work remains to be done.

Regarding the quadruped Leon, the first physical prototype has not yet been manufactured. While the design has been validated on paper, significant technical effort is still required to implement the first functional robot, and only its final deployment will confirm the estimated performance. Nevertheless, the approach itself already provides inspiration for other researchers and designers: an agile platform can be made from commercial components, with a limited mechanical design and mechatronic integration effort. Research groups should not be demotivated by a lack of extensive knowledge in actuator development, as it is no longer a requirement for obtaining a functional agile quadrupedal platform.

Conversely, the DAGANA gripper is a mature design that has been built in multiple physical prototypes and has been thoroughly validated. The set of experiments provided to demonstrate the gripper's effectiveness is the most complete presented in the thesis, and this validation procedure aims to be a reference for others who want to introduce new high-force-capable designs. Prototypes of the gripper have also been used extensively in recent works, and testify to its validity [132, 133, 134]. Other than mechanical refinements (such as reduction in size, implementation of full ingress protection), no further work is required. Furthermore, thanks to its modular approach, the gripper can be used as a platform for devising innovative grasping and sensing modules that extend its dexterity and expand its sensing capabilities.

One physical prototype of the Smart Drill end-effector has been built. As reported in its validation, work remains to be done to improve the precision and accuracy of the drilling process. Further tests, involving experimenting with arm control strategies and installing the end-effector on other robotic arms, are required to fully validate the design. Nevertheless, the fundamental contribution of the conceptual design is demonstrated: with Smart Drill, the end-effector commands the execution of the task, without requiring complex installation procedures on the robotic platform to perform real-world tasks. A collaborative drilling task is presented and, once precision is addressed, can be deployed in a construction environment with minimal changes to the end-effector's design.

Overall, the work reported provides examples of new approaches and applications of robotics in unstructured environments, with the aim of expanding their industrial deployment. The relatively simple inspection tasks that currently involve these robots in industrial settings may evolve, ultimately allowing the replacement of human operators in dangerous or physically demanding assignments. The hope is that, by observing the robotic design developments reported herein, readers are encouraged to experiment in the creation of new devices and approaches, bringing the industrial deployment of robots for unstructured environments another small step closer.

Bibliography

[1] J. F. Engelberger. Historical Perspective and Role in Automation. *Handbook of Industrial Robotics*. John Wiley & Sons, Ltd, 1999. Chap. 1, pp. 1–10. DOI: 10.1002/9780470172506.ch1.

[2] J. E. Colgate, W. Wannasuphoprasit, and M. A. Peshkin. Cobots: Robots for Collaboration With Human Operators. *ASME International Mechanical Engineering Congress and Exposition*. Vol. Dynamic Systems and Control. 1996, pp. 433–439. DOI: 10.1115/IMECE1996-0367.

[3] S. Robla-Gómez, V. M. Becerra, J. R. Llata, E. González-Sarabia, C. Torre-Ferrero, and J. Pérez-Oria. Working Together: A Review on Safe Human-Robot Collaboration in Industrial Environments. *IEEE Access* 5 (2017), pp. 26754–26773. DOI: 10.1109/ACCESS.2017.2773127.

[4] G. Ullrich. The History of Automated Guided Vehicle Systems. *Automated Guided Vehicle Systems: A Primer with Practical Applications*. Berlin, Heidelberg: Springer Berlin Heidelberg, 2015, pp. 1–14. DOI: 10.1007/978-3-662-44814-4_1.

[5] J. Zhang, X. Yang, W. Wang, J. Guan, L. Ding, and V. C. S. Lee. Automated Guided Vehicles and Autonomous Mobile Robots for Recognition and Tracking in Civil Engineering. *Automation in Construction* 146 (2023), p. 104699. DOI: 10.1016/j.autcon.2022.104699.

[6] M. Spenko, S. Buerger, and K. Lagnemma, eds. The DARPA Robotics Challenge Finals: Humanoid Robots to the Rescue. Vol. 121. Springer Tracts in Advanced Robotics. Cham: Springer International Publishing, 2018. DOI: 10.1007/978-3-319-74666-1.

[7] T. Rouček, M. Pecka, P. Čížek, T. Petříček, J. Bayer, V. Šalanský, D. Heřt, M. Petrlík, T. Báča, V. Spurný, F. Pomerleau, V. Kubelka, J. Faigl, K. Zimmermann, M. Saska, T. Svoboda, and T. Krajník. DARPA Subterranean Challenge: Multi-Robotic Exploration of Underground Environments. *Modelling and Simu-*

lation for Autonomous Systems. Vol. 11995. Lecture Notes in Computer Science. MESAS 2019, Palermo, Italy. Cham: Springer International Publishing, 2019, pp. 274–290. DOI: 10.1007/978-3-030-43890-6_22.

[8] C. Wong, E. Yang, X.-T. Yan, and D. Gu. Autonomous robots for harsh environments: a holistic overview of current solutions and ongoing challenges. *Systems Science & Control Engineering* 6.1 (2018), pp. 213–219. DOI: 10.1080/21642583.2018.1477634.

[9] L. Wijayathunga, A. Rassau, and D. Chai. Challenges and Solutions for Autonomous Ground Robot Scene Understanding and Navigation in Unstructured Outdoor Environments: A Review. *Applied Sciences* 13.17 (2023). DOI: 10.3390/app13179877.

[10] D. C. Guastella and G. Muscato. Learning-Based Methods of Perception and Navigation for Ground Vehicles in Unstructured Environments: A Review. *Sensors* 21.1 (2021). DOI: 10.3390/s21010073.

[11] D. Kragic, J. Gustafson, H. Karaoguz, P. Jensfelt, and R. Krug. Interactive, Collaborative Robots: Challenges and Opportunities. *Proceedings of the Twenty-Seventh International Joint Conference on Artificial Intelligence, IJCAI-18*. International Joint Conferences on Artificial Intelligence Organization, 2018, pp. 18–25. DOI: 10.24963/ijcai.2018/3.

[12] K. Darvish, L. Penco, J. Ramos, R. Cisneros, J. Pratt, E. Yoshida, S. Ivaldi, and D. Pucci. Teleoperation of Humanoid Robots: A Survey. *IEEE Transactions on Robotics* 39.3 (2023), pp. 1706–1727. DOI: 10.1109/TRO.2023.3236952.

[13] O. Brock, J. Park, and M. Toussaint. Mobility and Manipulation. *Springer Handbook of Robotics*. Ed. by B. Siciliano and O. Khatib. Cham: Springer International Publishing, 2016, pp. 1007–1036. DOI: 10.1007/978-3-319-32552-1_40.

[14] E. Ackerman. Robots Conquer the Underground: What Darpa's Subterranean Challenge Means for the Future of Autonomous Robots. *IEEE Spectrum* 59.5 (2022), pp. 30–37. DOI: 10.1109/MSPEC.2022.9771355.

[15] G. Li, T.-W. Wong, B. Shih, C. Guo, L. Wang, J. Liu, T. Wang, X. Liu, J. Yan, B. Wu, F. Yu, Y. Chen, Y. Liang, Y. Xue, C. Wang, S. He, L. Wen, M. Tolley, A.-M. Zhang, and T. Li. Bioinspired soft robots for deep-sea exploration. *Nature Communications* 14 (2023). DOI: 10.1038/s41467-023-42882-3.

[16] K. Hambuchen, J. Marquez, and T. Fong. A Review of NASA Human-Robot Interaction in Space. *Current Robotics Reports* 2.3 (2021), pp. 265–272. DOI: 10.1007/s43154-021-00062-5.

[17] D. Kim, D. Carballo, J. Di Carlo, B. Katz, G. Bledt, B. Lim, and S. Kim. Vision Aided Dynamic Exploration of Unstructured Terrain with a Small-Scale Quadruped Robot. *2020 IEEE International Conference on Robotics and Automation (ICRA)*. 2020, pp. 2464–2470. DOI: 10.1109/ICRA40945.2020.9196777.

[18] T. Bandyopadhyay, R. Steindl, F. Talbot, N. Kottege, R. Dungavell, B. Wood, J. Barker, K. Hoehn, and A. Elfes. Magneto: A Versatile Multi-Limbed Inspection Robot. *2018 IEEE/RSJ International Conference on Intelligent Robots and Systems (IROS)*. 2018, pp. 2253–2260. DOI: 10.1109/IROS.2018.8593891.

[19] O. Menendez, F. A. Auat Cheein, M. Perez, and S. Kouro. Robotics in Power Systems: Enabling a More Reliable and Safe Grid. *IEEE Industrial Electronics Magazine* 11.2 (2017), pp. 22–34. DOI: 10.1109/MIE.2017.2686458.

[20] R. R. Murphy, S. Tadokoro, and A. Kleiner. Disaster Robotics. *Springer Handbook of Robotics*. Ed. by B. Siciliano and O. Khatib. Cham: Springer International Publishing, 2016, pp. 1577–1604. DOI: 10.1007/978-3-319-32552-1_60.

[21] H. Hildmann and E. Kovacs. Review: Using Unmanned Aerial Vehicles (UAVs) as Mobile Sensing Platforms (MSPs) for Disaster Response, Civil Security and Public Safety. *Drones* 3.3 (2019). DOI: 10.3390/drones3030059.

[22] H.-H. Wei, Y. Zhang, X. Sun, J. Chen, and S. Li. Intelligent Robots and Human-Robot Collaboration in the Construction Industry: A Review. *Journal of Intelligent Construction* 1.1 (2023), pp. 1–12. DOI: 10.26599/JIC.2023.9180002.

[23] P. Gonzalez de Santos, J. Cobano, E. Garcia, J. Estremera, and M. Armada. A six-legged robot-based system for humanitarian demining missions. *Mechatronics* 17.8 (2007), pp. 417–430. DOI: 10.1016/j.mechatronics.2007.04.014.

[24] I. Vitanov, I. Farkhatdinov, B. Denoun, F. Palermo, A. Otaran, J. Brown, B. Omarali, T. Abrar, M. Hansard, C. Oh, S. Poslad, C. Liu, H. Godaba, K. Zhang, L. Jamone, and K. Althoefer. A Suite of Robotic Solutions for Nuclear Waste Decommissioning. *Robotics* 10.4 (2021). DOI: 10.3390/robotics10040112.

[25] B. Burger, P. M. Maffettone, V. V. Gusev, C. M. Aitchison, Y. Bai, X. Wang, X. Li, B. M. Alston, B. Li, R. Clowes, N. Rankin, B. Harris, R. S. Sprick, and A. I. Cooper. A mobile robotic chemist. *Nature* 583.7815 (2020), pp. 237–241. DOI: 10.1038/s41586-020-2442-2.

[26] Q. Li, F. Cicirelli, A. Vinci, A. Guerrieri, W. Qi, and G. Fortino. Quadruped Robots: Bridging Mechanical Design, Control, and Applications. *Robotics* 14.5 (2025). DOI: 10.3390/robotics14050057.

[27] M. H. Raibert. Legged Robots That Balance. MIT Press series in artificial intelligence. Cambridge, MA: MIT Press, 1986, p. 233. URL: https://mitpress.mit.edu/9780262681193/legged-robots-that-balance/.

[28] R. S. Mosher. Exploring the Potential of a Quadruped. *SAE Transactions* 78 (1969), pp. 836–843. URL: https://www.jstor.org/stable/44564284.

[29] S. Hirose and K. Kato. Study on quadruped walking robot in Tokyo Institute of Technology—Past, present and future. *Proceedings of the 2000 IEEE International Conference on Robotics and Automation (ICRA)*. Vol. 1. 2000, pp. 414–419. DOI: 10.1109/ROBOT.2000.844091.

[30] P. Biswal and P. K. Mohanty. Development of quadruped walking robots: A review. *Ain Shams Engineering Journal* 12.2 (2021), pp. 2017–2031. DOI: 10.1016/j.asej.2020.11.005.

[31] M. Raibert, K. Blankespoor, G. Nelson, and R. Playter. BigDog, the Rough-Terrain Quadruped Robot. *IFAC Proceedings Volumes* 41.2 (2008). 17th IFAC World Congress, pp. 10822–10825. DOI: 10.3182/20080706-5-KR-1001.01833.

[32] C. Semini, N. G. Tsagarakis, E. Guglielmino, M. Focchi, F. Cannella, and D. G. Caldwell. Design of HyQ – a Hydraulically and Electrically Actuated Quadruped Robot. *Proceedings of the Institution of Mechanical Engineers, Part I: Journal of Systems and Control Engineering* 225.6 (2011), pp. 831–849. DOI: 10.1177/0959651811402275.

[33] C. Semini, V. Barasuol, J. Goldsmith, M. Frigerio, M. Focchi, Y. Gao, and D. G. Caldwell. Design of the Hydraulically Actuated, Torque-Controlled Quadruped Robot HyQ2Max. *IEEE/ASME Transactions on Mechatronics* 22.2 (2017), pp. 635–646. DOI: 10.1109/TMECH.2016.2616284.

[34] C. Semini, V. Barasuol, M. Focchi, C. Boelens, M. Emara, S. Casella, O. Villarreal, R. Orsolino, G. Fink, S. Fahmi, G. Medrano-Cerda, D. Sangiah, J. Lesniewski, K. Fulton, M. Donadon, M. Baker, and D. G. Caldwell. Brief introduction to the quadruped robot HyQReal. *Italian Conference on Robotics and Intelligent Machines (I-RIM)*. 2019. URL: `https://iris.unitn.it/retrieve/f78624e9-153b-4322-964a-388de319c0e7/semini19irim.pdf`.

[35] W. Roozing, Z. Ren, and N. G. Tsagarakis. Design of a Novel 3-DoF Leg with Series and Parallel Compliant Actuation for Energy Efficient Articulated Robots. *2018 IEEE International Conference on Robotics and Automation (ICRA)*. 2018, pp. 6068–6075. DOI: `10.1109/ICRA.2018.8460493`.

[36] D. W. Haldane, M. M. Plecnik, J. K. Yim, and R. S. Fearing. Robotic vertical jumping agility via series-elastic power modulation. *Science Robotics* 1.1 (2016), eaag2048. DOI: `10.1126/scirobotics.aag2048`.

[37] F. Negrello, M. Garabini, M. G. Catalano, J. Malzahn, D. G. Caldwell, A. Bicchi, and N. G. Tsagarakis. A modular compliant actuator for emerging high performance and fall-resilient humanoids. *2015 IEEE-RAS 15th International Conference on Humanoid Robots (Humanoids)*. 2015, pp. 414–420. DOI: `10.1109/HUMANOIDS.2015.7363567`.

[38] G. A. Pratt and M. M. Williamson. Series Elastic Actuators. *Proceedings of the 1995 IEEE/RSJ International Conference on Intelligent Robots and Systems: Human Robot Interaction and Cooperative Robots*. Vol. 1. 1995, pp. 399–406. DOI: `10.1109/IROS.1995.525827`.

[39] P. M. Wensing, A. Wang, S. Seok, D. M. Otten, J. H. Lang, and S. Kim. Proprioceptive Actuator Design in the MIT Cheetah: Impact Mitigation and High-Bandwidth Physical Interaction for Dynamic Legged Robots. *IEEE Transactions on Robotics* 33.3 (2017), pp. 509–522. DOI: `10.1109/TRO.2016.2640183`.

[40] M. Hutter. StarlETH & Co.: Design and Control of Legged Robots with Compliant Actuation. PhD thesis. ETH Zurich, 2013. DOI: `10.3929/ethz-a-009915229`.

[41] M. Hutter, C. Gehring, D. Jud, A. Lauber, C. D. Bellicoso, V. Tsounis, J. Hwangbo, K. Bodie, P. Fankhauser, M. Bloesch, R. Diethelm, S. Bachmann, A. Melzer, and M. Hoepflinger. ANYmal - a Highly Mobile and Dynamic Quadrupedal Robot. *2016 IEEE/RSJ International Conference on Intelligent Robots and Systems (IROS)*. 2016, pp. 38–44. DOI: `10.1109/IROS.2016.7758092`.

[42] M. Hutter, C. Gehring, A. Lauber, F. Gunther, C. D. Bellicoso, V. Tsounis, P. Fankhauser, R. Diethelm, S. Bachmann, M. Bloesch, H. Kolvenbach, M. Bjelonic, L. Isler, and K. Meyer. ANYmal - Toward Legged Robots for Harsh Environments. *Advanced Robotics* 31.17 (2017), pp. 918–931. DOI: 10.1080/01691864.2017.1378591.

[43] N. Kashiri, L. Baccelliere, L. Muratore, A. Laurenzi, Z. Ren, E. M. Hoffman, M. Kamedula, G. F. Rigano, J. Malzahn, S. Cordasco, et al. CENTAURO: A Hybrid Locomotion and High Power Resilient Manipulation Platform. *IEEE Robotics and Automation Letters* 4.2 (2019), pp. 1595–1602. DOI: 10.1109/LRA.2019.2896758.

[44] A. Singh, N. Kashiri, and N. Tsagarakis. Design of a Quasi-Direct-Drive Actuator for Dynamic Motions. *Proceedings* 64.1 (2020). DOI: 10.3390/IeCAT2020-08516.

[45] B. G. Katz. A Low Cost Modular Actuator for Dynamic Robots. S.M. thesis. Cambridge, MA: Massachusetts Institute of Technology, 2018. URL: https://hdl.handle.net/1721.1/118671.

[46] G. Bledt, M. J. Powell, B. Katz, J. Di Carlo, P. M. Wensing, and S. Kim. MIT Cheetah 3: Design and Control of a Robust, Dynamic Quadruped Robot. *2018 IEEE/RSJ International Conference on Intelligent Robots and Systems (IROS).* 2018, pp. 2245–2252. DOI: 10.1109/IROS.2018.8593885.

[47] S. Kim and P. M. Wensing. Design of Dynamic Legged Robots. *Foundations and Trends in Robotics* 5.2 (2017), pp. 117–190. DOI: 10.1561/2300000044.

[48] B. Katz, J. Di Carlo, and S. Kim. Mini Cheetah: A Platform for Pushing the Limits of Dynamic Quadruped Control. *2019 International Conference on Robotics and Automation (ICRA).* 2019, pp. 6295–6301. DOI: 10.1109/ICRA.2019.8793865.

[49] P. Arm, R. Zenkl, P. Barton, L. Beglinger, A. Dietsche, L. Ferrazzini, E. Hampp, J. Hinder, C. Huber, D. Schaufelberger, F. Schmitt, B. Sun, B. Stolz, H. Kolvenbach, and M. Hutter. SpaceBok: A Dynamic Legged Robot for Space Exploration. *2019 International Conference on Robotics and Automation (ICRA).* 2019, pp. 6288–6294. DOI: 10.1109/ICRA.2019.8794136.

[50] S. Seok, A. Wang, M. Y. Chuah, D. J. Hyun, J. Lee, D. M. Otten, J. H. Lang, and S. Kim. Design Principles for Energy-Efficient Legged Locomotion and Implementation on the MIT Cheetah Robot. *IEEE/ASME Transactions on Mechatronics* 20.3 (2015), pp. 1117–1129. DOI: 10.1109/TMECH.2014.2339013.

[51] Y.-H. Shin, S. Hong, S. Woo, J. Choe, H. Son, G. Kim, J.-H. Kim, K. Lee, J. Hwangbo, and H.-W. Park. Design of KAIST HOUND, a Quadruped Robot Platform for Fast and Efficient Locomotion with Mixed-Integer Nonlinear Optimization of a Gear Train. *2022 International Conference on Robotics and Automation (ICRA)*. 2022, pp. 6614–6620. DOI: 10.1109/ICRA46639.2022.9811755.

[52] G. Valsecchi, N. Rudin, L. Nachtigall, K. Mayer, F. Tischhauser, and M. Hutter. Barry: A High-Payload and Agile Quadruped Robot. *IEEE Robotics and Automation Letters* 8.11 (2023), pp. 6939–6946. DOI: 10.1109/LRA.2023.3313923.

[53] S. D. Potter, Z. J. Jackowski, and A. Young. "Screw Actuator for a Legged Robot". US20180172121A1 (United States). Filed 2016-12-15; granted 2019-04-09; adjusted expiration 2037-03-03. 2018. URL: https://patents.google.com/patent/US20180172121A1.

[54] F. Grimminger, A. Meduri, M. Khadiv, J. Viereck, M. Wüthrich, M. Naveau, V. Berenz, S. Heim, F. Widmaier, T. Flayols, J. Fiene, A. Badri-Spröwitz, and L. Righetti. An Open Torque-Controlled Modular Robot Architecture for Legged Locomotion Research. *IEEE Robotics and Automation Letters* 5.2 (2020), pp. 3650–3657. DOI: 10.1109/LRA.2020.2976639.

[55] N. Kau, A. Schultz, N. Ferrante, and P. Slade. Stanford Doggo: An Open-Source, Quasi-Direct-Drive Quadruped. *2019 International Conference on Robotics and Automation (ICRA)*. 2019, pp. 6309–6315. DOI: 10.1109/ICRA.2019.8794436.

[56] D. Dholakiya, S. Bhattacharya, A. Gunalan, A. Singla, S. Bhatnagar, B. Amrutur, A. Ghosal, and S. Kolathaya. Design, Development and Experimental Realization of A Quadrupedal Research Platform: Stoch. *2019 5th International Conference on Control, Automation and Robotics (ICCAR)*. 2019, pp. 229–234. DOI: 10.1109/ICCAR.2019.8813480.

[57] A. Singh, B. G. Goswami, K. Nehete, and S. N. Y. Kolathaya. A Chain-Driven, Sandwich-Legged Quadruped Robot: Design and Experimental Analysis. *arXiv preprint* (2025). DOI: 10.48550/arXiv.2503.14255. arXiv: 2503.14255 [cs.RO].

[58] T. Asfour, L. Kaul, M. Wächter, S. Ottenhaus, P. Weiner, S. Rader, R. Grimm, Y. Zhou, M. Grotz, F. Paus, D. Shingarey, and H. Haubert. ARMAR-6: A Collaborative Humanoid Robot for Industrial Environments. *2018 IEEE-RAS 18th International Conference on Humanoid Robots (Humanoids)*. 2018, pp. 447–454. DOI: 10.1109/HUMANOIDS.2018.8624966.

[59] Y. Wu, P. Balatti, M. Lorenzini, F. Zhao, W. Kim, and A. Ajoudani. A Teleoperation Interface for Loco-Manipulation Control of Mobile Collaborative Robotic Assistant. *IEEE Robotics and Automation Letters* 4.4 (2019), pp. 3593–3600. DOI: 10.1109/LRA.2019.2928757.

[60] Z. Samadikhoshkho, K. Zareinia, and F. Janabi-Sharifi. A Brief Review on Robotic Grippers Classifications. *2019 IEEE Canadian Conference of Electrical and Computer Engineering (CCECE)*. 2019, pp. 1–4. DOI: 10.1109/CCECE.2019.8861780.

[61] J. Hernandez et al. Current Designs of Robotic Arm Grippers: A Comprehensive Systematic Review. *Robotics* 12.1 (2023). DOI: 10.3390/robotics12010005.

[62] E. Brown, N. Rodenberg, J. Amend, A. Mozeika, E. Steltz, M. R. Zakin, H. Lipson, and H. M. Jaeger. Universal Robotic Gripper Based on the Jamming of Granular Material. *Proceedings of the National Academy of Sciences* 107.44 (2010), pp. 18809–18814. DOI: 10.1073/pnas.1003250107.

[63] C. Piazza, G. Grioli, M. Catalano, and A. Bicchi. A Century of Robotic Hands. *Annual Review of Control, Robotics, and Autonomous Systems* 2.1 (2019), pp. 1–32. DOI: 10.1146/annurev-control-060117-105003.

[64] F. Negrello, H. S. Stuart, and M. G. Catalano. Hands in the Real World. *Frontiers in Robotics and AI* 6 (2020). DOI: 10.3389/frobt.2019.00147.

[65] M. Catalano et al. From Soft to Adaptive Synergies: The Pisa/IIT SoftHand. Springer Int. Publishing, 2016. Chap. 8, pp. 101–125. DOI: 10.1007/978-3-319-26706-7_8.

[66] R. Deimel and O. Brock. A novel type of compliant and underactuated robotic hand for dexterous grasping. *The International Journal of Robotics Research* 35.1-3 (2016), pp. 161–185. DOI: 10.1177/0278364915592961.

[67] Z. Ren, N. Kashiri, C. Zhou, and N. G. Tsagarakis. HERI II: A Robust and Flexible Robotic Hand Based on Modular Finger Design and Underactuation Principles. *2018 IEEE/RSJ International Conference on Intelligent Robots and Systems (IROS)*. 2018, pp. 1449–1455. DOI: 10.1109/IROS.2018.8594507.

[68] C.-H. Liu, F.-M. Chung, Y. Chen, C.-H. Chiu, and T.-L. Chen. Optimal Design of a Motor-Driven Three-Finger Soft Robotic Gripper. *IEEE/ASME Trans. Mechatronics* 25.4 (2020), pp. 1830–1840. DOI: 10.1109/TMECH.2020.2997743.

[69] J.-H. Bae et al. Development of a low cost anthropomorphic robot hand with high capability. *IEEE/RSJ Int. Conf. Intell. Robots Syst.* 2012, pp. 4776–4782. DOI: 10.1109/IROS.2012.6386063.

[70] S. W. Ruehl, C. Parlitz, G. Heppner, A. Hermann, A. Roennau, and R. Dillmann. Experimental evaluation of the Schunk 5-Finger gripping hand for grasping tasks. *IEEE Int. Conf. on Robotics and Biomimetics* (2014), pp. 2465–2470. DOI: 10.1109/ROBIO.2014.7090710.

[71] G. Walck, U. Cupcic, T. O. Duran, and V. Perdereau. A Case Study of ROS Software Re-usability for Dexterous In-Hand Manipulation. *Journal of Software Engineering in Robotics* (2014). URL: https://hdl.handle.net/10446/87663.

[72] C. Schwarke, V. Klemm, M. van der Boon, M. Bjelonic, and M. Hutter. Curiosity-Driven Learning of Joint Locomotion and Manipulation Tasks. *Proceedings of the 7th Conference on Robot Learning*. Ed. by J. Tan, M. Toussaint, and K. Darvish. Vol. 229. Proceedings of Machine Learning Research. PMLR, 2023, pp. 2594–2610. DOI: 10.3929/ethz-b-000650515.

[73] K. Telegenov, Y. Tlegenov, and A. Shintemirov. A Low-Cost Open-Source 3-D-Printed Three-Finger Gripper Platform for Research and Educational Purposes. *IEEE Access* 3 (2015), pp. 638–647. DOI: 10.1109/ACCESS.2015.2433937.

[74] C. Liu, A. Moncada, H. Matusik, D. I. Erus, and D. Rus. A Modular Bio-inspired Robotic Hand with High Sensitivity. *IEEE Int. Conf. Soft Robotics*. 2023, pp. 1–7. DOI: 10.1109/RoboSoft55895.2023.10121946.

[75] G. Maeda, N. Fukaya, and S.-i. Maeda. F1 Hand: A Versatile Fixed-Finger Gripper for Delicate Teleoperation and Autonomous Grasping. *IEEE Robotics and Automation Letters* 7.3 (2022), pp. 6734–6741. DOI: 10.1109/LRA.2022.3177293.

[76] R. R. Ma, A. Spiers, and A. M. Dollar. M2 Gripper: Extending the Dexterity of a Simple, Underactuated Gripper. *Advances in Reconfigurable Mechanisms and Robots II*. Ed. by X. Ding, X. Kong, and J. S. Dai. Cham: Springer International Publishing, 2016, pp. 795–805. DOI: 10.1007/978-3-319-23327-7_68.

[77] Z. Kappassov, J.-A. Corrales, and V. Perdereau. Tactile sensing in dexterous robot hands — Review. *Robotics and Autonomous Systems* 74 (2015), pp. 195–220. DOI: 10.1016/j.robot.2015.07.015.

[78] J. M. Romano, K. Hsiao, G. Niemeyer, S. Chitta, and K. J. Kuchenbecker. Human-Inspired Robotic Grasp Control With Tactile Sensing. *IEEE Trans. on Robotics* 27.6 (2011), pp. 1067–1079. DOI: 10.1109/TRO.2011.2162271.

[79] A. Yamaguchi and C. G. Atkeson. Combining Finger Vision and Optical Tactile Sensing: Reducing and Handling Errors While Cutting Vegetables. *2016 IEEE-RAS 16th International Conference on Humanoid Robots (Humanoids)*. 2016, pp. 1045–1051. DOI: 10.1109/HUMANOIDS.2016.7803400.

[80] T. Narita, S. Nagakari, W. Conus, T. Tsuboi, and K. Nagasaka. Theoretical Derivation and Realization of Adaptive Grasping Based on Rotational Incipient Slip Detection. *IEEE Int. Conf. Robot. Autom.* 2020, pp. 531–537. DOI: 10.1109/ICRA40945.2020.9196615.

[81] P. Cigliano, V. Lippiello, F. Ruggiero, and B. Siciliano. Robotic Ball Catching with an Eye-in-Hand Single-Camera System. *IEEE Transactions on Control Systems Technology* 23.5 (2015), pp. 1657–1671. DOI: 10.1109/TCST.2014.2380175.

[82] F. Hundhausen, R. Grimm, L. Stieber, and T. Asfour. Fast Reactive Grasping with In-Finger Vision and In-Hand FPGA-accelerated CNNs. *IEEE/RSJ Int. Conf. Intell. Robots Syst.* 2021, pp. 6825–6832. DOI: 10.1109/IROS51168.2021.9636043.

[83] A. Cirillo, G. Laudante, and S. Pirozzi. Proximity Sensor for Thin Wire Recognition and Manipulation. *Machines* 9.9 (2021), p. 188. DOI: 10.3390/machines9090188.

[84] J. Mejia, V. Dean, T. Hellebrekers, and A. Gupta. Hearing Touch: Audio-Visual Pretraining for Contact-Rich Manipulation. *Proceedings of the 2024 IEEE International Conference on Robotics and Automation (ICRA)*. 2024, pp. 6912–6919. DOI: 10.1109/ICRA57147.2024.10611305.

[85] D. Tor, L. Bertoni, F. Fusaro, N. Tsagarakis, and L. Muratore. ROS End-Effector: A Hardware-Agnostic Software and Control Framework for Robotic End-Effectors. *Journal of Intelligent & Robotic Systems* 108.4 (2023), p. 70. DOI: 10.1007/s10846-023-01911-5.

[86] B. Denoun, M. Hansard, B. León, and L. Jamone. Statistical Stratification and Benchmarking of Robotic Grasping Performance. *IEEE Trans. on Robotics* 39.6 (2023), pp. 4539–4551. DOI: 10.1109/TRO.2023.3306613.

[87] P. Sotiropoulos et al. A Benchmarking Framework for Systematic Evaluation of Compliant Under-Actuated Soft End Effectors in an Industrial Context. *IEEE-RAS Int. Conf. Humanoid Robots*. 2018, pp. 280–283. DOI: 10.1109/HUMANOIDS.2018.8624924.

[88] A. B. Clark, L. Cramphorn-Neal, M. Rachowiecki, and A. Gregg-Smith. Household Clothing Set and Benchmarks for Characterising End-Effector Cloth Manipulation. *IEEE Int. Conf. Robot. Autom.* 2023, pp. 9211–9217. DOI: 10.1109/ICRA48891.2023.10161398.

[89] J. Falco, K. Van Wyk, S. Liu, and S. Carpin. Grasping the Performance: Facilitating Replicable Performance Measures via Benchmarking and Standardized Methodologies. *IEEE Robot. Autom. Mag.* 22.4 (2015), pp. 125–136. DOI: 10.1109/MRA.2015.2460891.

[90] M. Sujan Kumar and R. Deivanathan. Effect of process parameters on drilling — An overview. *Materials Today: Proceedings* 46 (2021). 28th International Conference on Processing and Fabrication of Advanced Materials (PFAM28), pp. 1401–1406. DOI: 10.1016/j.matpr.2021.02.574.

[91] S. M. Wu. An End Effector for Robotic Drilling. *Handbook of High-Speed Machining Technology*. Ed. by R. I. King. Boston, MA: Springer US, 1985, pp. 317–326. DOI: 10.1007/978-1-4684-6421-4_14.

[92] A. J. Fields. The analysis and design of a flexible robotic fixturing and drilling system. M.S. thesis. Cambridge, MA: Massachusetts Institute of Technology, 1986. URL: https://hdl.handle.net/1721.1/151028.

[93] A. Verl, A. Valente, S. Melkote, C. Brecher, E. Ozturk, and L. T. Tunc. Robots in machining. *CIRP Annals* 68.2 (2019), pp. 799–822. DOI: 10.1016/j.cirp.2019.05.009.

[94] S. H. Kim, E. Nam, T. I. Ha, S.-H. Hwang, J. H. Lee, S.-H. Park, and B.-K. Min. Robotic Machining: A Review of Recent Progress. *International Journal of Precision Engineering and Manufacturing* 20.9 (2019), pp. 1629–1642. DOI: 10.1007/s12541-019-00187-w.

[95] S. Bi and J. Liang. Robotic Drilling System for Titanium Structures. *The International Journal of Advanced Manufacturing Technology* 54.5 (2011), pp. 767–774. DOI: 10.1007/s00170-010-2962-2.

[96] J. Atkinson, J. Hartmann, S. Jones, and P. Gleeson. Robotic Drilling System for 737 Aileron. *Aerospace Technology Conference and Exposition, September 17, 2007*. 2007-01-3821. SAE International, 2007. DOI: 10.4271/2007-01-3821.

[97] R. DeVlieg, K. Sitton, E. Feikert, and J. Inman. ONCE (ONe-Sided Cell End Effector) Robotic Drilling System. *Presented at the 2002 SAE Automated Fastening Conference & Exhibition, September 30, 2002*. 2002-01-2626. SAE International, 2002. DOI: 10.4271/2002-01-2626.

[98] B. Hempstead, R. DeVlieg, R. Mistry, and M. Sheridan. Drill and Drive End Effector. *SAE Technical Paper* 2001-01-2576 (2001). Presented at the 2001 Automated Fastening Conference & Exposition, published September 10, 2001. DOI: 10.4271/2001-01-2576.

[99] Y. Liu, Z. Shi, P. Yuan, D. Chen, M. Lin, and Z. Li. A visual positioning and measurement system for robotic drilling. *2016 IEEE 14th International Workshop on Advanced Motion Control (AMC)*. 2016, pp. 461–466. DOI: 10.1109/AMC.2016.7496393.

[100] J. Liang and S. Bi. Design and Experimental Study of an End Effector for Robotic Drilling. *The International Journal of Advanced Manufacturing Technology* 50.1 (2010), pp. 399–407. DOI: 10.1007/s00170-009-2494-9.

[101] A. Frommknecht, J. Kuehnle, I. Effenberger, and S. Pidan. Multi-Sensor Measurement System for Robotic Drilling. *Robotics and Computer-Integrated Manufacturing* 47 (2017). SI: FAIM 2015, pp. 4–10. DOI: 10.1016/j.rcim.2017.01.002.

[102] P. Maurice, V. Padois, Y. Measson, and P. Bidaud. Human-Oriented Design of Collaborative Robots. *International Journal of Industrial Ergonomics* 57 (2017), pp. 88–102. DOI: 10.1016/j.ergon.2016.11.011.

[103] A. Madani, P. P. Niaz, B. Guler, Y. Aydin, and C. Basdogan. Robot-Assisted Drilling on Curved Surfaces with Haptic Guidance under Adaptive Admittance Control. *2022 IEEE/RSJ International Conference on Intelligent Robots and Systems (IROS)*. 2022, pp. 3723–3730. DOI: 10.1109/IROS47612.2022.9982000.

[104] L. Peternel, L. Rozo, D. Caldwell, and A. Ajoudani. A Method for Derivation of Robot Task-Frame Control Authority from Repeated Sensory Observations. *IEEE Robotics and Automation Letters* 2.2 (2017), pp. 719–726. DOI: 10.1109/LRA.2017.2651368.

[105] X. Wang, S. Dong, P. Prajapati, O. Kravchenko, and K. Kaipa. Combining Force-Controlled Adaptive Feedrate and Human-Robot Collaborative Strategies to Handle Non-Repetitive Micro-Drilling Tasks. *2020 IEEE 16th International Conference on Automation Science and Engineering (CASE)*. 2020, pp. 1602–1607. DOI: 10.1109/CASE48305.2020.9216893.

[106] R. Berenstein, A. Wallach, P. E. Moudio, P. Cuellar, and K. Goldberg. An Open-Access Passive Modular Tool Changing System for Mobile Manipulation Robots. *2018 IEEE 14th International Conference on Automation Science and Engineering (CASE)*. 2018, pp. 592–598. DOI: 10.1109/COASE.2018.8560398.

[107] V. Gurau, B. Ragland, D. Cox, A. Michaud, and L. Busby. Robot Operations for Pine Tree Resin Collection. *Technologies* 9.4 (2021). DOI: 10.3390/technologies9040079.

[108] D. Rempel, D. Star, A. Barr, B. Gibbons, and I. Janowitz. A New Method for Overhead Drilling. *Ergonomics* 52.12 (2009). PMID: 19941190, pp. 1584–1589. DOI: 10.1080/00140130903254338.

[109] C. Brosque, G. Skeie, J. Örn, J. Jacobson, T. Lau, and M. Fischer. Comparison of Construction Robots and Traditional Methods for Drilling, Drywall, and Layout Tasks. *2020 International Congress on Human-Computer Interaction, Optimization and Robotic Applications (HORA)*. 2020, pp. 1–14. DOI: 10.1109/HORA49412.2020.9152871.

[110] F. Liu, M. Trkov, J. Yi, and N. Gucunski. Modeling of Pure Percussive Drilling for Autonomous Robotic Bridge Decks Rehabilitation. *2013 IEEE International Conference on Automation Science and Engineering (CASE)*. 2013, pp. 1063–1068. DOI: 10.1109/CoASE.2013.6654053.

[111] C. Guo and J. Yi. Vibration Suppression Control in Robotic Percussive Drilling. *2018 Annual American Control Conference (ACC)*. 2018, pp. 3702–3707. DOI: 10.23919/ACC.2018.8431813.

[112] A. B. Okon. Mars Science Laboratory Drill. *Proceedings of the 40th Aerospace Mechanisms Symposium*. NASA Technical Report 20100021931. Pasadena, CA, United States: NASA Kennedy Space Center, 2010. URL: https://ntrs.nasa.gov/citations/20100021931.

[113] S. Seok, A. Wang, D. Otten, and S. Kim. Actuator Design for High Force Proprioceptive Control in Fast Legged Locomotion. *2012 IEEE/RSJ International Conference on Intelligent Robots and Systems*. 2012, pp. 1970–1975. DOI: 10.1109/IROS.2012.6386252.

[114] M. Hutter, C. D. Remy, M. A. Hoepflinger, and R. Siegwart. High Compliant Series Elastic Actuation for the Robotic Leg ScarlETH. *Field Robotics*, pp. 507–514. DOI: 10.1142/9789814374286_0059.

[115] C. Semini, N. G. Tsagarakis, B. Vanderborght, Y. Yang, and D. G. Caldwell. HyQ - Hydraulically Actuated Quadruped Robot: Hopping Leg Prototype. *2008 2nd IEEE RAS & EMBS International Conference on Biomedical Robotics and Biomechatronics*. 2008, pp. 593–599. DOI: 10.1109/BIOROB.2008.4762913.

[116] G. Brantner and O. Khatib. Controlling Ocean One: Human–Robot Collaboration for Deep-Sea Manipulation. *Journal of Field Robotics* 38.1 (2021), pp. 28–51. DOI: 10.1002/rob.21960.

[117] J. K. A. Langowski, P. Sharma, and A. Leylavi Shoushtari. In the Soft Grip of Nature. *Science Robotics* 5.49 (2020), eabd9120. DOI: 10.1126/scirobotics.abd9120.

[118] Y. T. Tefera, I. Sarakoglou, S. N. Deore, Y. Kim, V. Barasuol, M. Villa, S. Anastasi, D. G. Caldwell, N. Tsagarakis, C. Semini, and N. Deshpande. ROBOT TELEOPERATIVO: Collaborative Cybernetic Systems for Immersive Remote Teleoperation. *2024 IEEE Conference on Telepresence*. 2024, pp. 1–4. DOI: 10.1109/Telepresence63209.2024.10841491.

[119] F. Rollo, G. Raiola, A. Zunino, N. Tsagarakis, and A. Ajoudani. Artifacts Mapping: Multi-Modal Semantic Mapping for Object Detection and 3D Localization. *2023 European Conference on Mobile Robots (ECMR)*. 2023, pp. 1–8. DOI: 10.1109/ECMR59166.2023.10256373.

[120] E. Del Bianco, N. Kashiri, M. Roveri, and N. G. Tsagarakis. Mechanical Design of an Agile Quadruped Robot. *European Robotics Forum 2024*. Ed. by C. Secchi and L. Marconi. Cham: Springer Nature Switzerland, 2024, pp. 58–63. DOI: 10.1007/978-3-031-76424-0_11.

[121] E. Romiti, J. Malzahn, N. Kashiri, F. Iacobelli, M. Ruzzon, A. Laurenzi, E. M. Hoffman, L. Muratore, A. Margan, L. Baccelliere, et al. Toward a Plug-and-Work Reconfigurable Cobot. *IEEE/ASME Transactions on Mechatronics* 27.5 (2022), pp. 3219–3231. DOI: 10.1109/TMECH.2021.3106043.

[122] N. Kashiri, A. Abate, S. J. Abram, P. J. Clary, M. Daley, S. Faraji, R. Furnemont, M. Garabini, H. Geyer, A. M. Grabowski, J. Hurst, J. Malzahn, G. Mathijssen, C. D. Remy, W. Roozing, M. Shahbazi, S. N. Simha, J. Song, S. Stramigioli, and N. G. Tsagarakis. An Overview on Principles for Energy Efficient Robot Locomotion. *Frontiers in Robotics and AI* 5 (2018), p. 129. DOI: 10.3389/frobt.2018.00129.

[123] L. Muratore, A. Laurenzi, A. De Luca, L. Bertoni, D. Torielli, L. Baccelliere, E. Del Bianco, and N. G. Tsagarakis. A Unified Multimodal Interface for the RELAX High-Payload Collaborative Robot. *Sensors* 23.18 (2023). DOI: 10.3390/s23187735.

[124] N. Kashiri, A. Ajoudani, D. G. Caldwell, and N. G. Tsagarakis. Evaluation of Hip Kinematics Influence on the Performance of a Quadrupedal Robot Leg. *Proceedings of the 13th International Conference on Informatics in Control, Automation and Robotics (ICINCO 2016).* Lisbon, Portugal: SCITEPRESS, 2016, pp. 205–212. DOI: 10.5220/0005986502050212.

[125] E. Del Bianco, D. Torielli, F. Rollo, D. Gasperini, A. Laurenzi, L. Baccelliere, L. Muratore, M. Roveri, and N. G. Tsagarakis. A High-Force Gripper with Embedded Multimodal Sensing for Powerful and Perception Driven Grasping. *2024 IEEE-RAS 23rd International Conference on Humanoid Robots (Humanoids).* 2024, pp. 149–156. DOI: 10.1109/Humanoids58906.2024.10769951.

[126] M. Quigley, K. Conley, B. Gerkey, J. Faust, T. Foote, J. Leibs, R. Wheeler, and A. Y. Ng. ROS: an open-source Robot Operating System. *ICRA Workshop on Open Source Software.* Kobe, Japan, 2009, p. 5. URL: https://ai.stanford.edu/~mquigley/papers/icra2009-ros.pdf.

[127] J. Redmon, S. Divvala, R. Girshick, and A. Farhadi. You Only Look Once: Unified, Real-Time Object Detection. *2016 IEEE Conference on Computer Vision and Pattern Recognition (CVPR).* 2016, pp. 779–788. DOI: 10.1109/CVPR.2016.91.

[128] E. Del Bianco, F. Rollo, M. Roveri, and N. G. Tsagarakis. Smart Drill: an Autonomous Drilling End-Effector with Embedded Sensing and Intelligence for Mobile and Collaborative Robots. *2024 IEEE 20th International Conference on Automation Science and Engineering (CASE).* 2024, pp. 508–513. DOI: 10.1109/CASE59546.2024.10711514.

[129] I. O. for Standardization. Manipulating industrial robots – Mechanical interfaces – Part 1: Plates. ISO 9409-1:2004. ISO, 2004. URL: `https://www.iso.org/obp/ui/#iso:std:iso:9409:-1:ed-3:v1:en`.

[130] E. Barrett, E. M. Hoffman, L. Baccelliere, and N. G. Tsagarakis. Mechatronic Design and Control of a Light Weight Manipulator Arm for Mobile Platforms. *2021 IEEE/ASME International Conference on Advanced Intelligent Mechatronics (AIM)*. 2021, pp. 1255–1261. DOI: `10.1109/AIM46487.2021.9517389`.

[131] X. Wu, H. Hua, C. Zhao, N. Shi, and Z. Wu. A Back-Drivable Rotational Force Actuator for Adaptive Grasping. *Actuators* 12.7 (2023), p. 267. DOI: `10.3390/act12070267`.

[132] L. Rossini, E. Romiti, A. Laurenzi, F. Ruscelli, M. Ruzzon, L. Covizzi, L. Baccelliere, S. Carrozzo, M. Terzer, M. Magri, C. Morganti, M. Lei, L. Bertoni, D. Vedelago, C. Burchielli, S. Cordasco, L. Muratore, A. Giusti, and N. Tsagarakis. CONCERT: A Modular Reconfigurable Robot for Construction. *Journal of Field Robotics* (2025), pp. 1–31. DOI: `10.1002/rob.70092`.

[133] D. Torielli, L. Muratore, and N. Tsagarakis. An Intuitive Tele-Collaboration Interface Exploring Laser-Based Interaction and Behavior Trees. *Robotics and Autonomous Systems* 193 (2025), p. 105054. DOI: `10.1016/j.robot.2025.105054`.

[134] D. Gasperini, L. Muratore, and N. Tsagarakis. CRESTA: A Cognitivist Robot Execution Framework for Semantic-Driven Task Awareness. *Robotics and Autonomous Systems* 197 (2026), p. 105303. DOI: `10.1016/j.robot.2025.105303`.

Online resources

[135] Universal Robots. History of the Cobots - The Cobots from Universal Robots. Accessed in December 2025. URL: https://www.universal-robots.com/news-and-media/news-center/the-history-behind-collaborative-robots-cobots/.

[136] Boston Dynamics on YouTube. Spot's Got an Arm! Accessed in December 2025. URL: https://www.youtube.com/watch?v=6Zbhvaac68Y.

[137] ANYbotics. ANYmal - Autoomous Robotic Inspection Solution. Accessed in December 2025. URL: https://www.anybotics.com/robotics/anymal/.

[138] Unitree Quadruped Robot Empowers [Smart Power Inspection]. Unitree Robotics on YouTube. Accessed in December 2025. URL: https://www.youtube.com/watch?v=m5__1M6gYwM.

[139] Boston Dynamics. Boston Dynamics Atlas. Accessed in December 2025. URL: https://www.bostondynamics.com/atlas.

[140] PAL Robotics. SOLO 12 Advanced Quadruped Platform. Accessed in December 2025. URL: https://solo.pal-robotics.com/solo.

[141] Unitree Robotics. Unitree Robotics. Accessed in December 2025. URL: https://www.unitree.com/.

[142] DEEP Robotics. X20: The Ultimate Quadruped Bot series for Industrial Use. Accessed in December 2025. URL: https://www.deeprobotics.cn/en/index/product.html.

[143] Ghost Robotics. Vision 60. Accessed in December 2025. URL: https://www.ghostrobotics.io/vision-60.

[144] Robotiq. Grippers. Accessed in December 2025. URL: https://robotiq.com/products/.

[145] Schunk. Grippers. Accessed in December 2025. URL: https://schunk.com/us/en/gripping-systems/c/PUB_8293.

[146] OnRobot. Grippers. Accessed in December 2025. URL: https://onrobot.com/en/products?grippers=.

[147] Boston Dynamics. Spot Arm. Accessed in December 2025. URL: https://bostondynamics.com/wp-content/uploads/2020/10/spot-arm.pdf.

[148] Robotic Arm Z1 Mobile Robot On-board Robotic Arm. Unitree Robotics. Accessed in December 2025. URL: https://www.unitree.com/z1.

[149] Electroimpact. Aerospace Manufacturing Solutions. Accessed in December 2025. URL: https://www.electroimpact.com/.

[150] Red Dot. Red Dot Design Award 2021 Hilti Jaibot. Accessed in December 2025. URL: https://www.red-dot.org/project/hilti-jaibot-52326.

[151] nLink. Drilly - the first mobile drilling robot. Accessed in December 2025. URL: https://www.nlinkrobotics.com/projects/drilly-mobile-drilling-robot.

[152] Boston Dynamics. Boston Dynamics Spot. Accessed in December 2025. URL: https://www.bostondynamics.com/products/spot.

[153] Axios. Chinese robotics manufacturer left backdoor in product. Accessed in December 2025. URL: https://www.axios.com/2025/04/01/threat-spotlight-backdoor-in-chinese-robots-future-of-cybersecurity.

[154] IEEE Spectrum. Exploit Allows for Takeover of Fleets of Unitree Robots. Accessed in December 2025. URL: https://spectrum.ieee.org/unitree-robot-exploit.

[155] CubeMars. CubeMars AK10.9 V2.0 KV60 Robotic Actuator. Accessed in December 2025. URL: https://www.cubemars.com/product/ak10-9-v2-0-kv60-robotic-actuator.html.

[156] Robotiq. Wrist Camera. Accessed in December 2025. URL: https://robotiq.com/products/wrist-camera.

[157] Boston Dynamics on YouTube. What's in a humanoid hand? Accessed in December 2025. URL: https://www.youtube.com/watch?v=gS4rOqNDTBk.

[158] EtherCAT Technology Group. Why use EtherCAT? Accessed in December 2025. URL: https://www.ethercat.org/en/why_use_ethercat.htm.

[159] Robotnik. Robotnik Autonomous Mobile Robots Company. Accessed in December 2025. URL: https://robotnik.eu/.

[160] Universal Robots. Universal Robots Cobots. Accessed in December 2025. URL: https://www.universal-robots.com/.

[161] Franka Robotics. Franka Research 3. Accessed in December 2025. URL: https://franka.de/franka-research-3.

[162] NVIDIA. Jetson AGX Orin for Next-Gen Robotics. Accessed in December 2025. URL: https://www.nvidia.com/en-us/autonomous-machines/embedded-systems/jetson-orin/.

[163] Ouster. Os0: High-Precision Ultra-Wide Short-Range Lidar Sensor. Accessed in December 2025. URL: https://ouster.com/products/hardware/os0-lidar-sensor.

[164] RealSense. Depth Camera D455. Accessed in December 2025. URL: https://realsenseai.com/products/real-sense-depth-camera-d455f/.

[165] Unitree Robotics on GitHub. ROS simulation packages for Unitree robots. Accessed in December 2025. URL: https://github.com/unitreerobotics/unitree_ros/tree/master.

[166] IKO. Crossed Roller Bearings. Accessed in December 2025. URL: https://www.ikont.eu/files/Documents/Catalogues/CAT-57151UKv3_IKO_CRB.pdf.

[167] MatWeb Material Property Data. Aluminum 7075-T6; 7075-T651. Accessed in December 2025. URL: https://www.matweb.com/search/DataSheet.aspx?MatGUID=4f19a42be94546b686bbf43f79c51b7d.

[168] Synapticon. SOMANET Circulo 9. Accessed in December 2025. URL: https://catalog.synapticon.com/shop/category/integrated-motion-control/somanet-servo-drives/somanet-circulo-9-581.

[169] AAEON. UP Xtreme i11 | Intel Tiger Lake SBC for AI & Edge Computing. Accessed in December 2025. URL: https://www.aaeon.com/en/product/detail/developer-board-intel-11th-up-xtreme-i11.

[170] Intel. NUC 11 Pro. Accessed in December 2025. URL: https://www.intel.com/content/www/us/en/content-details/720882/intel-nuc-11-pro.html.

[171] Omron Industrial Automation. GX-JC03 / JC06 EtherCAT Junction Slave. Accessed in December 2025. URL: https://www.ia.omron.com/products/family/3079/.

[172] D-Link. DGS-105 5-Port Gigabit Unmanaged Desktop Switch. Accessed in December 2025. URL: https://www.dlink.com/uk/en/products/dgs-105-5-port-gigabit-ethernet-switch.

[173] Gable Technologied BV. EtherCAT IMU and Navigation solutions. Accessed in December 2025. URL: https://gable-imu.nl.

[174] MAP Batterie. IP 48V15. Accessed in December 2025. URL: https://www.mapbatterie.it/batterie-litio-bici-elettriche/646-ip-48v15.html.

[175] Stereolabs. Zed Mini Stereo Camera. Accessed in December 2025. URL: https://www.stereolabs.com/en-it/store/products/zed-mini.

[176] Alberobotics. Actuators Datasheet. Accessed in December 2025. URL: https://alberobotics.it/images/datasheets/alberobotics-actuators-datasheet.pdf.

[177] SKF. KDN.KAA15XL0 - Thin section bearings. Accessed in May 2026. URL: https://www.skf.com/group/products/thin-section-bearings/reali-slim-thin-section-bearings/productid-KDN.KAA15XL0.

[178] Misumi. FL6805ZZ Deep groove ball bearings / single row / small diameters / outer ring with flange). Accessed in May 2026. URL: https://uk.misumi-ec.com/vona2/detail/110300107650/?HissuCode=FL6805ZZ.

[179] Arduino. Nicla Vision. Accessed in December 2025. URL: https://docs.arduino.cc/hardware/nicla-vision/.

[180] Raspberry Pi. Raspberry Pi Zero 2 W. Accessed in December 2025. URL: https://www.raspberrypi.com/products/raspberry-pi-zero-2-w/.

[181] Raspberry Pi. Camera Module 2 NoIR. Accessed in December 2025. URL: https://www.raspberrypi.com/products/pi-noir-camera-v2/.

[182] ST Microelectronics. VL53L1X-SATEL - Two Breakout boards with VL53L1X long distance ranging sensor. Accessed in December 2025. URL: https://www.st.com/en/evaluation-tools/vl53l1x-satel.html.

[183] Ubuntu. Enterprise Open Source and Linux. Accessed in December 2025. URL: https://ubuntu.com/.

[184] AlphaCephei. VOSK Offline Speech Recognition API. Accessed in December 2025. URL: https://alphacephei.com/vosk/.

[185] Bosch Professional. GSR 12V-15 Cordless Drill/Driver. Accessed in December 2025. URL: https://www.bosch-professional.com/gb/en/products/gsr-12v-15-060186817A.

[186] Milwaukee Tool. M12 FUEL 1/2" Drill/Driver Bare Tool. Accessed in December 2025. URL: https://www.milwaukeetool.com/products/3403-20.

[187] DEWALT. 12V XR Brushless Sub-Compact Drill Driver. Accessed in December 2025. URL: https://www.dewalt.co.uk/product/dcd701d2-gb/12v-xr-brushless-sub-compact-drill-driver-2-x-2ah-batteries.

[188] Raspberry Pi. 4 Model B. Accessed in December 2025. URL: https://www.raspberrypi.com/products/raspberry-pi-4-model-b/?variant=raspberry-pi-4-model-b-8gb.

[189] Adafruit Industries. PiRTC - Precise DS3231 Real Time Clock for Raspberry Pi. Accessed in December 2025. URL: https://www.adafruit.com/product/4282.

[190] SUNFOUNDER. 2 Channel DC 5V Relay Module - Low Level Trigger. Accessed in December 2025. URL: https://www.sunfounder.com/products/2-channel-dc-5v-relay-module-low-level-trigger.

[191] ST Microelectronics. VL53L1X - Time-of-Flight (ToF) ranging sensor based on ST's FlightSense technology. Accessed in December 2025. URL: https://www.st.com/en/imaging-and-photonics-solutions/vl53l1x.html.

[192] Traco Power. TSR 3-1250 Non-Isolated DC/DC Converter. Accessed in December 2025. URL: https://www.tracopower.com/int/model/tsr-3-1250.

[193] APEM. 631H/2TK. Accessed in December 2025. URL: https://www.apem.com/panel-switches/toggles/600h-600nh/631h--2tk.

[194] Ubiquity Robotics on GitHub. ROS node for the Raspberry Pi Camera Module. Accessed in December 2025. URL: https://github.com/UbiquityRobotics/raspicam_node.

[195] okalachev on GitHub. STM VL53L1X time-of-flight rangefinder driver for ROS. Accessed in December 2025. URL: https://github.com/okalachev/vl53l1x_ros.

[196] Stratasys. FDM Nylon 12CF Thermoplastic Filament. Accessed in December 2025. URL: https://www.stratasys.com/en/materials/materials-catalog/fdm-materials/nylon-12cf/.

[197] Gazebo. Gazebo simulator. Accessed in May 2026. URL: https://gazebosim.org/home.

[198] Alberobotics. Sensors Datasheet. Accessed in December 2025. URL: https://alberobotics.it/images/datasheets/alberobotics-sensors-datasheet.pdf.

[199] ImageJ. ImageProcessing and Analysis in Java. Accessed in December 2025. URL: https://imagej.net/ij/.

[200] Keybotic. Technology. Accessed in May 2026. URL: https://keybotic.com/.

[201] PUDU Robotics. PUDU D5 | Industry-Grade Autonomous Quadruped Robot. Accessed in May 2026. URL: https://www.pudurobotics.com/en/products/d5.